



Institute of Biochemistry and Biology

Characterization of metal-binding synthetic coiled coil peptides

Master Thesis for the attainment of the academic degree

Master of Science (M. Sc.)

Submitted to the Mathematical/Natural Science Faculty

at the University of Potsdam

by

Isabell Tunn

Student Number: 759623

E-mail: schelske@uni-potsdam.de

Master degree course: Biochemistry and Molecular Biology

Potsdam, 02 August 2016

First referee: Dr. Matthew Harrington (Max-Planck-Institute of Colloids and Interfaces)

Second referee: Prof. Dr. Robert Seckler (University of Potsdam)

To my grandfather

Declaration of Originality/ Eigenständigkeitserklärung

I hereby declare that this thesis work "Characterization of metal-binding synthetic coiled coil peptides" is my own work and that only the denoted resources were used. This thesis has not been published or submitted in this or a similar form for the award of any other degree.

Ich versichere hiermit, dass ich die vorliegende Arbeit zum Thema "Characterization of metal-binding synthetic coiled coil peptides" selbständig und ausschließlich unter Verwendung der angegebenen Literatur sowie Hilfsmittel erstellt habe. Die Arbeit wurde bisher nicht veröffentlicht und nicht in gleicher oder ähnlicher Form einer anderen Prüfungsbehörde vorgelegt.

Potsdam, 02. August 2016

Isabell Tunn

Abstract

Coiled coils are often found as a structural motif in proteins with mechanical function, such as myosin or α -keratin. They are made up of two to seven α -helices, which are wound around each other, forming a superhelix. In the field of bioinspired materials, naturally occurring and *de novo* synthesized coiled coils with high binding specificity have become versatile material building blocks, especially as crosslinkers for hydrogels that find application as extra cellular matrix mimics in cell culture and tissue engineering. Little is currently known about the mechanical properties of the coiled coil crosslinkers. This information is needed, however, to control the bulk material properties and to understand how cells interact with their surrounding material mechanically. In the present work, mechanically calibrated and tunable coiled coils were developed that have the potential to be used as mechanosensitive crosslinkers. Towards this goal, metal coordination sites were engineered into a coiled coil. Protein-metal coordination bonds are strong, non-covalent interactions mediated by amino acid ligands, such as histidine (His) and cysteine. Specifically, two His residues were introduced into a well-characterized heterodimeric coiled coil from the literature with the goal of stabilizing helical turns.

Using Infrared, Raman and Circular Dichroism (CD) spectroscopy it was shown that the His-modified peptides maintain their α -helical structure and that they are able to coordinate the transition metal ions Ni^{2+} , Cu^{2+} and Zn^{2+} . Most importantly, His-metal coordination increases the thermodynamic and mechanical stability of the coiled coil. The thermodynamic stability increases by 6.0°C as determined from thermal unfolding experiments (CD). At the same time, the mechanical stability increases by 13 pN, when measured with single molecule force spectroscopy at a fixed pulling speed of 1000 nm/s. These results clearly validate the experimental approach of stabilizing helical turns using bioengineered Ni^{2+} -His coordination sites. The coordination sites are functional and the increased stability of helical turns directly affects the overall stability of the coiled coil, thermodynamically and mechanically. Thus, the current work does not only show new routes towards tuning coiled coil mechanics but also provides crucial information about the failure mechanism of coiled coils under load.

Future work will focus on the tunability of the His-modified coiled coils by changing the metal ion, the His-metal ratios or the position of His-residues. These strategies will allow for fully exploiting the potential of metal-coordinating coiled coils as tunable mechanosensitive, self-healing crosslinkers in hybrid hydrogels.

Zusammenfassung

Das Coiled Coil kommt als Faltungsmotiv in vielen Proteinen mit mechanischer Funktion, z.B. in α -Kreatin oder Myosin, vor. Ein Coiled Coil besteht aus zwei bis sieben α -Helices, die umeinander gewickelt sind und eine Superhelix bilden. Im Bereich der bio-inspirierten Materialforschung werden natürlich vorkommende und de novo synthetisierte Coiled Coils als vielseitige Bausteine für Materialien genutzt. Insbesondere werden Coiled Coils als Crosslinker in Hydrogelen eingesetzt, die Anwendung als extrazelluläre Matrix-Imitate in der Zellkultur und der Geweberegeneration finden. Über die mechanischen Eigenschaften der Coiled Coil Crosslinker ist bisher nur wenig bekannt. Die Erforschung dieser ist jedoch von hoher Wichtigkeit, um Materialeigenschaften zu kontrollieren und ein besseres Verständnis über die Wechselwirkungen von Zellen mit der Matrix, die sie umgibt, zu erlangen. In dieser Arbeit wurden mechanisch kalibrierte Coiled Coils entwickelt, die potentiell als mechanosensitive Crosslinker eingesetzt werden können. Um dies zu erreichen, wurden Histidin-Koordinierungsstellen in ein Coiled Coil eingefügt. Protein-Metall Koordinierungsbindungen sind starke nicht-kovalente Wechselwirkungen, die durch Aminosäuren, wie Histidin (His) oder Cystein als Liganden vermittelt werden. Mit dem Ziel die Helices zu stabilisieren, wurden in dieser Arbeit zwei Histidine in ein gut charakterisiertes Coiled Coil Heterodimer eingefügt.

Mit Infrarot, Raman und Circular Dichroismus Spektroskopie wurde gezeigt, dass die Sekundärstruktur der His-modifizierten Coiled Coils erhalten bleibt und Übergangsmetallionen, wie Ni^{2+} , Cu^{2+} und Zn^{2+} durch die Histidine koordiniert werden können. Zudem zeigt diese Arbeit, dass die Coiled Coils durch His-Metallionen Koordination thermodynamisch und mechanisch stabilisiert werden. Mittels thermischer Entfaltung im CD Spektrometer wurde ein Anstieg der Schmelztemperatur um 6°C ermittelt. Des Weiteren, wurde ein Anstieg der mechanischen Stabilität um 13 pN mittels Einzelmolekülkraftspektroskopie bei einer konstanten Zuggeschwindigkeit von 1000 nm/s gemessen. Diese Ergebnisse zeigen deutlich, dass His-Metallionen Koordination als ein geeigneter experimenteller Ansatz zur Helix-Stabilisierung ist. Die Koordinationsstellen sind funktional und erhöhen nicht nur die Stabilität des betroffenen Helix-Abschnittes, sondern auch die mechanische und thermodynamische Stabilität des ganzen Coiled Coils. Daher ist diese Arbeit wegweisend hinsichtlich der gezielten Veränderung von Coiled Coils und liefert

wichtige Informationen über den Entfaltungsmechanismus von Coiled Coils unter mechanischer Belastung.

Zukünftige Studien werden sich mit der Untersuchung des Einflusses von verschiedenen Metallionen, vom Histidin-Metallionen Verhältnis und von der Position der Histidine, auf die Stabilität der modifizierten Coiled Coils beschäftigen. Diese Strategien können die Nutzung von Metallionen-koordinierenden Coiled Coils als potentielle gezielt veränderbare, mechanosensitive und selbstheilende Crosslinker in Hydrogelen ermöglichen.

Table of Contents

Abstract	II
Zusammenfassung	III
Table of Contents.....	V
List of Figures	VII
List of Tables.....	VIII
List of Abbreviations.....	IX
1 Introduction	1
1.1 Coiled coil peptides	2
1.1.1 Coiled coils in biological systems	2
1.1.2 Coiled coil peptides as mechanical building blocks	4
1.2 The mechanical role of metal ions in biological systems	6
1.3 Aim of this work.....	8
2 Methods	10
2.1 FTIR and Raman spectroscopy.....	10
2.1.1 FTIR spectroscopy.....	12
2.1.2 Raman spectroscopy	13
2.2 Circular Dichroism (CD) spectroscopy	15
2.2.1 CD spectroscopy for secondary structure determination.....	15
2.2.2 Thermal unfolding	16
2.3 Amino Acid Analysis	18
2.4 Analytical Ultracentrifugation (AUC).....	19
2.5 AFM-based single molecule force spectroscopy.....	20
2.5.1 Stability of molecular interactions under force	20
2.5.2 Working principle of the AFM.....	22
3 Materials and experimental procedures.....	25

Table of Contents

3.1	Chemicals	25
3.2	Peptides.....	26
3.3	FTIR spectroscopy.....	26
3.4	Raman spectroscopy	26
3.5	CD spectroscopy.....	27
3.5.1	Single spectra.....	27
3.5.2	Thermal unfolding curves.....	27
3.6	Amino Acid Analysis	28
3.7	Analytical Ultracentrifugation (AUC).....	28
3.8	Surface functionalization for AFM force spectroscopy	29
3.8.1	Preparation of cantilevers	29
3.8.2	Preparation of glass slides	31
3.8.3	Measurement conditions.....	31
4	Results.....	32
4.1	Peptide design.....	32
4.2	Secondary structure of the coiled coil peptides is depending on the buffer	33
4.3	Histidine-modified peptides are able to coordinate transition metal ions	37
4.4	Effect of Ni ²⁺ on the secondary structure of the Histidine-modified peptides	41
4.5	Changes in the thermodynamic stability of coiled coil peptides due to metal ion coordination.....	43
4.6	Mechanical stability of the coiled coil is tuned by metal ion coordination.....	51
5	Discussion	59
6	Conclusion and Outlook.....	66
	References.....	68
	Appendix	78
	Acknowledgements	89

List of Figures

Figure 1: A mechano-responsive polymer containing spiropyran.	1
Figure 2: Schematic representation of a dimeric coiled coil (A). Heptad repeats of a dimeric coiled coil (B).	3
Figure 3: Tensile, bending and unzipping mode of a coiled coil.	5
Figure 4: Hierarchical structure and building blocks of a byssus thread core.....	7
Figure 5: A dimeric coiled coil tuned by Histidine-metal ion coordination.....	8
Figure 6: Infrared absorption and Raman scattering processes.	11
Figure 7: ATR-FTIR measurement setup.	13
Figure 8: Histidine Protonation states after Takeuchi [66].....	15
Figure 9: Scheme of characteristic CD signatures of different secondary structures.....	16
Figure 10: Thermal unfolding curve of an α -helical protein.	17
Figure 11: The free energy landscape of a two state system is affected by an applied force...	21
Figure 12: Schematic setup of an Atomic Force Microscope (AFM).	22
Figure 13: Steps of a single molecule force measurement.	24
Figure 14: Functionalization of surface and cantilever for AFM.	30
Figure 15: ATR-FTIR spectra of the single peptides and the coiled coils in water.	34
Figure 16: CD Spectra of the coiled coil peptides in water pH 8.5 (A), 10 mM NaP, pH 8.1 (B) and 5 mM PIPPS, pH 8.1 (C).	36
Figure 17: Raman spectra for HA4 (A) HB4 (B) and HA4HB4 (C) in 10mM NaP pH 8.1.	38
Figure 18: Raman spectra for HA4 (A) HB4 (B) and HA4HB4 (C) in 10mM PIPPS pH 8.1.	40
Figure 19: Influence of Ni ²⁺ on the secondary structure of the individual peptides and the coiled coils studied with CD spectroscopy.....	42
Figure 20: Thermal unfolding curves of the control peptides (A) and the His-modified peptides (B) at 222 nm from 8°C-90°C.....	44
Figure 21: CD spectra of A4B4 (A), HA4HB4 (B) and HA4 (C) at different temperatures during the unfolding experiment.	45
Figure 22: CD spectra for the peptides before (black) and after (red) the heating process at 20°C.....	46
Figure 23: Thermal unfolding curves of HA4 (A) in 2 M GdmCl and HB4 (B) without GdmCl at 222 nm in the presence or absence of Ni ²⁺	47

List of Figures

Figure 24: Thermal unfolding curves of HA4HB4 (A) and A4B4 (B) at 222 nm in 2 M GdmCl in the presence or absence of Ni ²⁺	49
Figure 25: Sedimentation coefficient distribution of A4 (black), B4 (red), HA4 (green) and HB4 (blue).....	51
Figure 26: The dimeric coiled coil HA4HB4 tuned by His-metal coordination.	52
Figure 27: Comparison of the HA4HB4 system measured with a regular spring holder and the SmallCell.	53
Figure 28: Force curves obtained for 1000 nm/s pulling speed in without metal ions (black) and with 2 mM Ni ²⁺ (green) in PBS at 25°C.....	54
Figure 29: Rupture force and loading rate histograms for the HA4HB4 system in the absence of Ni ²⁺	55
Figure 30: Rupture force and Loading rate histograms for the HA4HB4 system in the presence of 2 mM Ni ²⁺	56
Figure 31: Loading rate dependency of the most probable rupture force.	58
Figure 32: Possible shapes of the free energy landscape in the absence (black) and presence of Ni ²⁺ (green).....	64

List of Tables

Table 1: Composition of the buffers used in this work.	25
Table 2: Sequences of the peptides used in this work.	32
Table 3: Assignments of the ATR-FTIR peaks of the peptides in Figure 15.....	35
Table 4: Positions of the minima in the CD spectra and $r_{222/208}$ of the His-modified peptides and the control peptides in water, PIPPS and NaP buffer.	36
Table 5: Assignments of the Raman peaks of the peptides in NaP buffer (pH 8.1), see Figure 16.	41
Table 6: Melting temperatures T_m of the peptides in different buffers and conditions determined with CD spectroscopy.....	50
Table 7: Loading rate (\dot{F}) dependency of the rupture force (F_R) of the HA4HB4 system without and with 2 mM Ni ²⁺	57

List of Abbreviations

ATR	attenuated total reflectance
CD	Circular Dichroism
deg	degree
ECM	extra cellular matrix
FTIR	Fourier-transformed Infrared spectroscopy
GdmCl	guanidinium chloride
LR	loading rate
N	native/folded state
NA	numerical aperture
NaP	sodium phosphate buffer
MPIKG	Max Planck Institute for Colloids and Interfaces
PEG	poly-ethylene glycol
PIPPS	piperazine-1,4-bis(propanesulfonic acid)
RT	room temperature
SMFS	single molecule force spectroscopy
T	temperature
TCEP	tris(2-carboxyethyl)phosphine
U	unfolded state
WLC	Wormlike Chain

1 Introduction

The development of mechano-responsive materials is a major focus of current materials research. The general aim is to engineer smart materials, which report mechanical manipulation or damage using an optical readout [1]. Examples of materials, which respond to mechanical loading, include polymeric materials tuned with spiropyran (Figure 1) [2] or the rod-like molecule oligo(*p*-phylene vinylene) [1]. For example, when a mechanical load is applied on the polymer, the colorless spiropyran undergoes isomerization to the red merocyanine; thus, self-reporting the mechanical manipulation. Moreover, materials, which self-report their mechanical loading, can also be engineered by the insertion of FRET pairs into polymers [3]. Mechano-responsive materials have potential application as molecular machines in nanomaterials and microdevices, while self-reporting materials are useful to detect damage on the micron scale, thereby reducing the risk of failure in load-bearing materials (e.g. in aerospace engineering). However, most of these materials undergo irreversible damage and information about the structural changes on the molecular level is hard to obtain. Moreover, many of these materials are not suitable for biological and biomedical applications, such as cell culture.

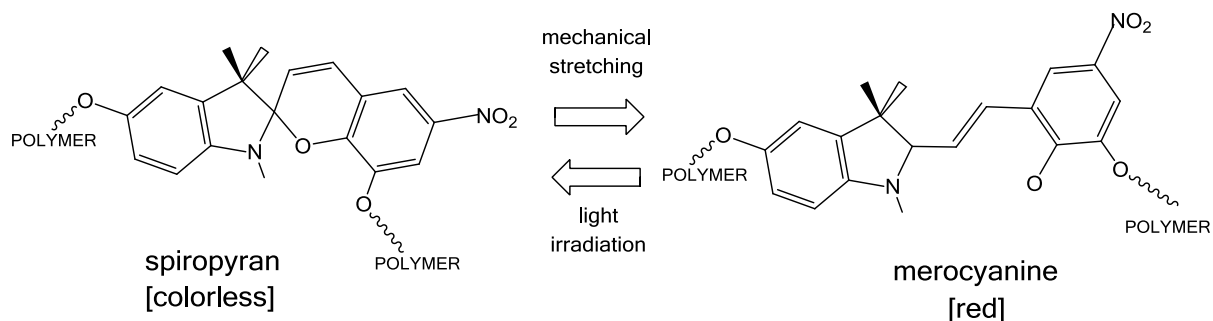


Figure 1: A mechano-responsive polymer containing spiropyran. When a mechanical load (stretching) is applied, the colorless spiropyran undergoes an isomerization. The resulting merocyanine, has a red color and can be converted back to spiropyran by light irradiation.

Thus, there is a need for biocompatible materials comprised of mechanically well-characterized and stimuli-responsive building blocks. A promising candidate for such a building block is the coiled coil folding motif in proteins. Coiled coils are often found in proteins, such as α -kreatin and myosin, which fulfill mechanical functions. In biomaterials research, the high binding specificity of natural or *de novo* designed α -helical peptides has been used to create coiled coil hydrogels and hybrid hydrogels comprised of a coiled coil crosslinked polymer [4]–[6]. Hydrogels crosslinked by coiled coils have the potential to serve as versatile extra cellular matrix (ECM) mimics for cell culture and tissue engineering [7],

because they are responsive to changes of the surrounding conditions, such as pH, ionic strength and mechanical loading. Thus, coiled coils could provide a dual function as crosslinkers and as tunable mechano-responsive building blocks, enabling the further investigation of the magnitude, geometry and duration of forces applied by cells on the ECM. It is known that the bulk mechanical properties of a material affect many cellular processes, including cell growth and differentiation [8]–[10]. To understand and control the underlying signaling pathways, materials with well-defined and tunable mechanical building blocks are required. Ultimately, the bulk properties of a material are determined by its molecular building blocks, such as reversible material crosslinkers.

Hence, there is a need for engineering and characterizing bio-compatible and tunable crosslinkers, e.g. based on coiled coils. Motivated by this need, the current work aims at bioengineering metal-chelating histidine side chains into coiled coil peptide sequences with the goal of increasing and tuning the stability of coiled coils via metal coordination. Here, metal coordination involves the formation of strong, yet labile bonds between amino acid ligands (e.g. Histidine) and transition metal ions (e.g. Ni^{2+} , Cu^{2+} , Zn^{2+}). Metal coordination is a proven means of stabilizing protein structures, as observed in both biological materials, such as the mussel byssus and spider fangs [11], as well as in bioengineered proteins [12]. If this work is successful, it could lead to a new toolkit of mechano-responsive crosslinkers with a wide range of applications.

1.1 Coiled coil peptides

1.1.1 Coiled coils in biological systems

Coiled coils are an abundant structural motif in proteins. In biological organisms coiled coils occur in proteins with very different functions. For example, α -keratin functions as an essential component of the cornified part of the skin, while tropomyosin can be found in muscle cells where it contributes to the regulation of muscle contraction [13]. Moreover, coiled coils are an important part of molecular motor proteins, such as myosin and dynein [14], [15]. A coiled coil consists of two to seven right-handed α -helices that are wound around each other to build up a left-handed superhelix [16]–[18]. Whereas dimeric coiled coils, such as myosin and dynein, are predominantly found in intracellular proteins, most of the extracellular coiled coils, such as fibrin, are trimeric [19]. The supercoil is characterized by the pitch, which is the distance of one complete turn, and the pitch angle, which describes the relative angle of each helix to the supercoil. In contrast to a single α -helix with 3.6

residues per turn, a dimeric supercoil is distorted with 3.5 per turn [14], [16]. Thus, the position of the side chain residues repeats every two turns or seven residues making up a so-called heptad repeat with the residues designated as *a*, *b*, *c*, *d*, *e*, *f*, *g* (Figure 2). The number of heptad repeats in a coiled coil can reach from only two in artificial peptides to 200 repeats in naturally occurring proteins [20].

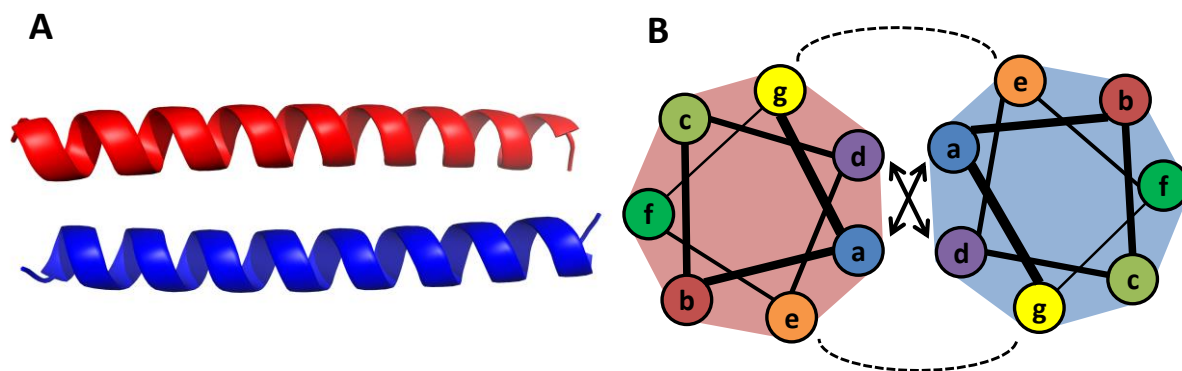


Figure 2: Schematic representation of a dimeric coiled coil (A). Heptad repeats of a dimeric coiled coil (B). The positions in one heptad are *a*, *b*, *c*, *d*, *e*, *f*, *g*. The hydrophobic core is made up of the positions *a* and *d* (Val, Leu, Ile). At the *e* and *g* positions charged amino acids, such as Glu or Lys can be found. *b*, *c* and *f* are solvent exposed and mostly hydrophilic residues. The arrows indicate Van-der-Waals interaction; the dashed lines indicate ionic interactions.

According to the “Peptide Velcro” hypothesis, every position of the repeat is occupied by a subset of amino acids with distinct properties in order to form a left-handed heterodimeric coiled coil [21]. At the *a* and *d* positions, which build up the interface between the helices, hydrophobic residues like valine (Val), leucine (Leu) or isoleucine (Ile) can be found. The Van-der-Waals interaction between the *a* and *d* residues of different helices results in a “knobs-into-holes” packing. The knob is represented by a hydrophobic side chain residue of one helix, while the hole is a cavity consisting of four side chain residues of the other helix [14]. The *e* and *g* positions are filled by charged amino acids like lysine (Lys) or glutamate (Glu), which enable specific electrostatic interaction of the helices in terms of orientation and pairing [16]. Specifically, the *g* residue of one helix forms a salt bridge with the *e* position of the next repeat of the other helix ($i \rightarrow i'+5$). The positions *b*, *c* and *f* are facing towards the solvent and are typically hydrophilic residues (e.g. glutamine, serine). Experimental studies revealed that there are certain rules to predict the oligomerization state and the orientation of a coiled coil depending on the amino acids at certain positions. For example, the charge pattern defines if parallel (N-termini at the same end of the supercoil) or antiparallel helices are formed and if homo- or heterodimeric supercoils are built up by the α -helices [17]. To favor heterodimerisation and prevent homodimer formation, two helices should have opposite charges at the *e* and *g* positions. Furthermore, an asparagine (Asn) in

complementary a positions of the two α -helical peptides is known to guide the formation of a parallel, “in-register” coiled coil by hydrogen bonding [22]. If the e and g positions are occupied by more hydrophobic residues, the probability of oligomers consisting of more than two α -helices increases. Moreover, the interhelical salt bridges between g and e contribute to the formation and stability of the supercoil and can be influenced by pH and salt concentration [23], [24]. To improve the thermal and maybe also the mechanical stability of a coiled coil, the number of heptad repeats or the hydrophobicity of the residues at the a and d position can be increased [25], [26]. Furthermore, recent experiments suggest that the helix propensity of the solvent exposed residues may also contribute to the stability of coiled coils [22]. Alternatively, in the current work, bioengineered His-metal coordination sites will be utilized to enhance the stability of a coiled coil. Changing the amino acid sequence of coiled coil peptides may inhibit the formation of an α -helical structure and coiling, if the rules derived from the “Peptide Velcro” hypothesis are violated. Thus, the positions of bioengineered His-metal coordination sites in a coiled coil sequence have to be chosen carefully. If successful, this work will allow to obtain more detailed insights into how the stability of the individual helices contributes to the overall stability of the coiled coil.

1.1.2 Coiled coil peptides as mechanical building blocks

Biological organisms often use coiled coils as building blocks for constructing tissues, (e.g. α -keratin), or as mechanical linkers between protein domains (e.g. myosin and dynein). Depending on their function, coiled coils can be exposed to very different forces with regards to loading geometry, loading rate, duration and magnitude of the applied force. For example, rotation or sliding of helices in receptor proteins transports signals across membranes, such as in the dimeric HAMP domain, which connects the intra and extracellular part of about 7500 different receptors in animals, plants, fungi and protists [27]. Furthermore, dimeric dynein undergoes a conformational change via sliding of the helices against each other, which leads to coupling of ATPase and microtubule binding [28]. Mechanical loading of coiled coils can also result in an α -helix to β -sheet transition, as observed in α -keratin [29], desmin [30], hagfish slime [29] or whelk egg capsule [31]. This transition can be linked to energy dissipation (e.g. in whelk egg capsule) and is most likely also responsible for the non-linear viscoelastic properties of these structures (e.g. strain-hardening), which prevents overstretching induced damage [31].

Possible applications of coiled coils for biological and biomedical purposes, such as protein purification and labeling, biosensing, drug delivery or stabilization of antibody fragments, are

based on the specificity between two α -helices [32]–[35]. This specificity has also been utilized in synthetic biomaterials research, where coiled coils have been implemented for the synthesis of responsive materials, such as hybrid hydrogels [5], [6], [32], [36].

However, little attention has been paid to the mechanical properties of the coiled coils, such as the loading geometry (Figure 3). The energy barrier to unfold and dissociate a coiled coil mechanically depends on the geometry of the applied force and can be different from the thermodynamic energy barrier [37], [38]. For unzipping of coiled coils, forces of 9-15 pN were found depending on length and sequence [37]. In the stretching mode of a dimeric myosin coiled coil, forces of 20-25 pN were observed, which emphasizes the critical role of the loading geometry [39].

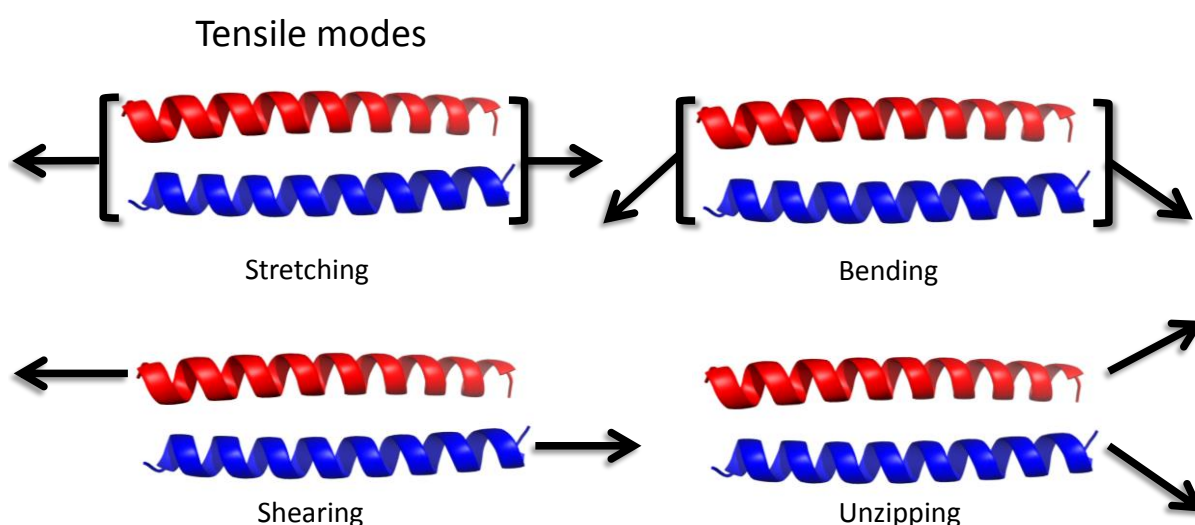


Figure 3: Tensile, bending and unzipping mode of a coiled coil. Stretching and Shearing are modes in the tensile geometry.

Up to now, it is not known which intra- and intermolecular helical interactions contribute most to the stability of a coiled coil, depending on the geometry of the applied force. In order to engineer mechanosensitive coiled coil hybrid hydrogels, the contributions of the different interactions on the stability and the response mechanism of coiled coils to forces need to be well understood. Applying force in the shear geometry, it has been shown using Molecular Dynamics simulations that the coiled coil helices start to unravel at the terminus where the force is applied. In the present work, histidine-metal ion coordination bonds will be introduced into these mechanically loaded heptads with the goal of stabilizing the helical structure. This will allow the investigation of the possible helix-stabilizing effect of these metal-coordination bonds on the overall stability of the coiled coil.

1.2 The mechanical role of metal ions in biological systems

About 40% of all known proteins interact with metal ions, which contribute to functions in catalysis, oxygen transport, photosynthesis, stabilization of proteins, nitrogen fixation and signal transduction [40], [41]. Metal ions can be coordinated by cofactors, such as the heme cofactor, or amino acids. The amino acid residue that is most often found in metal coordination spheres is histidine (His) followed by aspartate (Asp) and cysteine (Cys) [42]. Moreover, serine (Ser), threonine (Thr), tyrosine (Tyr), methionine (Met) and glutamate (Glu) can take part in coordination processes [42], [43]. The present study will focus on bioengineering His residues as metal ion ligands into a coiled coil peptide. The His side chain consists of an imidazole moiety, which contains two nitrogen atoms. These nitrogen atoms can potentially donate a lone pair of electrons to form a coordination bond with a metal ion. Under acidic conditions both nitrogen atoms are protonated and unable to coordinate metal ions. However, His has a pK_a of about 6.5 depending on the surrounding amino acids, indicating that at physiological pH one nitrogen will be deprotonated, facilitating the coordination of metal ions [44], [45]. In enzymes, His takes part in the coordination of Mn in Mn-superoxide dismutase of *Thermus thermophilus*, Cu in galactose oxidase, Fe in ribonucleotide reductase and Zn in carbonic anhydrase [40], [46].

However, aside from their physiological roles, metal ion coordination facilitated by His has been shown to play an essential role in the performance of biogenic acellular materials, such as the mussel byssus, ragworm mandibles and spider fangs [11]. In particular, the mussel byssus is a well-studied example of a protein-based biogenic material in which His-Zn²⁺ crosslinks have been implicated in increased mechanical stiffness, toughness and self-healing capacity [11], [47]. The crosslinks are associated with His-rich protein domains at the N- and C-terminal domains of the collagenous proteins called PreCol proteins, which comprise a significant portion of the threads by weight (Figure 4) [11], [48]. Peptides taken from the His-rich domain of the PreCols show a strong reversible interaction in the presence of metal ions [49].

Beyond functions in natural proteins and materials, the ability to rationally design protein sequences that are stabilized via metal coordination was demonstrated by Arnold and Haymore [50]. They showed that the insertion of a His-metal coordination site into an α -helix of cytochrome c, increases the thermodynamic stability of the protein by 4 kcal/mol in the presence of Cu²⁺.

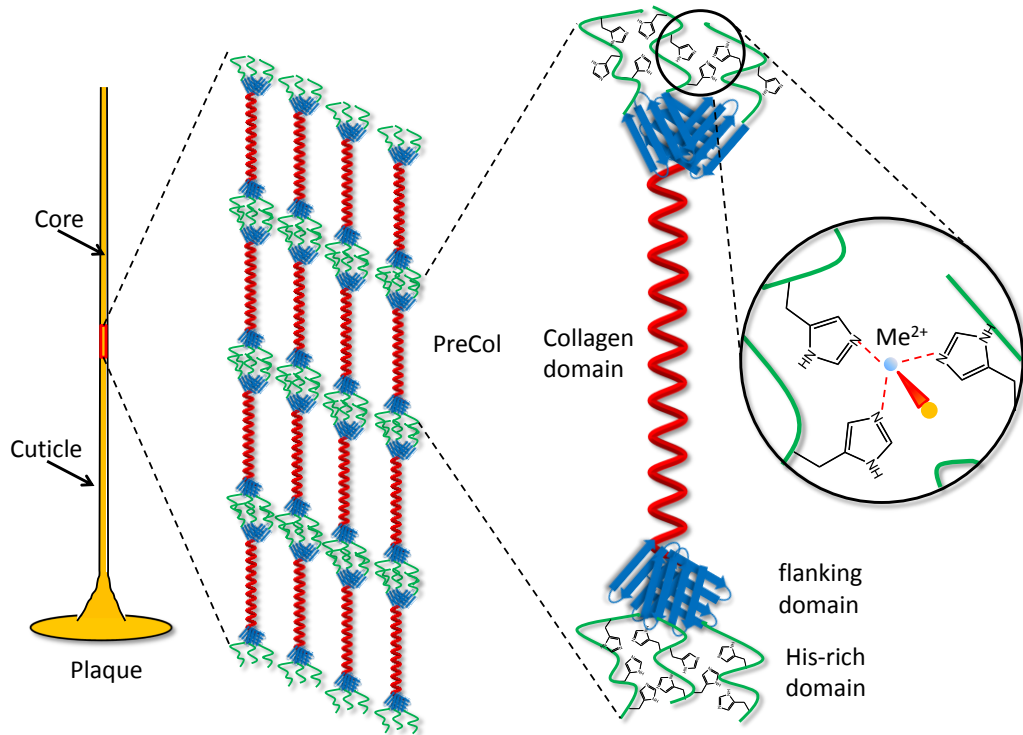


Figure 4: Hierarchical structure and building blocks of a byssus thread core. A thread is made up of the core, the cuticle and the plaque. The core contains staggered PreCol proteins with flanking domains and His-rich domains at the N- and C-terminus. The His residues are contributing to the self-healing ability through reversible metal ion coordination. Waite et al. [48] hypothesized that the His residues could bind reversibly to metal ions thereby the contributing to the stability and the self-healing properties of the mussel byssus threads after loading.

Specifically, the authors determined that two His residues bioengineered into an α -helical region of the protein with a three-amino-acid spacing (i.e. HXXXH), resulted in a suitable geometric configuration for chelating a single metal ion [50]. Rationally designed metal coordination sites were further shown to mechanically stabilize the small β -sheet protein GB1. In this protein, Cao et al. [12] engineered a bi-histidine metal chelation complex was across two β -strands and demonstrated a threefold higher mechanical stability of the protein against unfolding, using single molecule force spectroscopy [12]. The unfolding force of this protein was further shown to be pH dependent, which can be explained with electrostatic repulsion of the protonated (positively charged) His residues at acidic pH [51]. These examples clearly demonstrate that the insertion of His residues as metal ion coordination sites is a promising means for tuning the thermodynamic and mechanical stability, which may hold potential for coiled coil peptide design, as well as for investigating the response mechanism of coiled coil peptides to an applied force.

1.3 Aim of this work

The main aim of this thesis is to design coiled coil peptides, whose mechanical stability can be tuned via His-metal coordination bonds. If successful, these coiled coils will be implemented as tunable mechanosensitive crosslinkers in biomimetic hydrogel materials. Towards this goal, a thorough understanding of the mechanical response mechanism of coiled coils to an applied force is required. Molecular Dynamics simulations of the dimeric myosin coiled coil suggest the following response mechanism to shear forces: The α -helices unfold in the direction of the applied force and the unfolding starts at the point-of-origin of the force [52]. According to this prediction, stabilizing the heptad repeats closest to the point of force application will prevent α -helix and, consequently, coiled coil unfolding. Up to now, this predicted mechanism has not been studied experimentally.

In order to test this prediction, a well-characterized heterodimeric coiled coil is modified such that metal coordination bonds can form in the heptads that are primarily loaded with the applied shear force (Figure 5). The four-heptad coiled coil introduced by Thomas et al. [53] is used as the template for the current work. To facilitate metal-coordination, two histidine residues are introduced at the solvent exposed positions in the corresponding heptads. As the exchange of these residues to histidine may affect the secondary structure of the peptides, it needs to be determined first if the His-modified peptides are still able form α -helices. For this purpose, Attenuated total reflectance-Fourier transformed Infrared spectroscopy (ATR-FTIR) as well as Circular Dichroism (CD) spectroscopy is used.

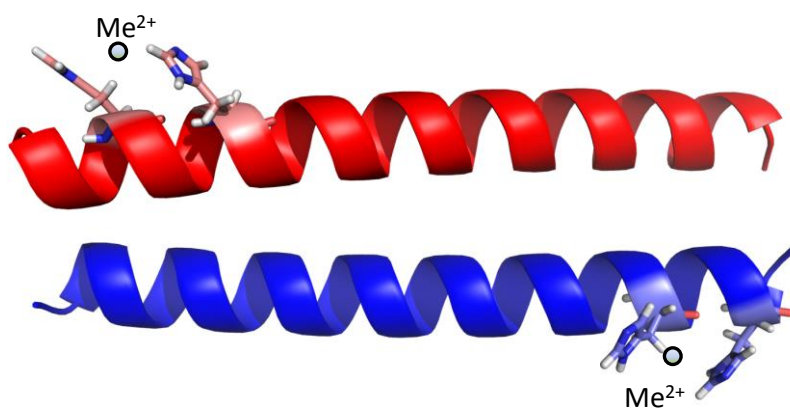


Figure 5: A dimeric coiled coil tuned by Histidine-metal ion coordination. The structure was predicted by CC-Builder [54]. The red peptide has two His in the first heptad and the blue peptide has two His in the fourth heptad repeat.

In order to bioengineer tunable crosslinkers, it is of high interest to know which metal ions are chelated by the His-modified peptides. Distinct metal ions are known to favor different coordination geometries, which may lead to differential stabilization of the coiled coil. To test

whether transition metal ions, such as Ni^{2+} , Cu^{2+} or Zn^{2+} , are chelated by the peptides, Raman spectroscopy is used.

As the ultimate proof of the design strategy, the effect of coordinated metal ions on the thermodynamic and mechanical stability of the coiled coils needs to be determined. Thermal unfolding of the coiled coils is monitored in the absence and presence of metal ions using CD spectroscopy. Single molecule force spectroscopy (SMFS) with an atomic force microscope (AFM) is used to investigate the effect of His-metal chelation on the mechanical stability. These measurements are expected to provide the molecular rupture forces of the coiled coil in the absence and presence of metal coordination. Thus, these experiments can yield the desired information about the mechanical stabilization of the loaded heptads and serve as the starting point for tuning the mechanical response of the coiled coil to shear forces. It is expected that metal-coordinating coiled coils will provide a new platform for the synthesis of tunable and mechanosensitive hydrogels.

2 Methods

In order to characterize the secondary structure of His-modified peptides, spectroscopic techniques, such as ATR-FTIR, Raman and CD spectroscopy, were used. The thermodynamic stability of the coiled coil was studied using thermal unfolding monitored by CD spectroscopy. To determine the effect of metal ion coordination on the mechanical stability of the coiled coil, AFM based single molecule force spectroscopy was used. This section gives a short theoretical background about the techniques used in this thesis.

2.1 FTIR and Raman spectroscopy

Fourier-transformed (FT) IR and Raman spectroscopy are complementary vibrational spectroscopy techniques based on the interaction of light with matter. They are useful for studying the conformation and structure of protein molecules as well as more complex materials and biological tissues. Both techniques are non-destructive, require small amounts of sample and have a high reproducibility [55]. Moreover, the techniques are complementary to each other, since both use light to probe the vibrational modes of molecules in a given sample [56]. However, the two forms of spectroscopy are different in the manner in which light energy is transferred to the molecule, thus changing its vibrational state. While FTIR spectroscopy is used to observe transitions between molecular vibrational energy states, due to absorption of a broad range of IR radiation, Raman spectroscopy is based on an inelastic scattering process (Stokes Raman scattering), caused by the interaction of incident, monochromatic light with molecules and molecular groups (Figure 6). Here, the vibrational quantum energies of the discrete vibrational energy states of the molecule do not match the energy of the incident photon, which loses part of its energy distorting (polarizing) the electron cloud of the atoms. As a result the molecule gets into a virtual energy state and a photon with reduced energy is scattered by the molecule.

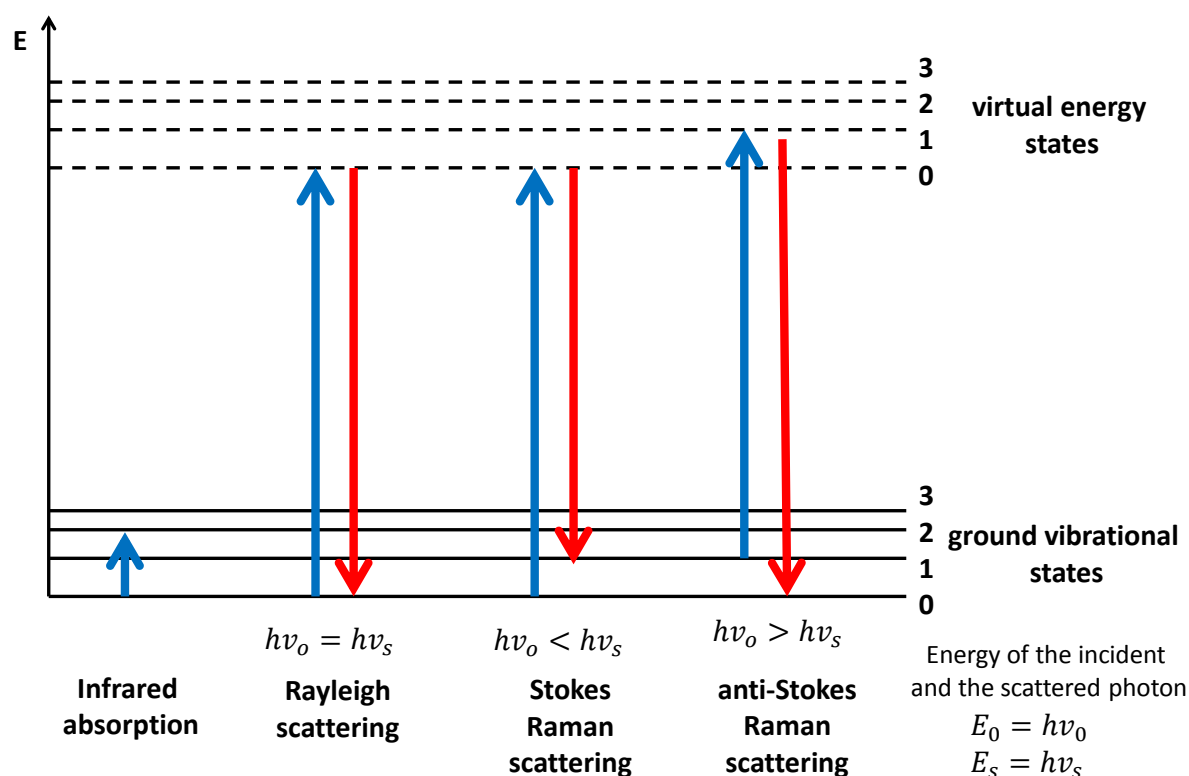


Figure 6: Infrared absorption and Raman scattering processes. The absorption of IR light elevates the molecule into a higher vibrational energy state. Rayleigh scattering is elastic. The initial energy (E_0) to bring the molecule in a higher virtual energy state equals the scattering energy (E_s). Stokes Raman scattering is inelastic and less probable than Rayleigh scattering. In anti-Stokes Raman scattering the initial energy is smaller than the energy of the scattering because the molecule possessed a higher ground vibrational state initially. The energy of the photons can be described by $E = h\nu$, where h is the Planck's constant and ν is the wavenumber of the photon.

In case of FTIR spectroscopy, the transition between the vibrational energy levels depends on the electric dipole of the molecules in the sample, while in Raman spectroscopy the interactions between the light and the sample involve the Raman polarizability of the molecules [56]. As a consequence of these differences, FTIR- spectroscopy is more suitable to detect asymmetric vibrations of polar groups, while Raman spectroscopy is more sensitive to symmetric vibrations of non-polar groups. However, there are also molecules, such as CO_2 , H_2O or benzene, which are both Raman and IR active [56]. The resulting bands in the FTIR and Raman spectra are characterized by their frequency, intensity and the band shape, which depend on the environment of the molecular groups. The frequencies of the molecular vibrations change depending on the mass of the atoms, the bond strength and the geometric arrangement, thus, providing information on structure, environment and dynamics of molecules [56]. To obtain a clear picture of the molecular structure of a sample, it is advisable to combine FTIR and Raman spectroscopy, which are described in more detail below.

2.1.1 FTIR spectroscopy

FTIR is based on the absorption of IR-light (e.g. mid-IR: $\nu = 4000\text{-}400\text{ cm}^{-1}$) by molecules, which leads to transition of the molecules into a higher vibrational energy state (Figure 6). In particular, all the IR frequencies are emitted simultaneously by the broad band light source and the different wavelengths are modulated by a Michelson-Interferometer at different rates, so that certain wavelengths are transmitted or blocked periodically by interference. The molecules absorb the modulated IR-light of a specific wavelength corresponding to distinct vibrational frequencies of IR active molecular structures and chemical bonds [55]. A molecule is IR active if its electric dipole changes when it is excited to a higher vibrational energy state. The detected signal is an interferogram containing the spectral information about the whole wavelength range used for the excitation. Fourier transformation is used to convert the interferogram into a whole spectrum. Typically, a FTIR spectrum is obtained by plotting the absorbance (or transmittance) versus the wavenumber [cm^{-1}]. The absorbed wavelengths provide information about the type of bonds and therefore the molecules present in a sample. Important spectral regions giving information about the protein backbone conformation are the amide I/II bands ($1500\text{-}1700\text{ cm}^{-1}$) and the amide III band ($1180\text{-}1320\text{ cm}^{-1}$) [55], [57]. The secondary structure of proteins is most clearly reflected by the position of the amide I band [58], which is at $1650\text{-}1657\text{ cm}^{-1}$ for α -helical proteins, while for coiled coils the amide I band can even be shifted to lower wavenumbers ($1637\text{-}1654\text{ cm}^{-1}$) [59]. In this work, the FTIR measurements are carried out using the ATR (attenuated total reflectance) mode, which is useful for investigating liquid and solid samples. The major advantage of the ATR mode compared to the more typical transmission mode, is that only little or no sample preparation is required [60]. In the ATR mode the samples are measured on a crystal with a high refractive index. In the present study, a crystal composed of a layer of Si on top of a ZnSe layer was used. The IR-light is directed in a 45° angle to the ZnSe-crystal and totally internally reflected in the Si-crystal (Figure 7). Only the evanescent wave created by internal reflectance extends beyond the crystal and can be absorbed by the molecules in the sample, which is in contact to the crystal. The intensity of the evanescent wave decreases exponentially with the distance from the crystal-sample interface; thus, only molecules in the distance of 0.5 to $5\text{ }\mu\text{m}$ can absorb energy from the evanescent wave [61]. The evanescent wave is altered or attenuated by the interaction with the molecules. Thus, the absorption processes also alter the IR beam.

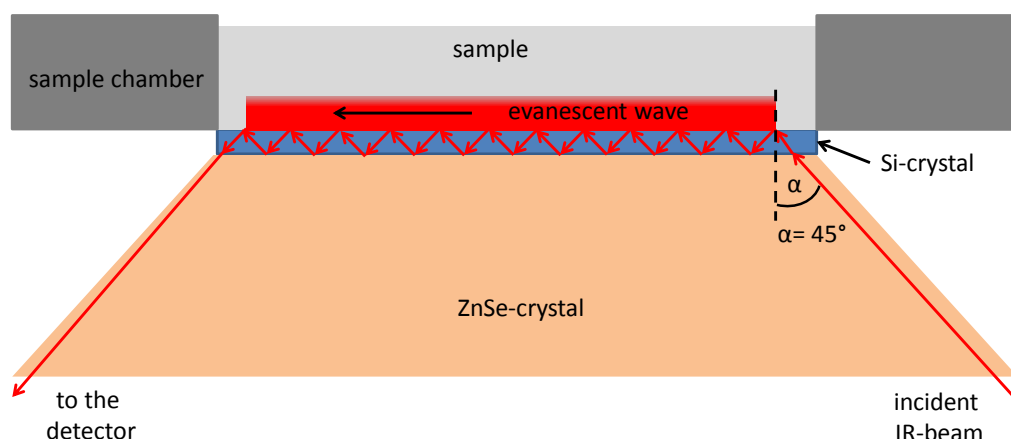


Figure 7: ATR-FTIR measurement setup. The incident IR-beam is total internal reflected by the Si-crystal if the incident angle is 45° . Distinct Energies of the resulting evanescent wave are absorbed by the IR active molecules. Attenuation of the evanescent wave causes changes in the IR-beam, which are recorded by a detector. Since the intensity of the evanescent wave decreases exponentially with the distance to the crystal-sample interface, molecules near the interface have a higher probability of being excited to a higher vibrational energy state.

One major drawback of FTIR is that water is highly IR active and has a characteristic peak that overlaps with the amide I band of proteins, which raises clear challenges for measuring samples in solution [55]. Thus, care must be taken for properly removing the water background if useful data about protein structure is to be extracted.

2.1.2 Raman spectroscopy

When photons interact with matter they are either absorbed or scattered. As mentioned, FTIR measures the frequencies (energies) of the IR-light, which are absorbed by molecules, corresponding to discrete transitions of molecular vibrations in the sample. In contrast, Raman spectroscopy measures the energy of the photons scattered by a sample. In this case the incident photon has a higher energy than the distinct vibrational energy states of a molecule, which is therefore not excited to a higher vibrational energy level, but the electron clouds of the atoms are distorted [56], [62]. This distortion or polarization of the electron cloud brings the molecule into a virtual energy state (Figure 6). The most probable scattering that occurs, when a Raman active molecule goes back from a virtual energy state to the vibrational ground state, is the elastic or Rayleigh scattering. Here, there is no energy difference between the incident and the scattered photon. The inelastic or Stokes Raman scattering results from the transition of a molecule from a virtual energy level to the first excited vibrational energy level and is, thus, far less probable than Rayleigh scattering [56]. In case of inelastic scattering, the frequency of scattered photon is shifted towards higher wavenumbers or lower energy compared to the incident photon. An even less probable scattering process is Anti-Stokes Raman scattering, where the molecule is initially in an excited vibrational energy state and

goes back from the virtual energy state to the vibrational ground state. Thus, the scattered photon has a higher energy than the incident photon. The basis for Raman spectroscopy is founded on the frequency (energy) difference between the incident photon and the scattered photon obtained by inelastic Stokes Raman scattering, which contains information about the energy of specific vibrational modes of the molecules in the sample.

In practice, Raman spectra are obtained by exciting a sample with monochromatic laser light and using a sensitive detector to measure the intensity of the inelastically scattered light as a function of differences in the energy between the wavelength of the incident laser and those of the photons scattered by the molecules in the sample. This energy difference is termed the Raman shift and usually displayed in wavenumbers [cm^{-1}], which are a measure of spatial frequency (i.e. number of cycles in a unit distance) [62]. Raman peaks are often associated with vibrations of specific functional groups of macromolecules, including the polypeptide backbone of proteins, making the technique useful for determining the secondary structure of proteins and peptides or measuring conformational changes of biomolecules under different conditions. For proteins and peptides the amide I band ($1634\text{-}1676\text{ cm}^{-1}$), CH_2 -bending/stretching (1450 cm^{-1}), the amide III band ($1100\text{-}1375\text{ cm}^{-1}$) and the bands for aromatic amino acids (e.g. Phe 1004 cm^{-1}) give important information about structures and conformations [62]. In the case of an α -helical conformation the amide I band can be found between 1645 and 1658 cm^{-1} , while the amide III band is typically between $1280\text{-}1320\text{ cm}^{-1}$ [63]–[65].

Relevant to the present study, Raman spectroscopy can also be used to investigate changes in the protonation and coordination state of the five-membered imidazole side chain of His. The distinctive peaks correspond to the $\text{C}_4=\text{C}_5$ double bond in the Histidine imidazole moiety and change according to the protonation and metal coordination state of the His residue as summarized in Figure 8. While His has two protonated nitrogen-atoms in the imidazole ring at acidic pH (< 6.5) (cationic imidazolium), the imidazole ring is deprotonated at neutral to basic pH [66]. In the latter case, there are two tautomers, where either the N_π -atom or the N_τ -atom has a bond to a hydrogen-atom. The deprotonated nitrogen-atom, which possesses a free electron pair, can function as a coordination site of transition metal ions. If a metal ion is coordinated by the N_τ -atom a band at $1594\text{-}1606\text{ cm}^{-1}$ is detected depending on the metal ion bound. Moreover, the fully deprotonated anionic imidazolate ring can bind to two metal ions (bridging) [66].

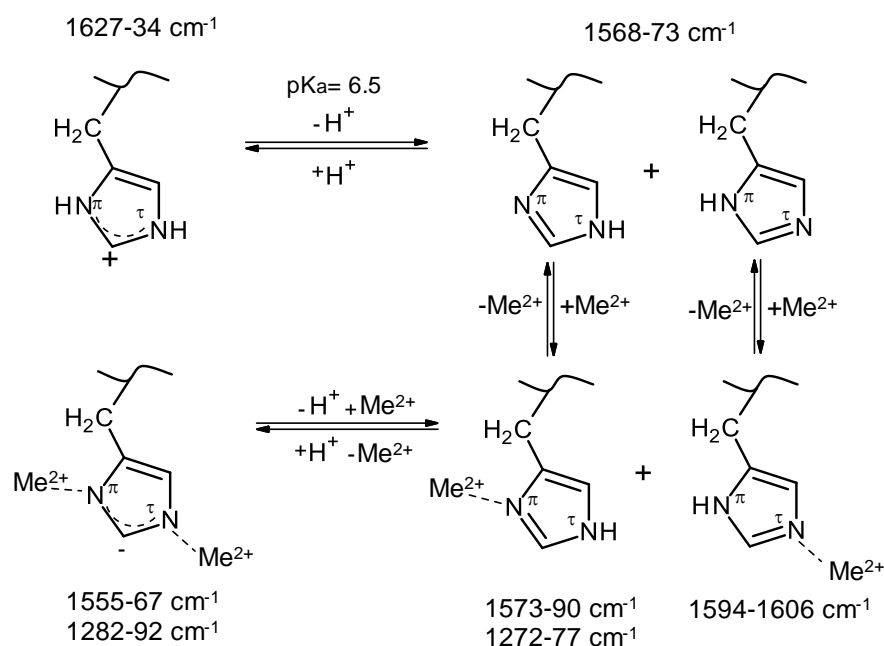


Figure 8: Histidine Protonation states after Takeuchi [66]. The imidazole side chain of His is predominantly protonated if the pH is below 6.5. Increasing pH leads to an increase in deprotonated His which is able to coordinate metal ions (Me^{2+}) at the N_π or N_τ -atom. At basic pH and high Me^{2+} concentration also both nitrogen-atoms can take part in coordination.

All the described states of the imidazole side chain of His can be observed in Raman spectra since they have a characteristic signature. To investigate changes in the state of His, it is beneficial if the sample does not contain aromatic amino acids (i.e. Trp, Tyr, Phe), which exhibit strong Raman peaks that overlap with the His peaks [66].

2.2 Circular Dichroism (CD) spectroscopy

2.2.1 CD spectroscopy for secondary structure determination

One of the most frequently used spectroscopic methods to investigate the secondary structure of a protein or peptide is CD spectroscopy. It is based on the ability of chiral molecules, like peptides, to differentially absorb left- and right-handed circularly polarized light. The monochromatic light is polarized through a suitable filter or prism. The resulting sinusoidal oscillation of the electric field E in a single plane can be described by two vectors E_R and E_L [67]. While E_R rotates clockwise, E_L rotates counterclockwise. The resulting vector traces describe a circle. When a chiral molecule interacts with circularly polarized light, it absorbs E_R and E_L to a different extent. This results in an elliptic polarization of the light. The CD spectrometer measures the ellipticity θ_{obs} in millidegree (mdeg). The mean residue molar ellipticity (θ_R) [$\text{deg cm}^2 \text{dmol}^{-1}$] can be calculated as

$$\theta_R = \frac{\theta_{\text{obs}}}{d \cdot c \cdot n} \quad (1)$$

with respect to the concentration c [mol/l], the number of amino acids (n) and the path length d [mm] [67]. Different protein or peptide secondary structures show distinct signatures in their CD spectra (Figure 9). Proteins in the α -helical conformation exhibit two minima at 222 nm and 208 nm as well as a maximum at 193 nm [67]. The formation of coiled coils can be estimated by calculating the ratio ($r_{222/208}$) between the two minima [θ_{222}]/[θ_{208}] [25]. A ratio ($r_{222/208}$) close to 1 or bigger than 1 indicates a well-defined coiled coil structure [22]. For proteins in β -sheet conformation, a minimum at 218 nm and a maximum at 195 nm can be observed and random coil proteins show a maximum of low intensity at 210 nm and a minimum at 195 nm.

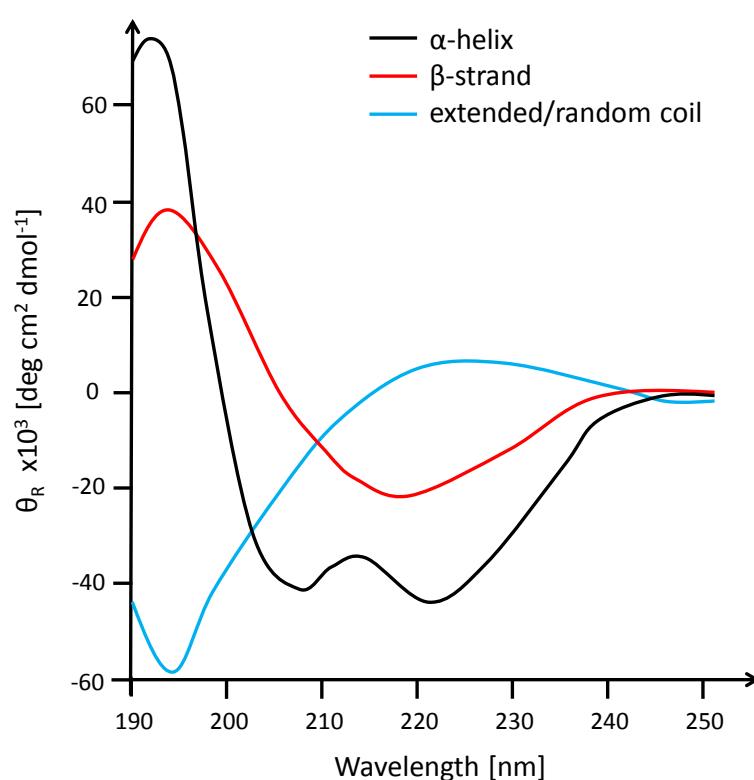


Figure 9: Scheme of characteristic CD signatures of different secondary structures. α -helix (black), β -strand (red), random coil (blue) [67].

2.2.2 Thermal unfolding

The stability of proteins can be influenced by temperature, pH, ionic strength or the addition of chemical denaturants, such as guanidinium chloride (GdmCl). The thermal unfolding of proteins and peptides leads to a loss of the secondary structure, which can be monitored using CD spectroscopy coupled with a heating element [68]. For example, CD spectra of proteins, which are completely unfolded, have a spectrum similar to random coils (Figure 9), whereas proteins with a higher thermal stability partially maintain their secondary structure even at

high temperatures. Relevant to this study, CD spectroscopy can be used to monitor the process of unfolding for α -helical proteins or peptides by monitoring changes in the ellipticity at 222 nm over a suitable temperature range. For most of the dimeric coiled coils, such as the leucine zipper, studies showed that helix formation and dimerization of the monomers are cooperative processes, which can be described by a two state transition [69], [70]:



For coiled coils, the native state is a folded dimer (N_2), which fully denatures to unfolded monomers ($2U$) during heating or chemical denaturation. The resulting unfolding curves have a sigmoidal shape (Figure 10) [71].

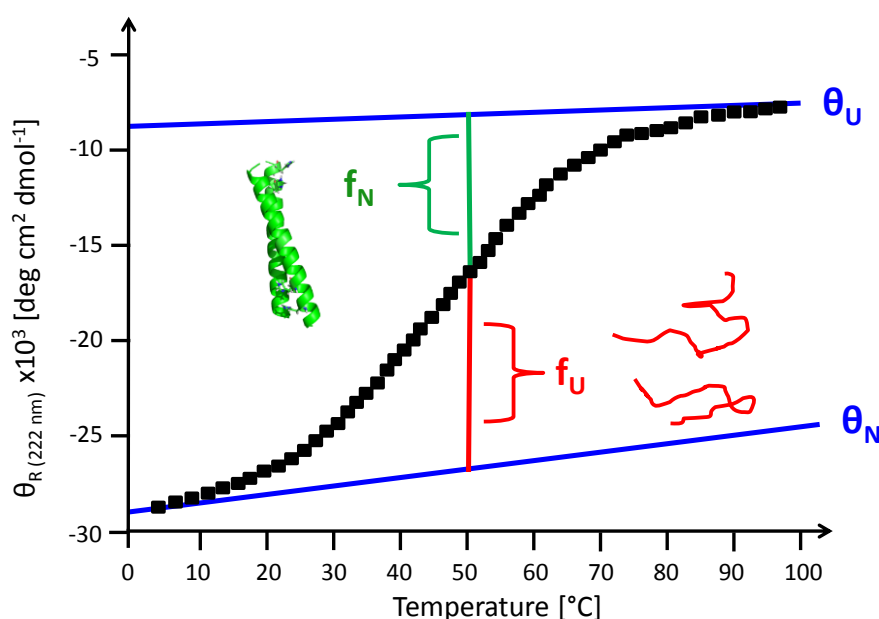


Figure 10: Thermal unfolding curve of an α -helical protein. The ellipticity is measured at 222 nm over a temperature range. fraction folded (f_N) and the fraction unfolded (f_U) as well as the ellipticities of the folded and the unfolded state θ_N and θ_U at every temperature can be determined.

For every temperature (T) the folded fraction f_N and the unfolded fraction f_U of the peptides can be calculated as

$$f_N = \frac{\theta_T - \theta_U}{\theta_N - \theta_U} \quad f_U = \frac{\theta_T - \theta_N}{\theta_U - \theta_N} \quad (2)$$

with θ_N being the ellipticity of the folded peptides, θ_U being the ellipticity of the unfolded peptides and θ_T being the mean residue molar ellipticity of the peptide at any temperature [68]. Moreover, $f_N + f_U$ equals 1. If the coiled coil peptides bind metal ions, there may be a change in the helicity and the helix stability, since the His-modified heptads should be stabilized in the presence of metal ions, as observed by Ghadiri and Choi [72]. These

effects can be investigated by determining the melting temperature T_m or the change in the unfolding constant K_U of the coiled coils at different metal ion concentrations. Equation 3 describes the relationship between the free energy ΔG of unfolding and K_U [73]:

$$\Delta G = -RT \ln K_U \quad (3)$$

The Gibbs Helmholtz equation is

$$\Delta G = \Delta H (T - T_m) \Delta C_p - T(\Delta S + \Delta C_p (\ln \left(\frac{T}{T_m}\right))) \quad (4)$$

where ΔH is the free enthalpy, T is the absolute temperature, ΔS is the entropy and ΔC_p in the change of the heat capacity of the peptides [73]. According to equation 2, the melting temperature T_m of the protein is defined as the temperature for that f_N equals f_U equals 0.5, so that $\ln K=1$ and $\Delta G=0$ and $\Delta S=\Delta H/T_m$. To describe the interaction between two different proteins or peptides, as in this work, the equation 4 has to be further modified. However, to study the effect of the His-metal chelation on the stability of the coiled coil peptides, the T_m can be determined by fitting the data to the equation 5 [74]:

$$\theta_R = \frac{\theta_u^o - \theta_n^o + (m_u - m_n)T}{1 + \exp\left(\frac{1}{R}\left(\Delta C_p \ln\left(\frac{T}{T_m}\right) - \left(\frac{1}{T} - \frac{1}{T_m}\right)(\Delta H_m - T_m \Delta C_p)\right)\right)} + \theta_n^o + m_n T \quad (5)$$

The parameters θ_u^o and θ_n^o are the mean residue molar ellipticities of the unfolded and the folded coiled coil at $T=0$ K and m_u and m_n are the constant temperature dependencies (slopes of the baselines) of the unfolded and the folded peptides. The parameters θ_u^o , θ_n^o , m_u and m_n are required to represent the pre- and post-transition baselines depending on the temperature. The thermodynamic parameters are ΔH_m , which is the molar change in the enthalpy of folding at T_m ; T_m , which is the midpoint of the transition (melting temperature) and ΔC_p , which is the molar isobaric heat capacity change. In the current work, the slope of the pre-transition curves was set to a constant value for the measurements with and without metal ions to guarantee the comparability of the obtained values. ΔC_p was set to 0, since also Thomas et al. [53] assumed that the change in the heat capacity of the coiled coil peptides is so small that it can be neglected.

2.3 Amino Acid Analysis

To calculate the correct mean residue molar ellipticity and related thermodynamic parameters from the CD measurements, it is essential to know the exact concentrations of the peptides in the samples. Because there are no aromatic amino acids or Cys in the peptides used for CD spectroscopy, Amino Acid Analysis based on a post-column ninhydrin derivatization was

used to determine the concentration of the peptides. After acid hydrolysis of the peptides the single amino acids are separated using an amino acid analyzer based on high pressure liquid chromatography [75]. To separate the amino acids, gradients in pH and ionic strength are used. The reaction of the free amines of the amino acids with ninhydrin leads to the formation of Ruhemann's purple, which can be quantified by measuring the absorbance at 440 nm and 570 nm [75]. A standard solution with known amino acid concentrations is used to establish a linear correlation of the peak area of amino acids to the concentration in mol%. The absolute nanomoles of the amino acids in the sample volume can be summed up to reliably determine the peptide concentration in the stock solutions.

2.4 Analytical Ultracentrifugation (AUC)

AUC is a powerful tool to analyze the shape and size of macromolecules in solution. In general, there are two different measurement setups: the sedimentation velocity and the sedimentation equilibrium mode. In the sedimentation velocity mode, biomolecules move in the high centrifugal field according to their shape, size and interaction with other molecules [76]. The sedimentation equilibrium mode uses lower centrifugal fields to analyze equilibrium concentration gradients. Parameters obtained from this method are the molecular mass, association stoichiometry, association constants and solution nonideality [76]. In this work the sedimentation velocity setup was used. The net force acting on the molecules in a sedimentation velocity experiment is

$$F = (M_p - M_s) \omega^2 r \quad (6)$$

M_p is the mass of the molecule, M_s is the mass of the solvent displaced by the molecule while it sediments, ω is the speed of the rotor (revolutions per second), and r is the distance to the center of the rotor. The M_s is also described as

$$M_s = M_p \bar{v} \rho \quad (7)$$

with the partial specific volume \bar{v} of the molecule and the density of the solvent ρ . Thus, the effective mass of a molecule is

$$M_{eff} = M_p(1 - \bar{v} \rho) \quad (8)$$

If also the frictional force (frictional coefficient f) acting on a molecule moving through the solvent with a velocity v is taken into account the sedimentation coefficient in Svedberg s [S] can be obtained:

$$s = \frac{v}{\omega^2 r} = \frac{M_{eff}}{f} \quad (9)$$

From a sedimentation velocity experiment the sedimentation coefficient distribution c can be calculated using the program SEDFIT by solution of equation 10:

$$c(t, r) = \int g^*(s)U(s, r, t)ds \quad (10)$$

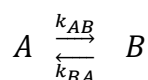
with $g^*(s)$ being the apparent sedimentation coefficient distribution using the least square principles, and $U(s,r,t)$ being the sedimentation profile of a non-diffusing species [77]. From the resulting data, conclusions about the mass and thus, the different oligomerization states of the peptides can be drawn.

2.5 AFM-based single molecule force spectroscopy

AFM-based single molecule force spectroscopy is a versatile, sensitive tool to investigate the mechanical stability as well as the force-induced unbinding kinetics of single molecular interactions. The basic kinetic model used in this work and the general working principle of the AFM are explained in the following two subchapters.

2.5.1 Stability of molecular interactions under force

A simple model for the transition of a molecule from a state A to a state B is the two state model.



For biomolecules, the two states can represent either the folded state N and the unfolded state U, or the bound and unbound state between two binding partners (e.g. in the coiled coil). The two states are separated by a transition state T (Figure 11 A). The potential width between the states is Δx . The rate constants for the reversible transitions are k_{AB} and k_{BA} , which show an exponential dependence on the height of the respective energy barrier ΔG [78].

$$k_{AB} = \nu_1 \cdot e^{\frac{-\Delta G_1}{k_B T}} \quad (11)$$

$$k_{BA} = \nu_2 \cdot e^{\frac{-\Delta G_2}{k_B T}} \quad (12)$$

According to the theory of Kramers [79], ν_1 and ν_2 are the attempt frequencies, k_B is the Boltzmann constant and T is the absolute Temperature. The equilibrium constant K can be calculated according to the law of mass action:

$$K = \frac{k_{AB}}{k_{BA}} = \frac{[B]}{[A]} \quad (13)$$

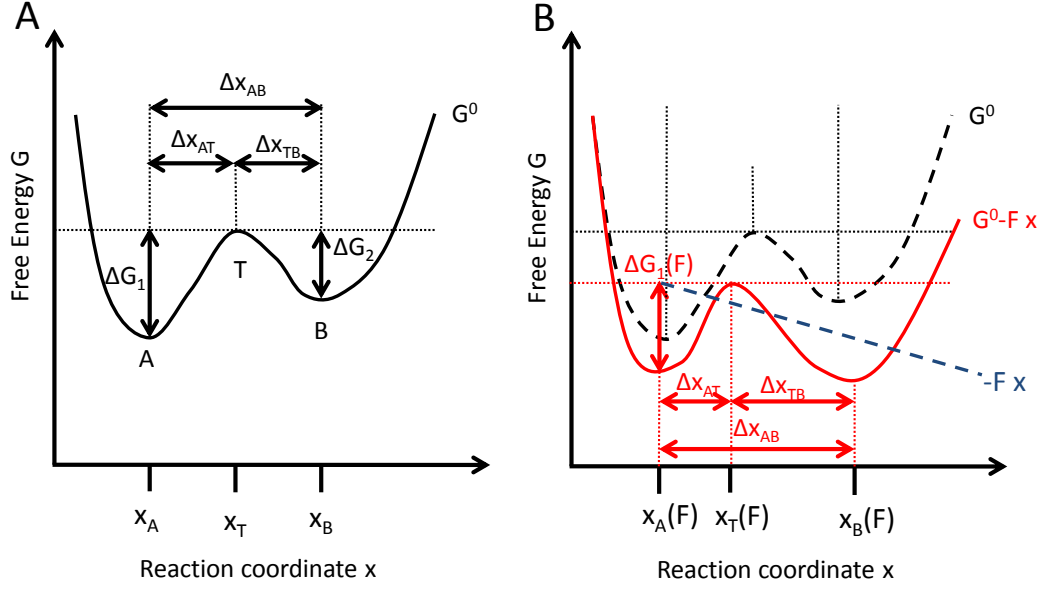


Figure 11: The free energy landscape of a two state system is affected by an applied force. A: Potential energy landscape of a two state system in the absence of force. A and B are the two states of a molecule, which are separated by the transition state T. ΔG_1 and ΔG_2 are the differences in the free energy between A and B and the transition state, respectively. The potential width is Δx . B: An externally applied force ($-Fx$) changes the free energy landscape (dashed curve) by lowering the energy of the transition state and state B relative to A (red curve). This increases the probability that a molecule resides in the state B. The Free energy minima and maxima may shift along the reaction coordinate according to the local structure of the free energy landscape.

Equation 13 can be used to calculate the free energy difference between the states A and B:

$$\Delta G_1 - \Delta G_2 = -k_B T \cdot \ln K \quad (14)$$

The energy landscape changes, if an external force is applied (Figure 11 B). Bell [80] first described these effects of an external force on a system and his model was further modified by Evans and Ritchie [81]. The Bell-Evans model is broadly used to analyze force measurements. It describes the tilting of the free energy landscape by an external force, which in effect decreases the free energy of the transition state. For deep potentials it can be assumed that the potential width Δx_{AT} is independent of the applied force. Thus, the rate constant for the A→B transition becomes:

$$k_{AB}(F) = v_1 \cdot e^{\frac{-\Delta G_1 - (F \cdot \Delta x_{AT})}{k_B T}} \quad (15)$$

Guthold et al. [82] distinguished two different reactions of a two state system under applied force. The system is considered to be at equilibrium, if the transition occurs on the timescale of the experiment, whereas non-equilibrium transitions occur if the time scale of the experiment is faster than the transitions between the states. In the latter case, the rupture force measured with the AFM depends on the loading rate \dot{F} [N/s], which is defined as

$$\dot{F} = \frac{dF}{dt} \quad (16)$$

Considering the energy landscape at ambient temperature, the system fluctuates around the bound state A, which results in a distribution of binding forces. Using the Bell-Evans model the most probable rupture force F_R can be described using the following equation, which also considers the influence of the loading rate

$$F_R(\dot{F}) = \frac{k_B T}{\Delta x_{AT}} \cdot \ln \frac{\dot{F} \cdot \Delta x_{AT}}{k_B T \cdot k_{off}} \quad (17)$$

This equation highlights that the rupture force is determined by both, the dissociation rate at zero force (equilibrium) $k_{off} = k_{AB}(0)$ [s^{-1}] and the potential width. These parameters can be obtained when plotting F_R against $\ln \dot{F}$. If the Bell-Evans model is valid, the resulting graph is linear, where k_{off} is the intercept with the x-axis at zero force and Δx_{AT} can be determined from the slope.

2.5.2 Working principle of the AFM

To be able to describe the free energy landscape of the coiled coils (i.e. to determine k_{off} and Δx_{AT}), the rupture force and the loading rate need to be determined in a single molecule force spectroscopy experiment. The following section describes how these parameters are obtained from AFM measurements.

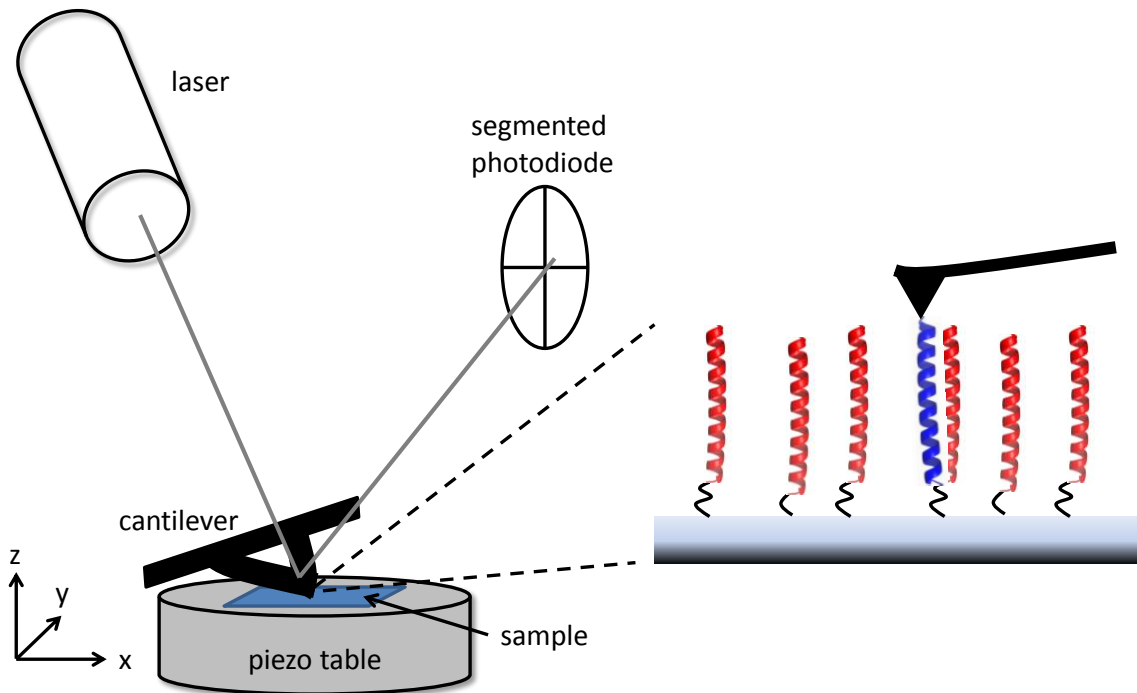


Figure 12: Schematic setup of an Atomic Force Microscope (AFM). The peptide functionalized cantilever is in contact with the peptide functionalized surface (sample), which is mounted on a piezo table. The deflection of the laser beam focused on the back of the cantilever is measured using a segmented photodiode.

To characterize a biomolecular interaction, one biomolecule is bound to the cantilever via a flexible polymer spacer and its binding partner is immobilized on a surface the same way (Figure 12). First, the cantilever is brought into contact with the surface, allowing the molecular interaction to form. Then, the cantilever is retracted from the surface, thereby mechanically loading the molecule. The applied force pulls the cantilever towards the surface. The resulting deflection, which is proportional to the applied force, is detected with a laser focused on the back of the cantilever and a segmented photodiode, which records the position of the laser beam (Figure 12). The measured deflection of the cantilever is converted to a force (F) using Hooke's law:

$$F = -k_s \cdot D \quad (18)$$

where k_s is the spring constant and D is the deflection of the cantilever [83].

The steps to acquire a single-molecule force curve are illustrated in more detail in Figure 13. When the cantilever approaches the surface (1) it bends backwards upon contact (2). When withdrawing the tip from the surface, the molecular interactions stabilizing the coiled coil exert a force on the tip so that it deflects towards the surface (3). The coiled coil peptides start unfolding and dissociate as a result of the applied force. The adhesive force right before the jump-off-contact corresponds to the force needed to disrupt the coiled coil, i.e. its rupture force (4) [83]. The slope of the force curve directly before the rupture events is extracted to calculate the loading rate by multiplying the slope [pN/nm] with the pulling velocity [nm/s]. This approach and retract cycle is then repeated until a sufficient number of force curves have been collected. Statistically, only 5-20% of the measured force curves originate from a single interaction that formed between the tip and the surface ("single pulls"). In many cases, no interaction has formed at all and in some rare cases also multiple interactions may have formed. For data analysis, only force curves representing a specific single molecular interaction are considered. To unambiguously identify the corresponding force curves, each individual curve is fitted with the Wormlike Chain model (WLC) [84], [85]. This model describes the stretching of the polymeric spacers that are used for immobilizing the peptides to the tip and the surface. For a specific interaction, both spacers should be stretched together with the coiled coil and this distance information can be used to discriminate specific from non-specific interactions.

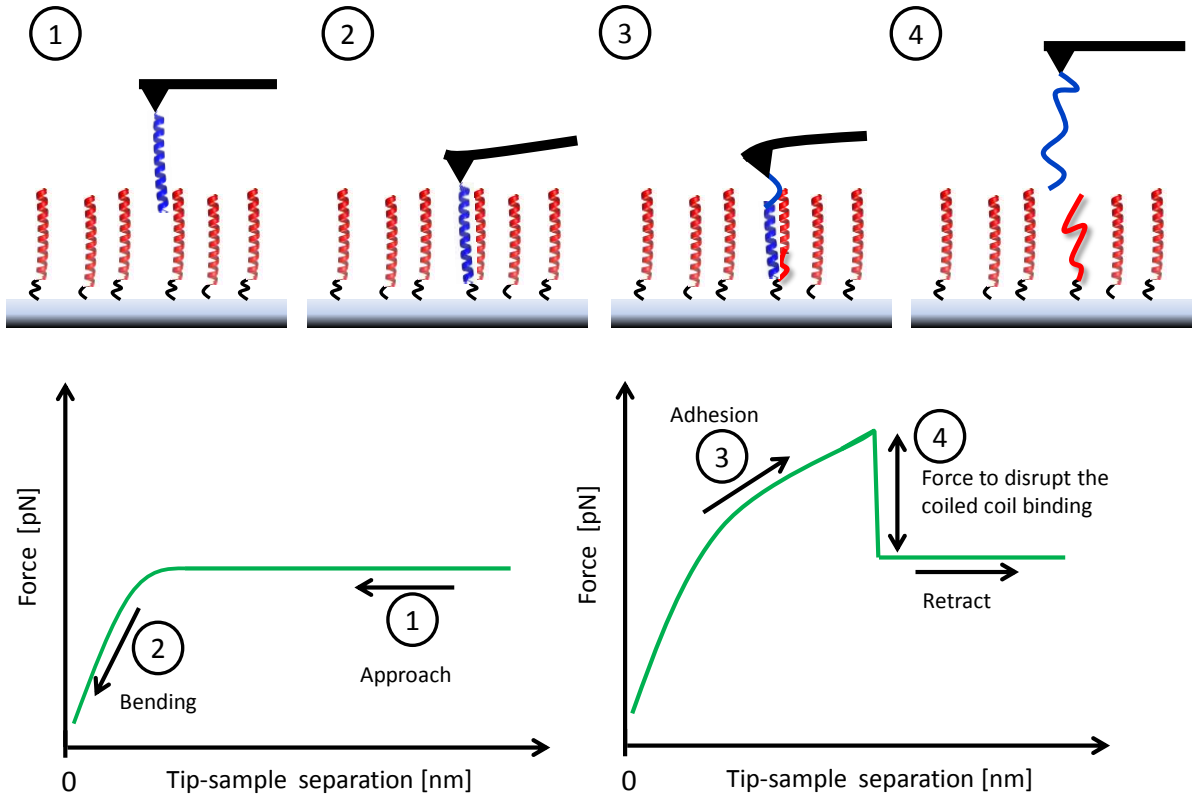


Figure 13: Steps of a single molecule force measurement. 1. The functionalized cantilever approaches to the surface. 2. Upon contact with the surface, the cantilever bends away from the surface. 3. During retraction, an adhesive force builds up, resulting from the coiled coil interaction. 4. The coiled coil ruptures, which results in a sudden decrease of the force back to the baseline value. The difference in force between the last adhesion point and the baseline is the rupture force.

Furthermore, the model describes the elasticity of the polymer spacer, which can be used to discriminate single pulls from multiple interactions. In more detail, the WLC model yields the contour length l_c (length of the fully extended polymer) as well as the persistence length l_p , which is a measure of the polymer elasticity. The WLC model describes polymers as thin homogenous rods with linear bending elasticity. The polymer is composed of N segments with the length l ($l_c = N \cdot l$) [86]. Using the WLC, the force acting on a polymer can be calculated as

$$F(x) = \frac{k_B T}{l_p} \left(\frac{1}{4 \left[1 - \frac{x}{L} \right]^2} - \frac{1}{4} + \frac{x}{L} \right) \quad (19)$$

where x is the extension of the polymer, k_B is the Boltzmann's constant and T is the absolute temperature [87].

3 Materials and experimental procedures

3.1 Chemicals

All chemicals had per analysis purity and were purchased from Roth (Karlsruhe, Germany) or Sigma Aldrich (Steinheim, Germany). The Piperazine-1,4-bis(propanesulfonic acid) (PIPPS) buffer was purchased from Merck Millipore (Darmstadt, Germany). All solutions were prepared with distilled water (Ultra clearTM Integra UV UF, Siemens, Germany) and filtered (pore size 0.2 μm). Additionally, solutions were degassed for thermal unfolding measurements in CD. For amino acid analysis, the standard solution was purchased from SYKAM GmbH (Eresing, Germany). The composition of the buffers used for the different measurements is summarized in Table 1.

Table 1: Composition of the buffers used in this work. All Buffer components had per analysis grade and were prepared with distilled water and filtered. The pH was adjusted with 1 M NaOH.

Name	Molarity (mM)	Components	pH	Technique
PIPPS	5	PIPPS	8.1	CD spectroscopy, Analytical Ultracentrifugation
	10			Raman spectroscopy
NaP	10	$\text{Na}_2\text{HPO}_4/\text{NaH}_2\text{PO}_4$	8.1	CD spectroscopy, Raman spectroscopy
1xPBS	10	Na_2HPO_4	7.4	AFM force spectroscopy
	2	KH_2PO_4		
	137	NaCl		
	2.7	KCl		
Sodium borate buffer	50	$\text{H}_3\text{BO}_3/\text{Na}_2\text{B}_4\text{O}_7$	8.5	Surface functionalization
Coupling buffer	50	Na_2HPO_4	7.2	Surface functionalization
	50	NaCl		
	10	EDTA		
Sample dilution buffer (SYKAM, (Germany))	40	trisodium citrate dehydrate	2.2	Amino acid analysis
	30	citric acid		
	116	(12 ml) Thiodiglycol		
	21	Phenol		

The pH of the measurement buffers for Raman and CD spectroscopy was set to 8.1 because His is mostly deprotonated at this pH and able to bind metal ions.

3.2 Peptides

N-terminally acetylated and C-terminally amidated peptides were purchased from Centic Biotech (Heidelberg, Germany) with a purity higher than 95% (determined with HPLC). The lyophilized peptides were dissolved in distilled water to a concentration of 5 mg/ml (~1.5 mM) and sonicated for 1 min to dissolve larger peptide aggregates which may have formed during the lyophilization process. The peptide stock solutions were stored at 4°C for at least one day before use to allow full folding of the peptides. HA4 and HB4 as well as A4 and B4 were mixed in a 1:1 ratio to yield the corresponding coiled coils HA4HB4 and A4B4.

3.3 FTIR spectroscopy

In this work, the FTIR measurements were performed with a Vertex 70 FTIR spectrometer (Bruker, USA) equipped with a HeNe-Laser (633 nm, power: 1 mW) in ATR-mode. Peptide solutions with a total concentration of 5 mg/ml (~1.5 mM) in distilled water were measured at RT on a Si-crystal, which is optically coupled to a ZnSe-crystal. To study the effect of metal ions, 2 mM NiCl₂, CuCl₂ (Alfa Aesar, USA) or ZnCl₂ were added so that the His-metal ion ratio was 2:1. The OPUS software package 7.0 (Bruker, USA) was used to record and evaluate the spectra. First, the reference spectrum of water was measured and directly subtracted from the sample spectrum. The number of accumulations for one spectrum was 32. The spectra were baseline corrected with the rubberband method (linear, 1 iteration) and smoothed (5 points).

3.4 Raman spectroscopy

Peptides were investigated by Raman micro-spectroscopy in the solid state as films prepared on glass slides. The total concentration of the peptides was 1.5 mM. 2 mM ZnCl₂ was added so that the His-metal ion ratio was 2:1. Dried films were washed with 10 mM PIPPS buffer or NaP buffer and measured. A Confocal Raman Microscope (alpha300, WITec, Germany) equipped with a piezo scanner (P-500, Physik Instrumente, Karlsruhe, Germany) and a 20x objective (Nikon, NA 0.4) was used. As laser source a linearly polarized laser ($\lambda = 532$ nm, Oxxius, Lannion, France) was focused on the sample with a polarization of 0° and no analyzer in the light path. The Raman scattered light was detected by a thermoelectrically cooled CCD detector (DU401A-BV, Andor, Belfast, North Ireland) with an integration time of 1 s and 30 accumulations. Spectra from at least three different spots of the sample were

collected and averaged. The ScanCtrlSpectroscopyPlus (Version 1.38, WITec, Germany) and the Project FOUR software (Version 4.1 WITec, Germany) were used to measure and average the spectra. OPUS was used for baseline correction (rubberband method, linear, 1 pt), normalized (0,100) and smoothing (5 pt).

3.5 CD spectroscopy

CD spectra were recorded to investigate the secondary structure and the thermal stability of the peptides in the absence and presence of Ni²⁺. The peptide stock solutions were diluted in PIPPS buffer or NaP buffer (pH 8.1) to a final concentration of 50 μM. For measuring the CD spectrum a quartz glass cuvette (Hellma, Germany) with a path length 1 mm was used. The exact concentrations of the peptides were determined by amino acid analysis (chapter 2.3). For baseline correction, the buffer spectra were recorded using identical parameters and subtracted from the peptide spectra. The mean residue molar ellipticity θ_R [deg cm² dmol⁻¹] was calculated according to equation 1 (chapter 2.2).

3.5.1 Single spectra

The single spectra were recorded with a Jasco Spectropolarimeter J-715 (Tokio, Japan). If not stated otherwise, all spectra were recorded from 200 nm to 250 nm, with a step resolution of 1 nm and a bandwidth of 1 nm at a temperature of 20°C. The scanning speed was 50 nm/min with an integration time of 2 s. To improve the signal-to-noise ratio, 10 scans were accumulated. NiCl₂ was added in different ratios (5:1; 3:1; 2:1; 1:1 and 1:2 His:Ni²⁺) to the histidine residues of the peptides.

3.5.2 Thermal unfolding curves

Thermal unfolding of the peptides was performed with the Jasco Spectropolarimeter J-715 (Tokio, Japan) equipped with a water bath (HAAKE DC3, Germany) and a custom built temperature control system (Klaus Bienert, MPIKG, Germany). Temperature ramps were set and monitored with the Multi Control Program (Version 1.6.1, Klaus Bienert, MPIKG, Germany). Before and after the heating process, complete spectra of the peptides were recorded as described to get information about the reversibility of peptide unfolding. The unfolding process was investigated using the Interval Scan mode at 222 nm (interval: 2 min, 1 accumulation). The wavelength of 222 nm was used, since samples with high α -helical content have a minimum at this wavelength and the signal to noise ratio is higher at 222 nm compared to 208 nm [68]. Since some of the peptides were so stable that it was not possible to determine their melting temperature in PIPPS buffer, the thermal unfolding was performed in

presence of 2 M GdmCl. To study the stability change of the coiled coils in the presence metal ions, Ni²⁺ was added in a 2:1 His:Ni²⁺ ratio. All measurements were performed in triplicate as not stated otherwise.

To validate the accuracy of the home-built temperature control system, the measurements for HA4HB4 were repeated with a Jasco Spectropolarimeter J-815-150S (Tokio, Japan) equipped with a Peltier element (JASCO PTC 423S/15) (University of Potsdam, Physical Biochemistry). The temperature ramp was set from 4 to 90°C with a heating rate of 1°C/ min. Before and after thermal unfolding single spectra were recorded at 20°C (5 accumulations, 4 s integration time). The temperature-wavelength scan measurements were performed at 222 nm in 1°C steps after at least 5 s with no temperature change bigger than 0.1°C. Additionally, single spectra with the same settings as described above were recorded at 4, 10, 25, 40, 55, 70 and 85°C.

3.6 Amino Acid Analysis

To calculate a correct mean residue molar ellipticity for the CD measurements, the concentration of the peptides was determined using Amino Acid Analysis. For acid hydrolysis, 10 µl of the peptide stock solutions and 10 µl 6 N HCl were mixed and hydrolyzed two times for 15 min at 150 °C under anoxic conditions with the Microwave CEM Discover Protein Hydrolysis (CEM, USA). The hydrolyzed samples were washed with 50 µl water and dried two times. The amino acid standard was measured at the beginning of the measurements and again after the measurements of the samples to get the correct retention times of the amino acids. Dried standards were resolved in 200 µl and the samples in 150 µl Sample Dilution Buffer (SYKAM, Germany). Then 100 µl of the samples were analyzed with the SYKAM S433 amino acid analyzer. The Chromatograms were obtained and evaluated using the program Chromstar 7 (SCPA, Germany).

3.7 Analytical Ultracentrifugation (AUC)

The oligomerization state of the individual peptides (1mg/ml) in 5 mM PIPPS (pH 8.1) was investigated with analytical ultracentrifugation in the sedimentation velocity mode. The sedimentation experiments have been performed on an Optima XLI centrifuge (Beckman Coulter, Palo Alto CA) using titanium 12 mm double sector center pieces (Nanolytics, Potsdam, Germany) and Raileigh interference optics at 25°C and 60000 rpm. The sedimentation coefficient distributions have been evaluated with the evaluation software SEDFIT (version 13.0b beta P. Schuck 2012) [88].

3.8 Surface functionalization for AFM force spectroscopy

For single molecule force spectroscopy (SMFS) the cantilever tip as well as the surface need to be functionalized with the biomolecules of interest. In this work, one coiled coil peptide was coupled to the surface and the other coiled coil peptide was coupled to the tip using the protocol from Zimmermann et al. [89] (Figure 14). First, the pre-cleaned surface and tip were modified with monoalkoxy amino silane. In the second step a bifunctional, linear 10 kDa poly-ethylene glycol (PEG) spacer carrying a maleimide group and a N-hydroxy succinimide ester (NHS) [NHS-PEG-maleimide] was covalently coupled to the amino functionalized silane [89]. The maleimide group of the PEG linker is coupled to the TCEP-reduced thiol group of the Cys containing peptide by Michael addition.

The peptides stock solutions were prepared as described in chapter 3.2, but dissolved in coupling buffer (pH 7.2). The 10 kDa NHS-PEG-maleimide was synthesized by Rapp Polymere (Tübingen, Germany).

3.8.1 Preparation of cantilevers

First, the cantilevers (MLCT, Bruker, USA) were placed into a glass petri dish and cleaned in an UV/Ozone Pro cleaner (BioForce Nanoscience, USA) for 20 min. For silanization, the cantilevers were submerged with 3-aminopropyl dimethyl ethoxysilane (abcr, Karlsruhe, Germany) for 10 min at RT. Afterwards, the cantilevers were washed with isopropanol and distilled water and dried under N₂ flow. The cantilevers were cured for 30 min at 80°C and incubated for 1 h in a humidity chamber with 30 µl of 50 mM of NHS-PEG-maleimide solved in sodium borate buffer (pH 8.5). Then, the cantilevers were washed intensively with distilled water, dried under N₂ flow and incubated for 1 h with 25 µl of 0.75 mM of peptide in the humidity chamber at 4°C. The functionalized cantilevers were washed intensively in PBS (pH 7.4) to remove unbound peptides.

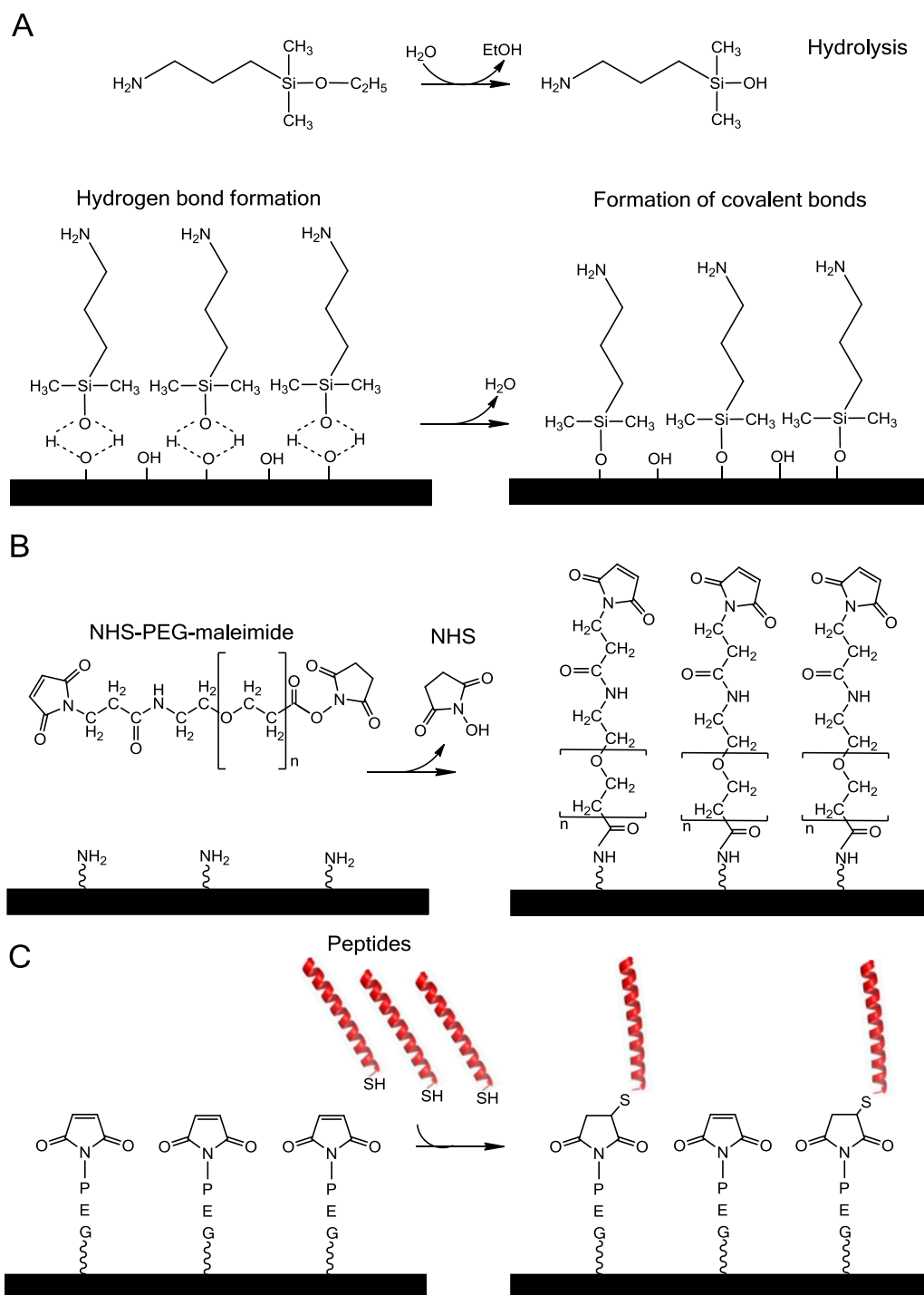


Figure 14: Functionalization of surface and cantilever for AFM. A: Cleaned surfaces or cantilevers are incubated with monoalkoxy amino silanes and baked to remove water and form covalent bonds. B: Coupling of a heterobifunctional NHS-PEG-maleimide spacer to the surface. C: TCEP reduced Cys-peptides are coupled through the reaction of the reduced thiol group with the maleimide.

3.8.2 Preparation of glass slides

Aminosilanized glass slides (Schott Nexterion, Germany) were washed in a quadriperm dish with borate buffer for 1 h and dried with N₂. A sandwich of two glass slides was incubated with 60 µl of NHS-PEG-maleimide or 1 h in a humidity chamber. After the removal of unbound NHS-PEG-maleimide with distilled water and drying under N₂ flow, the peptide was coupled to the PEG. For this 30 µl peptide solution (0.75 mM) was incubated on the glass slides in a humidity chamber for 1 h at 4°C. After incubation, most of the solution was removed carefully and the glass slides were washed twice for 5 min with PBS (pH 7.4) while gently shaking.

3.8.3 Measurement conditions

The force measurements were performed with a ForceRobot 300 (JPK instruments, Germany). To avoid evaporation effects the Small Cell (JPK instruments, Germany), which is a closed measurement system, was used. Measurements were carried out in PBS (pH 7.4) at 25°C with the following parameters: IGain 50 Hz, PGain 0.0048, relative setpoint 0.08 nN, z-length 0.4 µm. The pulling speed was varied (50, 200, 400, 1000, 2500, 5000 nm/s) to get information about the loading rate dependency of the system. To investigate the effect of metal ion coordination on the coiled coil stability, 2 mM NiCl₂ was added. The tip was calibrated after the measurements to determine the sensitivity and the spring constant. The data were analyzed using the JKPSPM Data processing software (Version 5.0.68, JPK instruments, Germany). “Single-pull” force curves were baseline corrected, the adhesion point was determined, the x-offset was adjusted and the curves were fitted with the implemented Wormlike-Chain model. The analysis program yields the rupture force as well as the loading rate of every force curve. The most probable rupture force and the most probable loading rate were determined by fitting a Gaussian distribution curve to the corresponding histogram. The resulting most probable rupture forces were plotted against the corresponding most probable loading rates and fitted with the Bell-Evans model (equation 17) to determine k_{off} and Δx_{AT} .

4 Results

4.1 Peptide design

The primary aim of this work was to modify an existing, well-characterized coiled coil from the literature with His-metal chelation sites to create tunable, mechano-responsive material building blocks. To reach this aim, the four heptad coiled coil sequences A4 and B4 published by Thomas et al. [53] were used. While the peptide A4 is acidic, containing Glu in the *e* and *g* positions, the B4 peptide is basic containing Lys at these positions (Table 2). It was shown, that these peptides reliably form stable, parallel heterodimeric α -helical coiled coils. Currently, the group Mechano(bio)chemistry at the MPIKG aims at characterizing the mechanical stability of this coiled coil in the shear geometry (Figure 3).

It was challenging to choose the positions for introducing the His residues into the α -helices. They had to be positioned in strict accordance to the stability rules of coiled coils, in order to maintain the α -helical structure of the peptides. Moreover, it is known from other bioengineered His-metal coordination sites, that two coordinating ligands with a three amino acid spacing (HXXXH) are enough to stabilize or crosslink α -helices [72], [90], [91]. The two His residues were inserted at the first heptad repeat to yield HA4 and at the fourth heptad repeat to yield HB4 at the register positions *b* and *f* instead of Ala and Gln (Table 2). Thus, both requirements are fulfilled: the His residues are solvent-exposed and should not interfere with the hydrophobic interactions stabilizing the core and they have a three-amino-acid spacing favoring metal coordination.

Table 2: Sequences of the peptides used in this work. The peptides are N-terminal acetylated and C-terminal amidated. The α -helix starts with the register position *g*. A Cys was added to the N-terminus of HA4 (CHA4) and the C-terminus of HB4 (CHB4) to enable the binding of the peptides to surfaces in order to perform single molecule force spectroscopy.

Full Name	Abbreviation	Sequence (Register starts with <i>g</i>) gabcdef gabcdef gabcdef gabcdef	MW (Da)
A4s-W21Q_noCys	A4	Ac-GG EIAALEQ EIAALEK ENAALEQ EIAALEQ GG-NH ₂	3325
B4-Y14Q_noCys	B4	Ac-GG KIAALKQ KIAALKQ KNAALKK KIAALKQ GG-NH ₂	3294
A4s-W21Q-H1_noCys	HA4	Ac-GG EI H ALE H EIAALEK ENAALEQ EIAALEQ GG-NH ₂	3324
B4-Y14Q-H4_noCys	HB4	Ac-GG KIAALKQ KIAALKQ KNAALKK KI H ALK H GG-NH ₂	3316
A4s-W21Q-H1	CHA4	Ac- C GG EI H ALE H EIAALEK ENAALEQ EIAALEQ GG-NH ₂	3445
B4-Y14Q-H14	CHB4	Ac-GG KIAALKQ KIAALKQ KNAALKK KI H ALK H G C -NH ₂	3437

For single molecule force spectroscopy (SMFS), a Cys was added at the N-terminal site of HA4 (CHA4) and the C-terminal site of HB4 (CHB4). The thiol group of the Cys was used to couple the peptides to the AFM cantilever or the glass surface. In this setup, the His residues should be able to stabilize the heptad repeat that is primarily experiencing the pulling force in shear geometry in the single molecule force spectroscopy experiments in the presence of metal ions. Thus, the SMFS experiments can reveal important information about the response mechanism of a coiled coil upon shearing.

Another important part of this work was to study the ability of the His residues to chelate metal ions using Raman spectroscopy. Since aromatic residues overlap with His-metal coordination peaks in Raman Spectroscopy [66], the Trp residues in the third heptad of the acidic peptides and Tyr residues in the second heptad of the basic peptides were changed to Gln to yield the His-modified peptides (HA4 and HB4) and the control peptides without His (A4 and B4).

4.2 Secondary structure of the coiled coil peptides is depending on the buffer

Before characterizing the His-modified peptides thermodynamically and mechanically, it is important to address the question whether the modified peptides are still able to form an α -helix. The sequences of the α -helical peptides published by Thomas et al. [53] were modified at three positions: two His were introduced instead of Ala and Gln in one heptad and the aromatic amino acids were changed to Gln. Since already small changes in the sequence can lead to large alterations in the secondary structure of a protein [92], it was investigated whether the His-modified peptides are still α -helical and able to form coiled coils. For that purpose, ATR-FTIR and CD spectroscopy were used.

Figure 15 shows the ATR-FTIR spectra of the control and the His containing peptides. The amide I peak of the individual peptides was centered at $1650/51\text{ cm}^{-1}$, which can be assigned to an α -helical conformation [93]. In A4B4, the amide I peak was slightly shifted to 1649 cm^{-1} . Usually the amide I band for α -helical proteins is assigned to $1655\text{-}1650\text{ cm}^{-1}$ and a peak at 1649 cm^{-1} is assigned to random coil [55], [58], [94]. However, for distorted helices and short helical segments, like the four heptad repeat α -helical peptides, a shift to lower wavenumbers is common [59]. Table 3 gives an overview about the peaks and their assignments. B4, A4B4 and the His-modified peptides all showed an additionally shoulder in the amide I region at $1674/75\text{ cm}^{-1}$. This shoulder is typically assigned to β -turns and was especially strong in B4 and HB4 [95], suggesting that these two peptides may adopt a

partially different structure. The shoulder at 1712 cm^{-1} arises from the Glu in the A peptide, but was only visible in the A4 and not in the HA4 peptide [96]. The amide II of all the peptides was at $1547/49\text{ cm}^{-1}$ and the amide III band was at 1204 cm^{-1} for all peptides. Both bands are caused by C-N stretching and N-H in plane bending of the peptide backbone and are relatively similar in the different peptides [55].

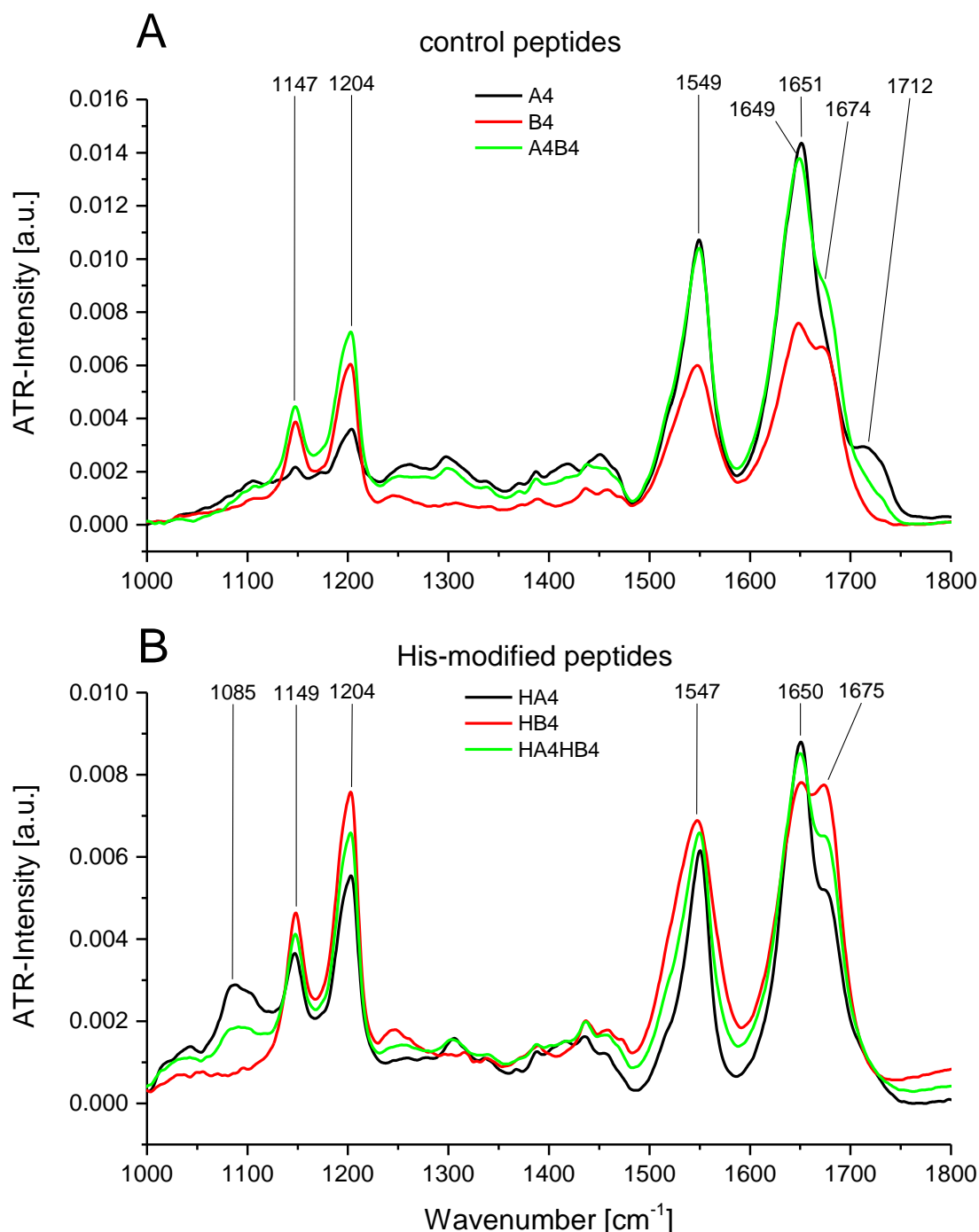


Figure 15: ATR-FTIR spectra of the single peptides and the coiled coils in water. A: Control peptides A4 (black), B4 (red) and A4B4 (green). B: His-modified peptides HA4 (black), HB4 (red) and HA4HB4 (green). The peptides were measured in the ATR-mode on a Si-crystal. The concentration was 1.5 mM, 32 scans were accumulated. The spectra were smoothed (5 point) and baseline corrected (rubberband method, linear, 1 iteration) with OPUS 7.0.

Results

Table 3: Assignments of the ATR-FTIR peaks of the peptides in Figure 15. The peaks were assigned using the references in brackets.

Peptide(s)	Peak position [cm ⁻¹]	Assignment
A4B4	1649	Amide I, α -helical structure [59], [93]
HA4, HB4, HA4HB4	1650	
A4, B4	1651	
HA4, HB4, HA4HB4	1547	Amide II (N-H bending, C-N stretching) [55]
A4, B4, A4B4	1549	
A4, B4, A4B4	1147	Amide III (N-H bending, C-N stretching) [55]
HA4, HB4, HA4HB4	1149	
A4, B4, A4B4, HA4, HB4, HA4HB4	1204	
A4	1712	C=O of Gln [96]
HA4	1085	C-N, C-C stretching mode of Gln [96]

It is well known that buffers can have an effect on the conformation of a protein and also metal coordination [97]. For that reason CD spectroscopy was performed in water, NaP buffer and PIPPS buffer. PIPPS is a non-complexing tertiary amine buffer, which could be useful to investigate the ability of the His-modified peptides to coordinate metal ions [98]. Since the coiled coils will most likely be used in phosphate containing media for final biological or biomedical applications, also NaP buffer was tested. The results for the different buffers revealed that the secondary structure of the individual peptides is influenced by the buffer composition (Figure 16). In water at pH 8.5 (Figure 16 A) all individual peptides besides HA4 show a minimum of low intensity at 224 nm and a minimum of higher intensity at 202 nm. Thus, the individual peptides are largely unfolded [53]. It has been demonstrated for several proteins, that unfolding can be initiated upon dilution, which may also happen in the case of the individual peptides tested here [99]. In contrast, the A4B4 showed an α -helical conformation with minima at 222 nm and 208 nm and $r_{222/208}=0.97$ [25], [67]. In the literature, a $r_{222/208}$ close or bigger than 1 is assigned to coiled coils [22]. Thus, A4 and B4 fold upon binding, forming a coiled coil. The spectrum of HA4HB4 had a minimum at 222 nm, but the second minimum was shifted to 206 nm in water. The $r_{222/208}$ of 0.89 indicated that there may be a part of the peptides not fully folded, so that less coiled coils were formed. Moreover, also HA4 showed the minima typical for α -helical conformation and $r_{222/208}$ was 1.00 in water.

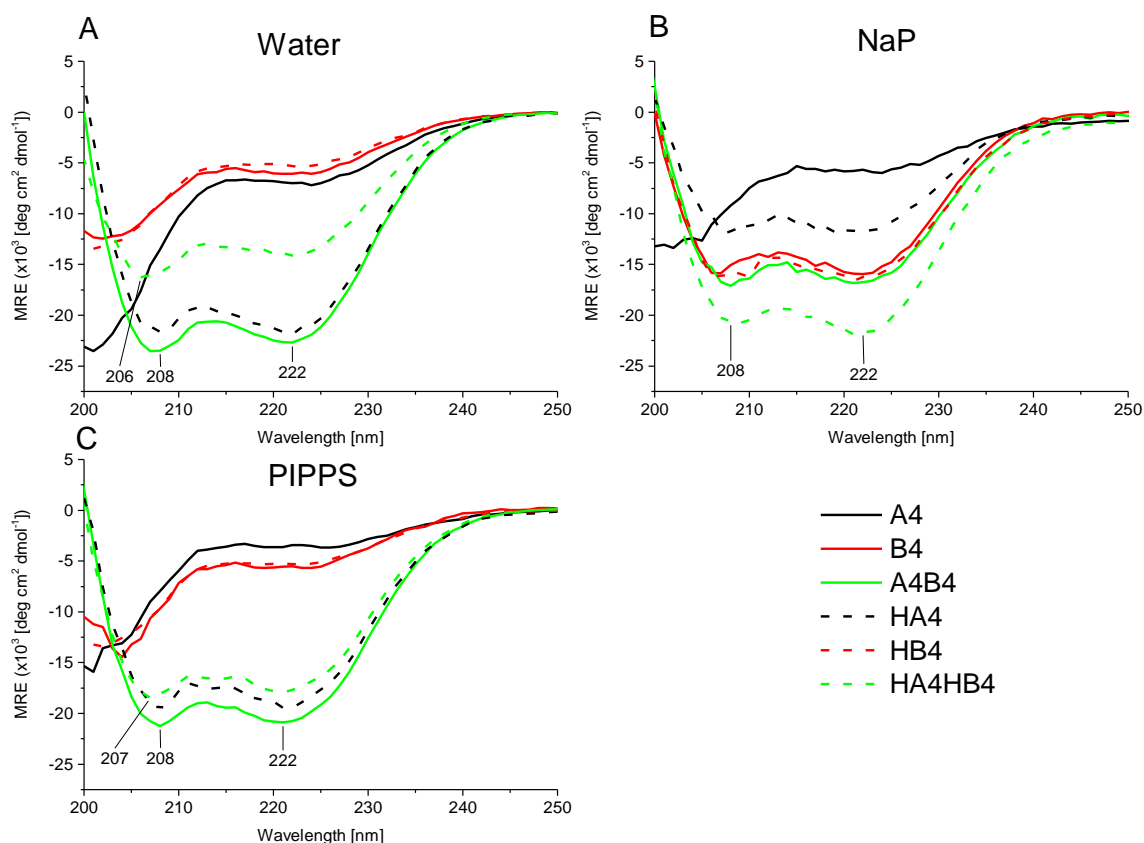


Figure 16: CD Spectra of the coiled coil peptides in water pH 8.5 (A), 10 mM NaP, pH 8.1 (B) and 5 mM PIPPS, pH 8.1 (C). Control peptides: solid line, His-modified peptides: dashed line, A4, HA4: black; B4, HB4: red; A4B4, HA4HB4: green. The spectra were taken at 20°C with a step resolution of 1 nm, a bandwidth of 1 nm, a scanning speed of 50 nm/min, an integration time of 2 s and 10 scans were accumulated. The mean residue molar ellipticity (MRE) was calculated using equation 1.

Table 4: Positions of the minima in the CD spectra and $r_{222/208}$ of the His-modified peptides and the control peptides in water, PIPPS and NaP buffer.

Peptide	water (pH 8.5)			5 mM PIPPS (pH 8.1)			10 mM NaP (pH 8.1)		
	Minima [nm]		$r_{222/208}$	Minima [nm]		$r_{222/208}$	Minima [nm]		$r_{222/208}$
HA4	208	222	1.00	208	222	0.95	208	222	0.97
HB4	202	224	0.59	202	224	0.58	208	222	0.95
HA4HB4	206	222	0.89	207	222	0.90	208	222	1.08
A4	202	224	0.53	202	224	0.46	202	224	0.62
B4	202	224	0.67	202	224	0.61	206	222	1.05
A4B4	208	222	0.97	208	222	0.97	208	222	0.98

The positions of the minima in the CD spectra and the $r_{222/208}$ of all peptides are summarized in Table 4. In PIPPS buffer (pH 8.1) the spectra of the peptides were very similar to the spectra in water, but the mean residue molar ellipticity (θ_R) of A4 decreased, while it increased for HA4HB4. The second minimum of HA4HB4 was also shifted to 207 nm. However, the conformation of the individual peptides HB4 and B4 changed if they were measured in NaP buffer (pH 8.1) (Figure 16 C). In this buffer, all spectra, except the spectrum of A4, showed an α -helix signature with minima at 222 nm and 208 nm. The second minimum of B4 was shifted to 206 nm. The θ_R -signal of HA4HB4 was more negative than in water and the $r_{222/208}$ was bigger than 1 (1.08), which is characteristic for coiled coils.

Based on these measurements, the individual peptides exhibit a predominantly α -helical conformation under high concentration conditions, measured with ATR-FTIR; however, at the lower concentrations used for CD spectroscopy, secondary structure is dependent on the buffer composition. A4B4 and HA4HB4 showed an α -helical conformation even at low concentration in water and the buffers used. Thus, although, the conformation of the individual peptides depends on the buffer, the changes made in the sequence do not seem to inhibit the formation of coiled coils.

4.3 Histidine-modified peptides are able to coordinate transition metal ions

It was shown that the His-residues introduced at the α -helical part of bovine somatotropin have the ability to coordinate transition metal ions, such as Cu^{2+} [90]. The main goal of this work was to stabilize coiled coil peptides with His-metal coordination. Raman spectroscopy is a suitable method to investigate whether there is an interaction of HA4 and HB4 with metal ions, since the distinctive peaks corresponding to the $\text{C}_4=\text{C}_5$ double bond in the histidine imidazole moiety depend on the protonation and metal coordination state of the imidazole side chain [66]. The Raman measurements were performed on thin peptide films (1.5 mM) with 2:1 His: $\text{Ni}^{2+}/\text{Cu}^{2+}/\text{Zn}^{2+}$ on glass slides. The ratio of His: Me^{2+} was kept at 2:1, because the two His residues in a heptad could coordinate the metal ion together with water molecules in a tetrahedral or square planar geometry [100]. Since future applications as tunable metal-chelating crosslinkers may be in phosphate containing systems, the measurements were performed using 10 mM NaP (pH 8.1). The pH was set to 8.1 because His is mostly deprotonated at this pH and able to bind metal ions. To compare the coordination behavior in NaP and the non-coordinating buffer PIPPS, measurements were performed in PIPPS as well.

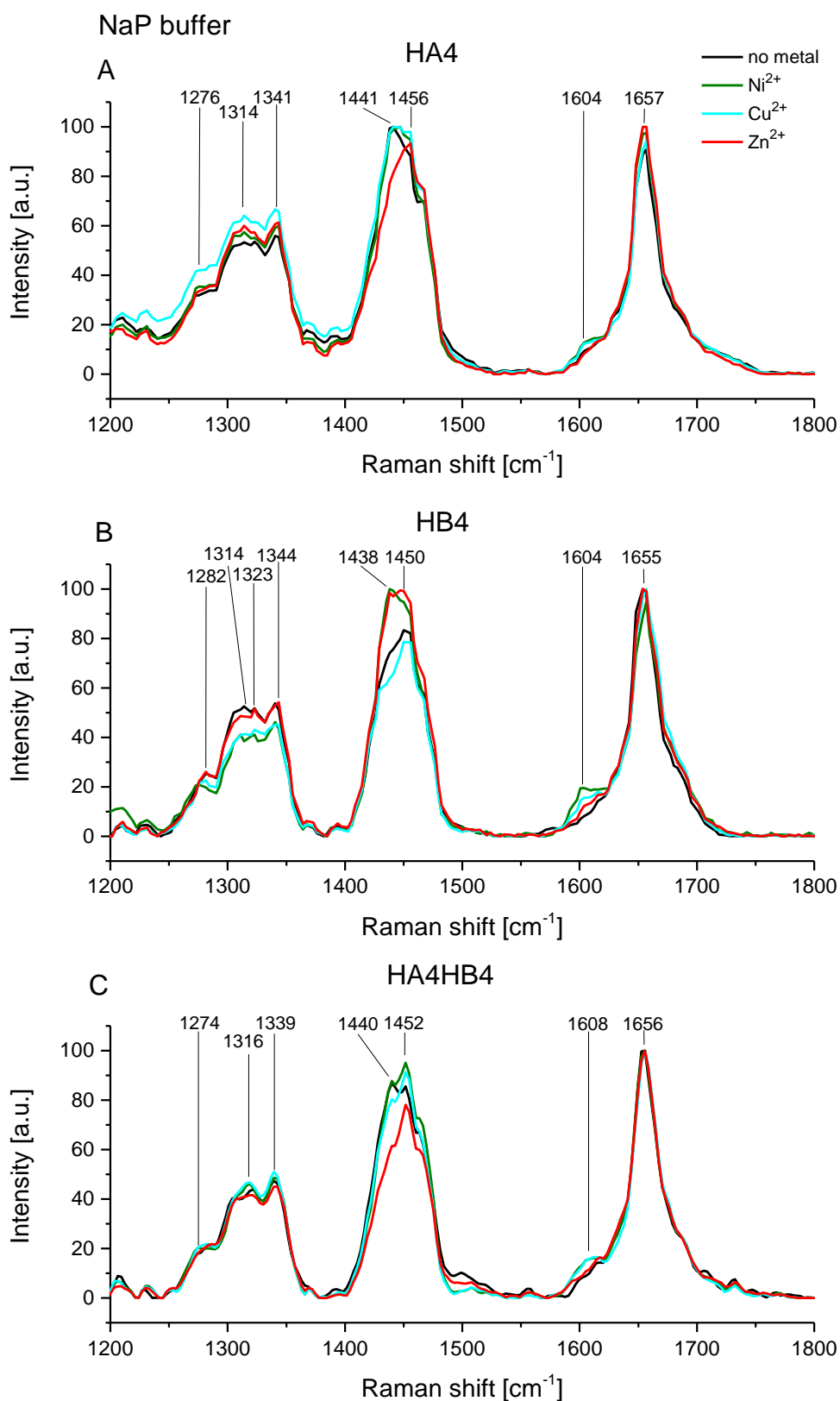


Figure 17: Raman spectra for HA4 (A) HB4 (B) and HA4HB4 (C) in 10mM NaP pH 8.1. Metal ions were added in 2:1 His:Me²⁺ ratio. No metal ions (black), Ni²⁺ (green), Cu²⁺ (blue) and Zn²⁺ (red). A 20x objective (Nikon, NA 0.4) was used with 0° polarization and no analyzer in the light path. Spectra from at least three points of the sample were measured (integration of 1 s and 30 accumulations) and averaged. The spectra are baseline corrected (rubberband method, linear, 1 pt) and smoothed (5 pt) with OPUS 7.0.

The amide I band in the Raman spectra of all peptide films with NaP buffer is at 1656 cm^{-1} or 1657 cm^{-1} , which is typically assigned to α -helical proteins (Figure 17) [62]. The relatively sharp amide I peak indicates that there is only little contribution of more extended secondary structures, such as β -strands. The amide III region is a complex Raman band with contributions from the peptide backbone, which was shown to be particularly dependent on the dihedral angles making it especially useful for assigning secondary structure [101]. The peaks around $1300\text{-}1270\text{ cm}^{-1}$ in combination with the absence of a band around 1230 cm^{-1} in the spectra are a clear indication for α -helix [101]. Thus, both, the amide I as well as the amide III, show that the coiled coil peptides are in a predominantly α -helical conformation, which is completely consistent with the results obtained with ATR-FTIR. All peaks in the Raman spectra of the His-modified peptides together with their assignments can be found in Table 5.

At basic pH, the coordination of metal ions by the N_{τ} -Atom of the imidazole side chain of His can be observed in the range of $1594\text{-}1606\text{ cm}^{-1}$ [66]. In NaP buffer the Raman spectra for HA4, HB4 (Figure 17 A, B) show a peak at 1604 cm^{-1} in presence of Ni^{2+} or Cu^{2+} which is partially overlapping with the amide I peak. For HA4HB4 the shoulder in the presence of Ni^{2+} or Cu^{2+} is shifted to 1608 cm^{-1} . With Zn^{2+} or without metal ions, there is no shoulder at these wavenumbers. In principle, His should be able to coordinate Zn ions, as reported in the carbonic anhydrase or Zn-Finger proteins [46], [102]. However, the coordination of Zn^{2+} by His may be inhibited by the phosphate of the NaP buffer, which can also interact with Zn^{2+} , forming a complex with low solubility [103], [104].

To test the coordination of metals by the His-modified peptides in a non-coordinating buffer, PIPPS (pH 8.1) was used (Figure 18). The spectra obtained in PIPPS show slightly shifted CH_2 -bending/stretching bands ($1400\text{-}1460\text{ cm}^{-1}$) and amide III peaks, but the amide I peak is always observed at 1656 cm^{-1} , consistent with an α -helical structure. More importantly, the His-modified peptides show a shoulder for metal ion coordination at 1605 cm^{-1} when mixed with Ni^{2+} , Cu^{2+} or Zn^{2+} . In contrast to the His-modified peptides, the control peptides A4, B4 and A4B4 show no metal coordination, but still maintain an α -helical structure (Figure A 3).

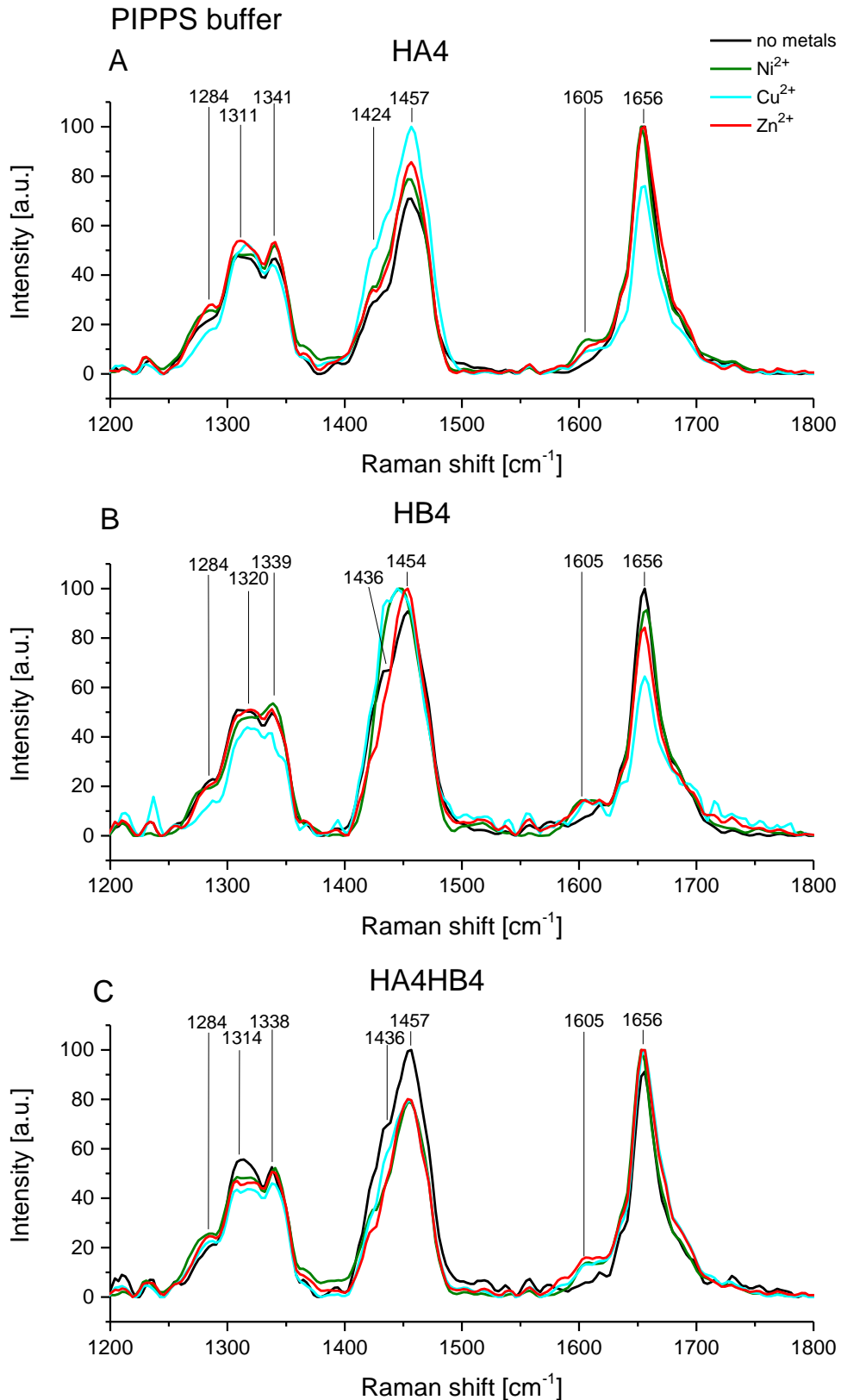


Figure 18: Raman spectra for HA4 (A) HB4 (B) and HA4HB4 (C) in 10mM PIPPS pH 8.1. Metal ions were added in 2:1 His:Me²⁺ ratio. No metal ions (black), Ni²⁺ (green), Cu²⁺ (blue) and Zn²⁺ (red). A 20x objective (Nikon, NA 0.4) was used with 0° polarization and no analyzer in the light path. Spectra from at least three points of the sample were measured (integration of 1 s and 30 accumulations) and averaged. The spectra are baseline corrected (1 pt) and smoothed (5 pt) with OPUS 7.0.

Table 5: Assignments of the Raman peaks of the peptides in NaP buffer (pH 8.1), see Figure 16. If not stated otherwise the peaks were the same in the samples without (w/o) metal ions, with Ni²⁺, Cu²⁺ and Zn²⁺. The peaks were assigned using the reference in brackets.

Peptide(s)	Peak position [cm ⁻¹]			Assignment
HA4	1657			Amide I, α -helical structure [62]
HB4	1655			
HA4HB4	1656			
HA4, HB4 (Ni ²⁺ , Cu ²⁺)	1604			Me-N _τ -coordination by Histidine [66]
HA4HB4 (Ni ²⁺ , Cu ²⁺)	1608			Not assigned, maybe Me-His coordination
HA4	1456	1441		CH ₂ - and CH ₃ -deformations [62]
HB4	1450	1438		
HA4HB4	1452	1440		
HA4	1341	1314	1276	Amide III, α -helix (N-H bending, C-N stretching) [55]
HB4	1344	1323/1314	1282	
HA4HB4	1339	1316	1274	

4.4 Effect of Ni²⁺ on the secondary structure of the Histidine-modified peptides

In Raman spectroscopy the His-modified peptides showed no change in the amide I peak for α -helical conformation. But the coordination of metal ions by His may cause a change in the secondary structure of the relatively low concentrated peptides used for the CD measurements. Since the change in the thermodynamic stability of the peptides in the presence of metal ions will be investigated, it is of special interest to determine if also the addition of metal ions to the peptides at a constant temperature would result in changes of the secondary structure. The Raman spectra in NaP showed that this buffer interferes with His-metal coordination (chapter 4.3). Therefore, the experiments were performed in 5 mM PIPPS (pH 8.1) and NiCl₂ was added to the peptides in ratios of 5:1, 3:1, 2:1, 1:1 and 1:2 His:Ni²⁺. Figure 19 shows, that Ni²⁺ has no effect on the structure of HB4 and HA4HB4 as well as the control peptides. However, HA4 (Figure 19 B), which has an α -helical signature without metal ions, showed a slight increase in θ_R at 222 nm already when Ni²⁺ was added in a ratio of 5:1 His:Ni²⁺ (Figure 19 B, red curve). Furthermore, the $r_{222/208}$ increases from 0.95 without Ni²⁺ to 1.05 with 1:2 His:Ni²⁺, indicating that HA4 could form a homomeric coiled coil in presence of metal ions. Additionally, ATR-FTIR measurements with a His:Me²⁺ ratio of 2:1

Results

showed no conformational change in the presence of Ni^{2+} , Cu^{2+} and Zn^{2+} for all peptides (Figure A 1, Figure A 2).

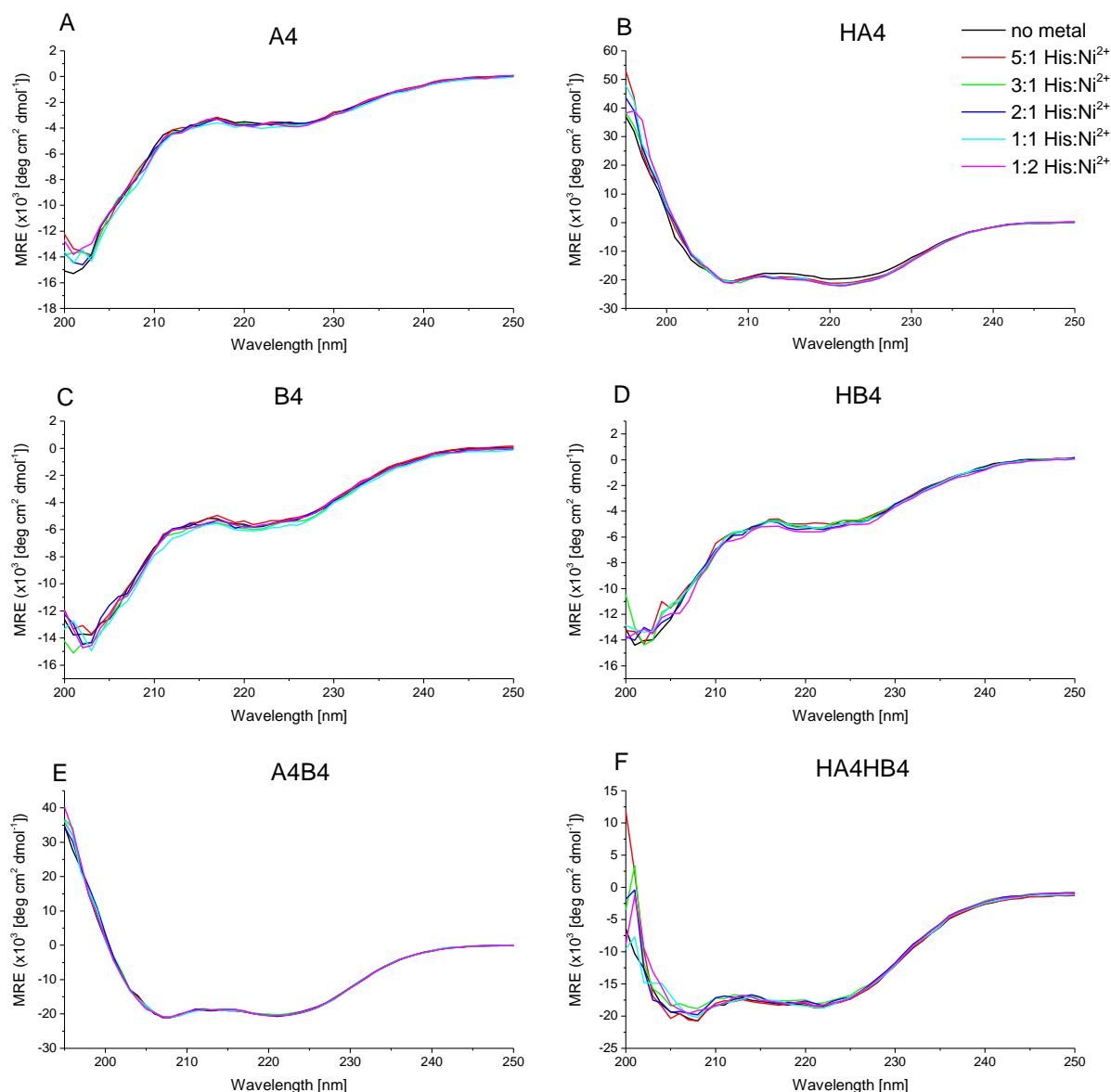


Figure 19: Influence of Ni^{2+} on the secondary structure of the individual peptides and the coiled coils studied with CD spectroscopy. The His: Ni^{2+} ratios used are: without Ni^{2+} (black), 5:1 (red), 3:1 (green), 2:1 (dark blue), 1:1 (light blue) and 1:2 (magenta). The spectra were taken at 20°C with a step resolution of 1 nm, a bandwidth of 1 nm, a scanning speed of 50 nm/min, an integration time of 2 s and 10 scans were accumulated. The mean residue molar ellipticity (MRE) was calculated using equation 1.

In summary, the His-modified peptides are able to coordinate transition metal ions, such as Ni^{2+} , Cu^{2+} and Zn^{2+} (chapter 4.3); however, with exception of HA4, changes in the secondary structure in the presence of metal ions could not be detected with CD spectroscopy. Nevertheless, there might be a change in the thermodynamic stability of the His-modified peptides.

4.5 Changes in the thermodynamic stability of coiled coil peptides due to metal ion coordination

To use coiled coils as tunable crosslinkers, it is not only important to mechanically characterize them, but also to investigate the temperature-dependent stability of their secondary structure. In this work, the thermodynamic stability of the peptides was investigated using thermal unfolding monitored by CD spectroscopy. The change in ellipticity was studied at 222 nm from 8 to 90°C with a custom built heating system (Klaus Bienert, MPIKG). Since the CD spectra in NaP and PIPPS buffer showed, that different buffers can influence the secondary structure of the individual peptides and metal binding (see Figure 16, Figure 17), the unfolding experiments were carried out in both, PIPPS buffer (pH 8.1) and NaP buffer (pH 8.1).

Figure 20 shows the thermal unfolding curves at 222 nm of the His-modified peptides and the control peptides in PIPPS buffer in absence of metal ions. For HB4, A4 and B4, which are already unfolded at 20°C (see Figure 16), the θ_R has a small intensity and shows only minimal changes upon heating. Thus, the melting temperature T_m for HB4, A4 and B4 is $< 8^\circ\text{C}$. The coiled coil peptides HA4HB4 and A4B4 as well as HA4, which have an α -helical signature in PIPPS buffer at 20°C, show a decrease in $\theta_{R,222\text{ nm}}$ of about $10,000\text{ deg cm}^2\text{ dmol}^{-1}$ if they are heated to 90°C. However, the shape of the curves was not sigmoidal and the remaining $\theta_{R,222\text{ nm}}$ was still high. Hence, it is concluded, that the coiled coil peptides and HA4 are only partially unfolded at 90°C. Fletcher et al. reported a similarly high stability for trimeric coiled coils [105]. The high stability of HA4HB4, A4B4 and HA4 is further emphasized by their CD spectra at different temperatures in Figure 21. Although these spectra are noisier since just one accumulation could be acquired in this measurement setup, they clearly indicate an α -helical signature with two minima of lower intensity. Moreover, all the peptides returned to the initial state again after cooling down to 20°C and even showed a slight increase in θ_R (Figure 22). This could be due to evaporation of buffer during the experiment, which leads to a slightly higher concentration of the peptides in the cuvette.

The stability of the peptides in PIPPS (pH 8.1) was compared with the stability in NaP buffer (Figure A 4). While HA4HB4, A4B4 as well as HA4 and A4 had a very similar unfolding curve also in NaP buffer, HB4 and B4 showed a sigmoidal unfolding curve in this buffer. The T_m of HB4 (33.9°C) and B4 (38.4°C) in NaP buffer was determined by fitting equation 5 to the curves (Figure A 5).

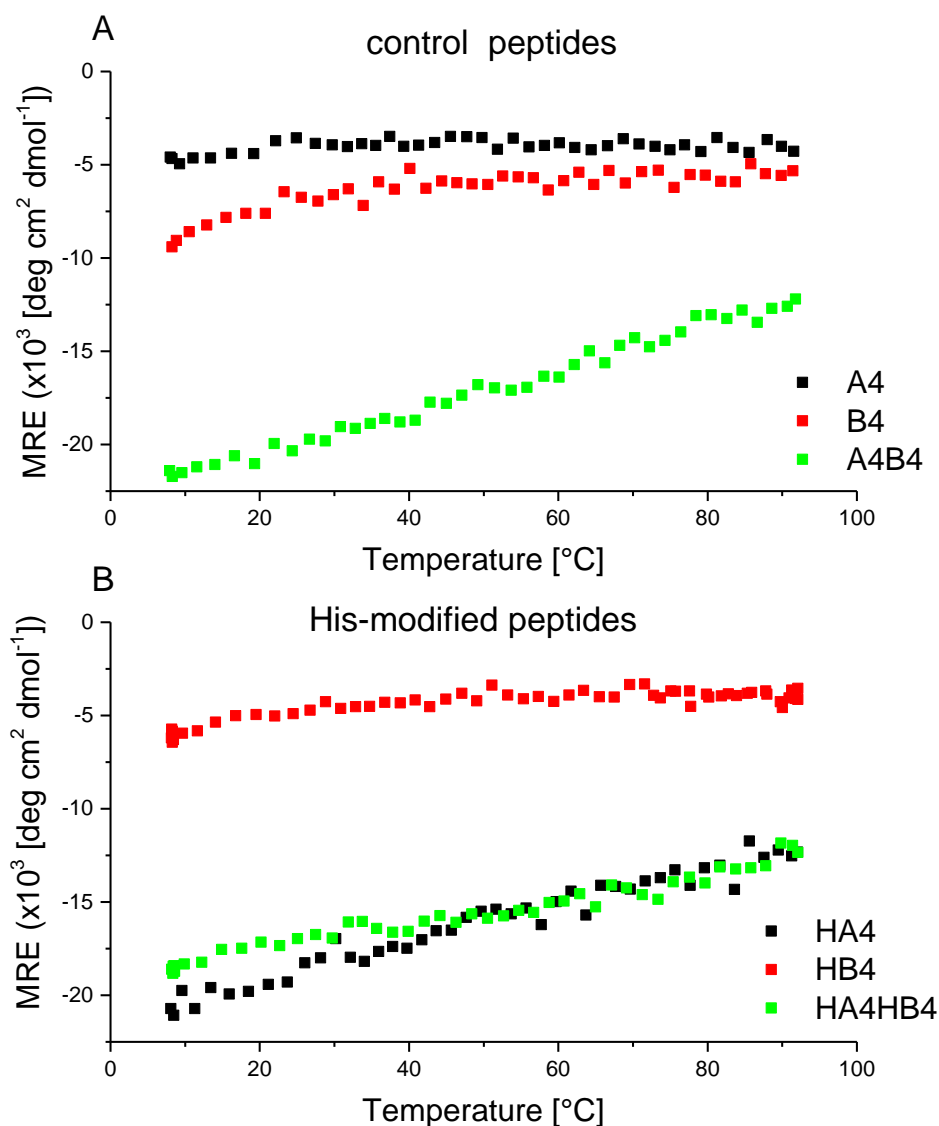


Figure 20: Thermal unfolding curves of the control peptides (A) and the His-modified peptides (B) at 222 nm from 8°C-90°C. The heating rate was 1°C/min. Measurements were performed in 5 mM PIPPS pH 8.1 in the interval scan mode (interval: 2 min, 1 accumulation, 2 s response). The mean residue molar ellipticity (MRE) was calculated using equation 1.

Since the NaP buffer is suspected to interact with the metal ions, thermal unfolding experiments with Ni^{2+} were also performed in the non-coordinating PIPPS buffer to study whether His-metal coordination has an effect on the stability of the peptides. In particular, measurements without and with Ni^{2+} in a ratio of 2:1 His: Ni^{2+} were performed. This ratio favors the coordination of one metal ion by the two His residues in one heptad of the His-modified peptides, which should be the optimal ratio for the stabilization of the α -helices. To obtain a mean melting temperature T_m , the measurements were performed in triplicate. Since the coiled coil peptides are highly stable in PIPPS buffer, 2 M GdmCl was added to the HA4HB4, HA4 and A4B4 samples. The addition of GdmCl is a standard procedure used to destabilize or denature proteins or peptides [106]. The presence of 2 M GdmCl shifts the

melting temperature of HA4HB4, HA4 and A4B4 into a temperature range that can be accessed by the experimental setup. This approach was also used by Fletcher et al. [105] to destabilize trimeric coiled coils.

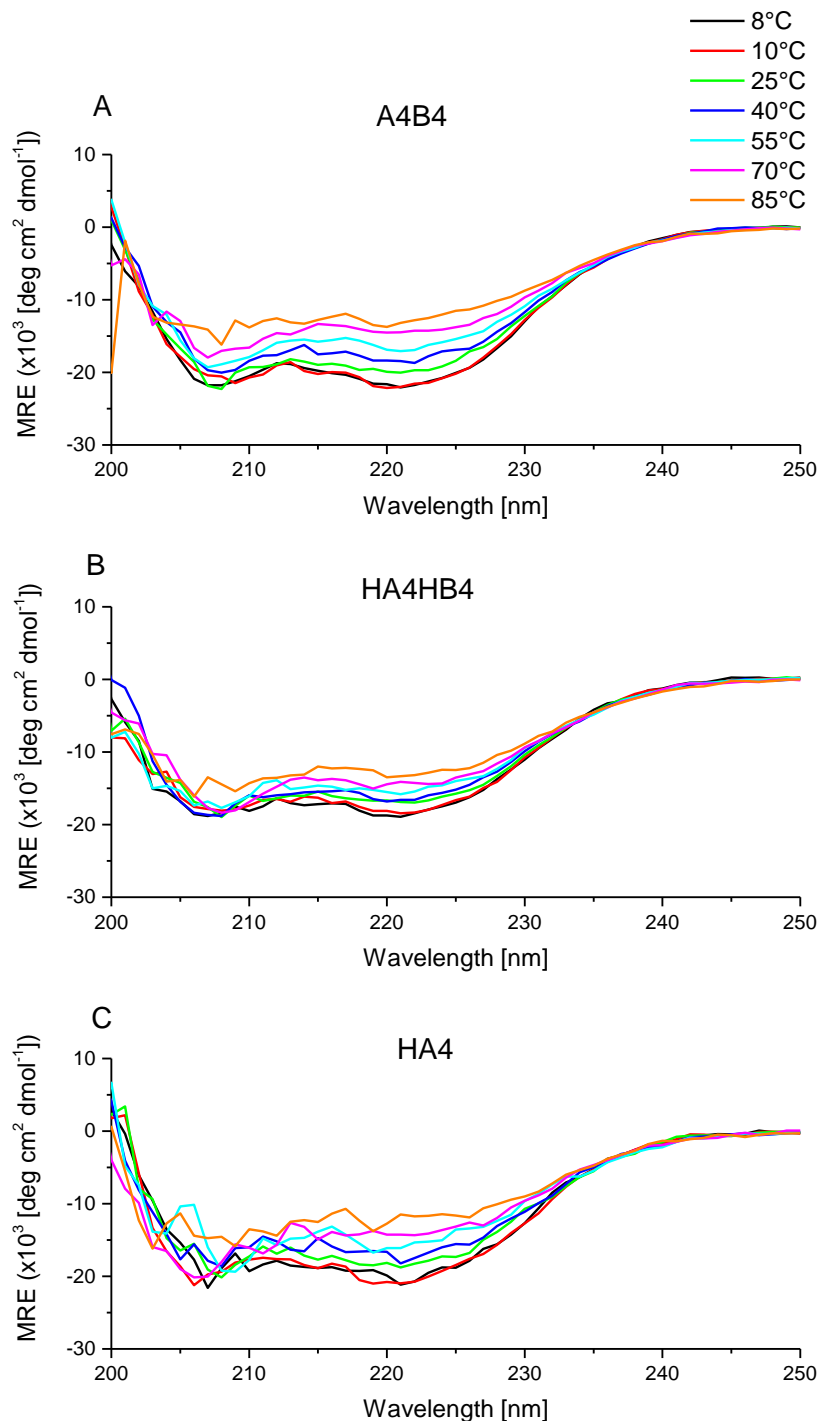


Figure 21: CD spectra of A4B4 (A), HA4HB4 (B) and HA4 (C) at different temperatures during the unfolding experiment. The spectra were taken in 5 mM PIPPS (pH 8.1) with a step resolution of 1 nm, a bandwidth of 1 nm, a scanning speed of 50 nm/min, an integration time of 2 s and 1 scans was accumulated. The mean residue molar ellipticity (MRE) was calculated using equation 1.

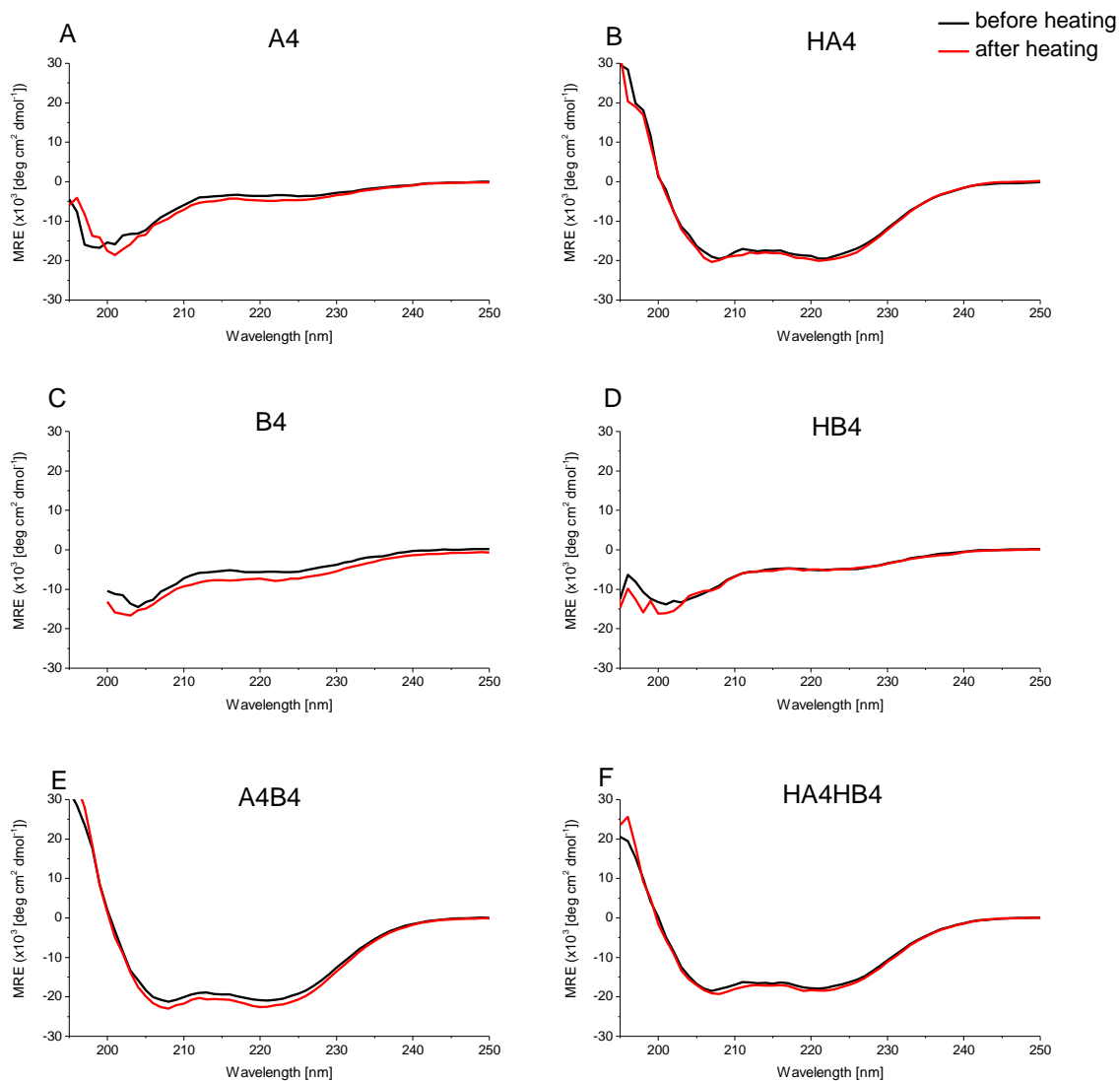


Figure 22: CD spectra for the peptides before (black) and after (red) the heating process at 20°C. The spectra were taken in 5 mM PIPPS (pH 8.1) with a step resolution of 1 nm, a bandwidth of 1 nm, a scanning speed of 50 nm/min, an integration time of 2 s and 10 scans were accumulated. The mean residue molar ellipticity (MRE) was calculated using equation 1.

The melting temperatures T_m of HA4HB4, A4B4 and HA4 in the presence and absence of Ni^{2+} were determined by nonlinear least-square fitting (chapter 2.2.2, equation 5) of the unfolding curves using the Excel Solver (MS Excel 14.0). Since the baseline before heating was not well defined, the slope m_n of this baseline was held constant at 14 deg cm²/dmol K for all the fits, to obtain comparable data. Moreover, it was assumed that the ΔC_p during the experiment was small and can be neglected, as described by Thomas et al. [53]. According to Kemmer and Keller [74], the melting temperature T_m is the kinetic parameter, which can be most reliably determined with equation 5. Thus, only T_m was used to evaluate the effect of metal ions on the stability of the peptides. A summary of all T_m values can be found in Table 6 and detailed results for all the parameters of the fits are summarized in Table A 2. The

sum of squared residuals (SSR) of the fits was still high. A reason for this could be the constrained measurement setup, which did not allow starting the measurement at lower temperatures. Hence, it was not possible to obtain a more defined baseline.

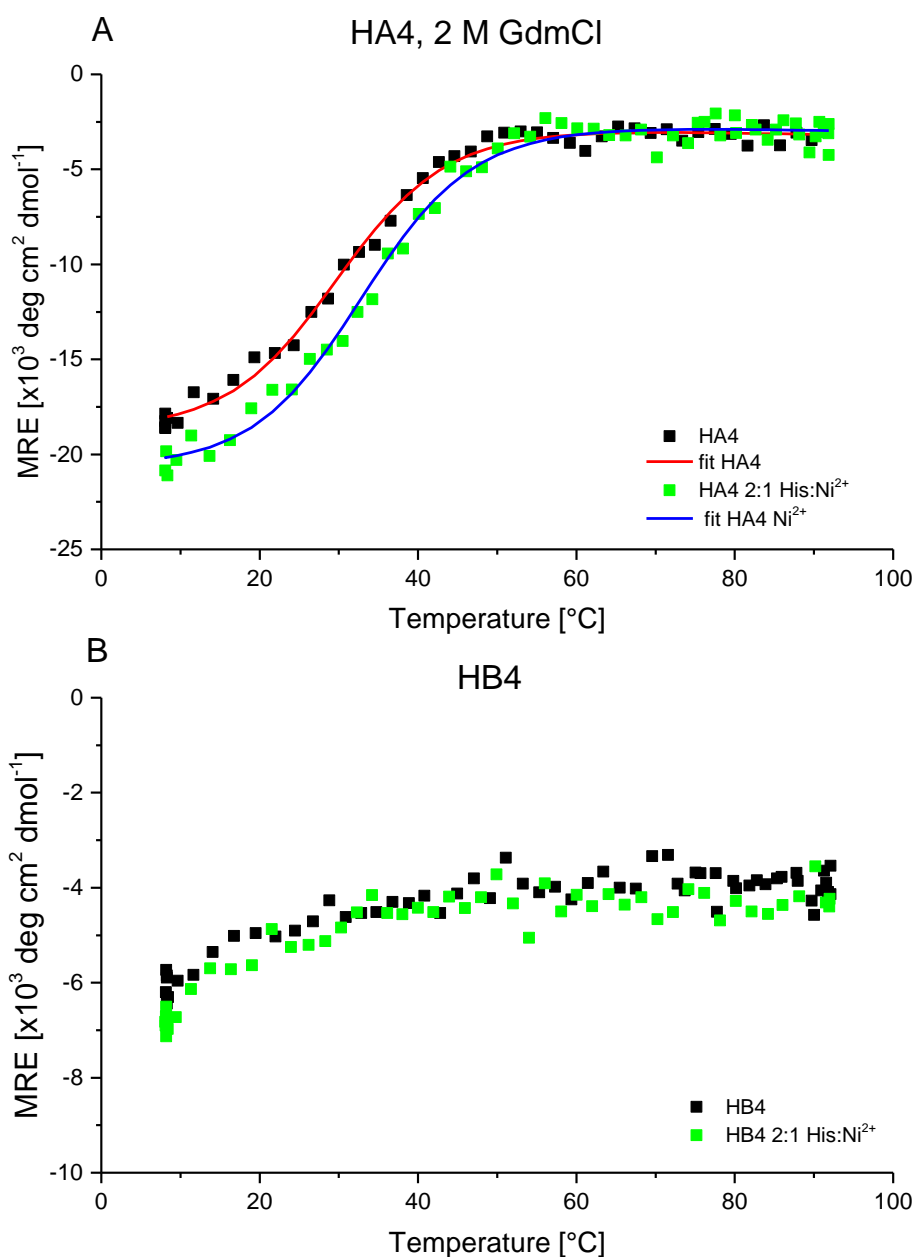


Figure 23: Thermal unfolding curves of HA4 (A) in 2 M GdmCl and HB4 (B) without GdmCl at 222 nm in the presence or absence of Ni^{2+} . The His: Ni^{2+} ratio was 2:1. The temperature range was 8-90 $^{\circ}\text{C}$ with a heating rate of 1 $^{\circ}\text{C}/\text{min}$. Measurements were performed in 5 mM PIPPS pH 8.1 in the interval scan mode (interval: 2 min, 1 accumulation, 2 s response). The mean residue molar ellipticity (MRE) was calculated using equation 1 and the equation 5 was fitted to the HA4 curves to obtain the melting temperature.

The molar enthalpy change ΔH_m at T_m in the fits of the HA4HB4 and HA4 in the presence and absence of Ni^{2+} is between 90 and 120 kJ/mol. There was no difference observed in ΔH_m of the coiled coil peptides with and without Ni^{2+} in the PIPPS buffer. The values obtained for ΔH_m are comparable to the ΔH of about 140 kJ/mol published by Thompson et al. [107] for the coiled coil domain of the bZIP transcription factor GCN4.

In general, the higher the T_m of a coiled coil, the more stable the structure is. Thus, significant shifts to higher T_m upon addition of Ni^{2+} are indicators for the stabilization or destabilization of the coiled coil peptides. First the effect of Ni^{2+} on the stability of the individual peptides was determined. The unfolding curves for HA4 with 2 M GdmCl had a sigmoidal shape and were also evaluated using nonlinear least-square fitting (equation 5) (Figure 23, A). The mean melting temperature T_m of HA4 without Ni^{2+} was $31.6 \pm 1.2^\circ\text{C}$, while T_m in the presence of 2:1 His: Ni^{2+} was $32.9 \pm 0.5^\circ\text{C}$ (replicate melting curves can be found in Figure A 6). Hence, the effect of Ni^{2+} on the thermodynamic stability of HA4 is quite small. The T_m with Ni^{2+} is in the range of the standard deviation (SD) of the T_m of HA4 without Ni^{2+} and a Student t-test (confidence interval 0.95, two-sided, unequal variance) confirmed that the difference in T_m for HA4 without and with Ni^{2+} is not significant ($p > 0.05$). HB4 was measured in PIPPS buffer without GdmCl, because it was already unfolded at 8°C (compare Figure 16). However, no change in the shape of the unfolding curve of HB4 was observed in the presence of Ni^{2+} (Figure 23, B).

Thermal unfolding of the His-modified HA4HB4, on the other hand, revealed that in the presence of Ni^{2+} the melting temperature T_m is about 6°C higher ($35.8 \pm 1.1^\circ\text{C}$) than without Ni^{2+} ($29.7 \pm 1.5^\circ\text{C}$). This change in T_m is significant ($p < 0.05$). The stabilizing effect of Ni^{2+} on HA4HB4 is emphasized in Figure 24 A, where the curve with a 2:1 His: Ni^{2+} ratio is left shifted and has a higher initial mean residue molar ellipticity. The effect of Ni^{2+} on T_m was corroborated by repeating the experiment three times with the custom built setup (Figure A 7; A, B). Furthermore, a control experiment was performed with a Jasco J-815 CD spectrometer equipped with a Peltier element (department Physical Biochemistry, University of Potsdam), which confirmed the results obtained with the custom build heating system (Figure A 7; C). Notably, the thermal unfolding process in 2 M GdmCl is fully reversible in the presence of Ni^{2+} , whereas HA4HB4 only refolds partially in the absence of Ni^{2+} (Figure A 8). For the control coiled coil A4B4, no change in T_m was detected in the presence of Ni^{2+} . A4B4 has a T_m of $37.9 \pm 1.5^\circ\text{C}$ in the presence of Ni^{2+} , while T_m is

$38.6 \pm 0.9^\circ\text{C}$ in the absence of Ni^{2+} . Moreover, the unfolding curves of A4B4 with and without Ni^{2+} showed a very similar intensity and shape (Figure 24 B; Figure A 7; D, E).

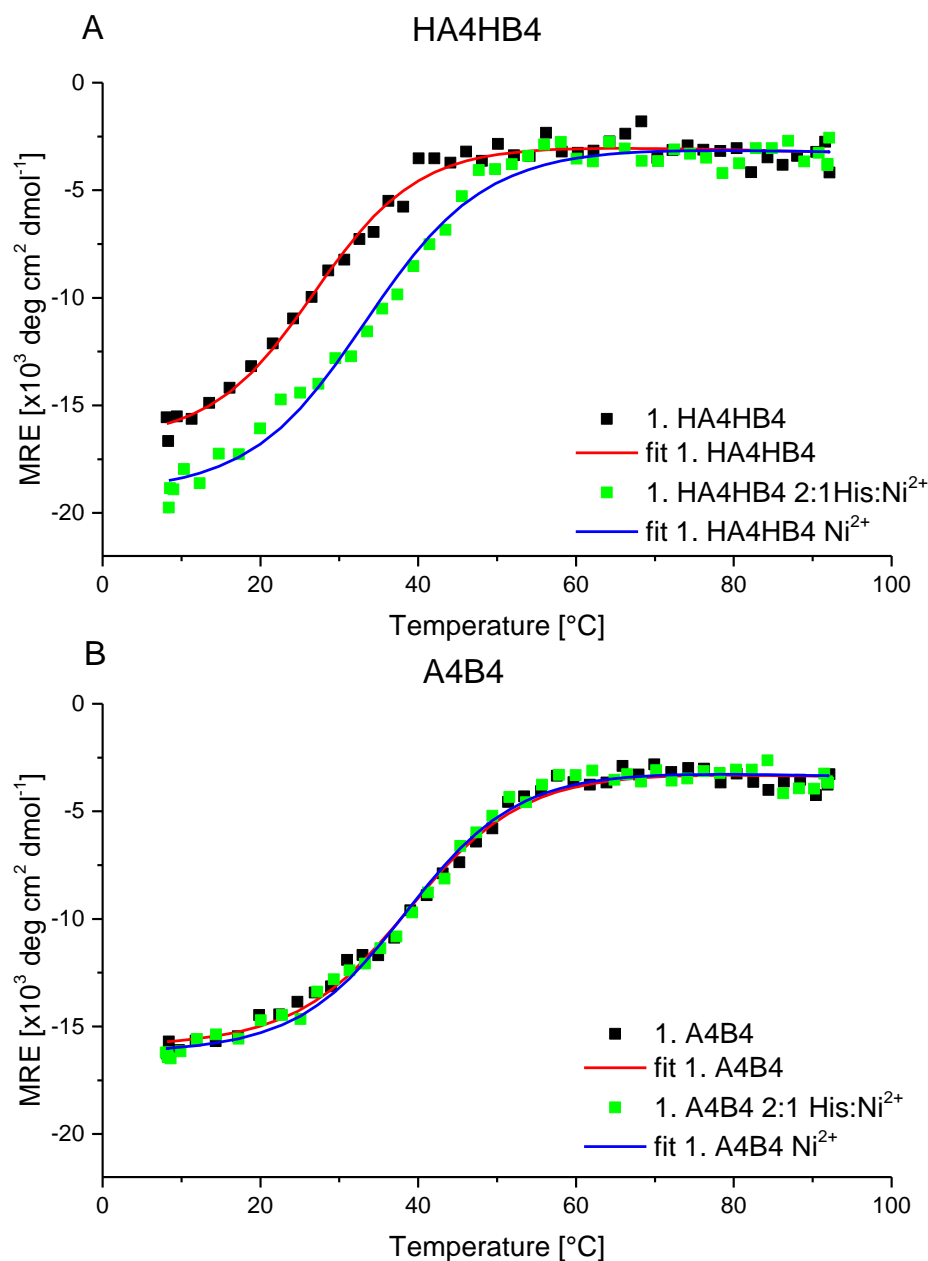


Figure 24: Thermal unfolding curves of HA4HB4 (A) and A4B4 (B) at 222 nm in 2 M GdmCl in the presence or absence of Ni^{2+} . The His: Ni^{2+} ratio was 2:1. The temperature range was 8-90 $^\circ\text{C}$ with a heating rate of 1 $^\circ\text{C}/\text{min}$. Measurements were performed in 5 mM PIPPS pH 8.1 in the interval scan mode (interval: 2 min, 1 accumulation, 2 s response). The mean residue molar ellipticity (MRE) was calculated using equation 1 and the equation 5 was fitted to the curves to obtain the melting temperature.

Results

Table 6: Melting temperatures T_m of the peptides in different buffers and conditions determined with CD spectroscopy. The melting temperatures were obtained by fitting the equation 5 to the unfolding curves. Detailed fitting results can be found in Table A 2. A dash means not determined. SD is the standard deviation.

Peptide(s)	10 mM NaP, pH 8.1	5 mM PIPPS, pH 8.1	5 mM PIPPS pH 8.1, 2 M GdmCl		5 mM PIPPS pH 8.1, 2 M GdmCl, 2:1 His:Ni ²⁺	
	T_m [°C]	T_m [°C]	T_m [°C]	Mean \pm SD	T_m [°C]	Mean \pm SD
HA4	> 90	> 90.0	33.1 30.4 31.4	31.6 \pm 1.2	32.8 32.4 33.6	32.9 \pm 0.5
HB4	33.9	< 8.0	-	-	-	-
HA4HB4	> 90.0	> 90.0	27.6 30.6 30.8	29.7 \pm 1.5	34.3 36.7 36.4	35.8 \pm 1.1
A4	< 8.0	< 8.0	-	-	-	-
B4	38.4	< 8.0	-	-	-	-
A4B4	> 90.0	> 90.0	39.8 38.4 37.7	38.6 \pm 0.9	39.4 38.4 35.8	37.9 \pm 1.5

The results of the thermal unfolding experiments show that the stability of HA4 is similarly high as the stability of the coiled coil HA4HB4 in the absence of Ni²⁺. This could be the result of a stabilizing effect of the acetylated N-terminus interacting with a His residue [108] or homo-oligomer formation of HA4. To test the last hypothesis, analytical ultracentrifugation in the sedimentation velocity mode was performed with the individual peptides. The apparent sedimentation coefficient distribution is visualized in Figure A 9. The obtained sedimentation coefficient distribution $c(s)$ is presented in Figure 25. B4 and HB4 just have one peak at 0.54 S and 0.56 S, which hints at a monodisperse distribution, while A4 and HA4 behave differently. Both of them have a big peak at low sedimentation coefficients of 0.12 S and 0.02 S, respectively. This indicates that there are impurities or peptide fragments in these samples. Nevertheless, A4 shows one peak at 0.47 S, which is broader than the peaks for B4 and HB4. In contrast, HA4 has two peaks of very low intensity at 0.47 S and 1.2 S (Figure 25 B). Thus, HA4 could also be forming oligomers, such as dimers. Experiments in

the sedimentation equilibrium mode with purified HA4 and A4 will be required to determine the exact oligomerization state of HA4.

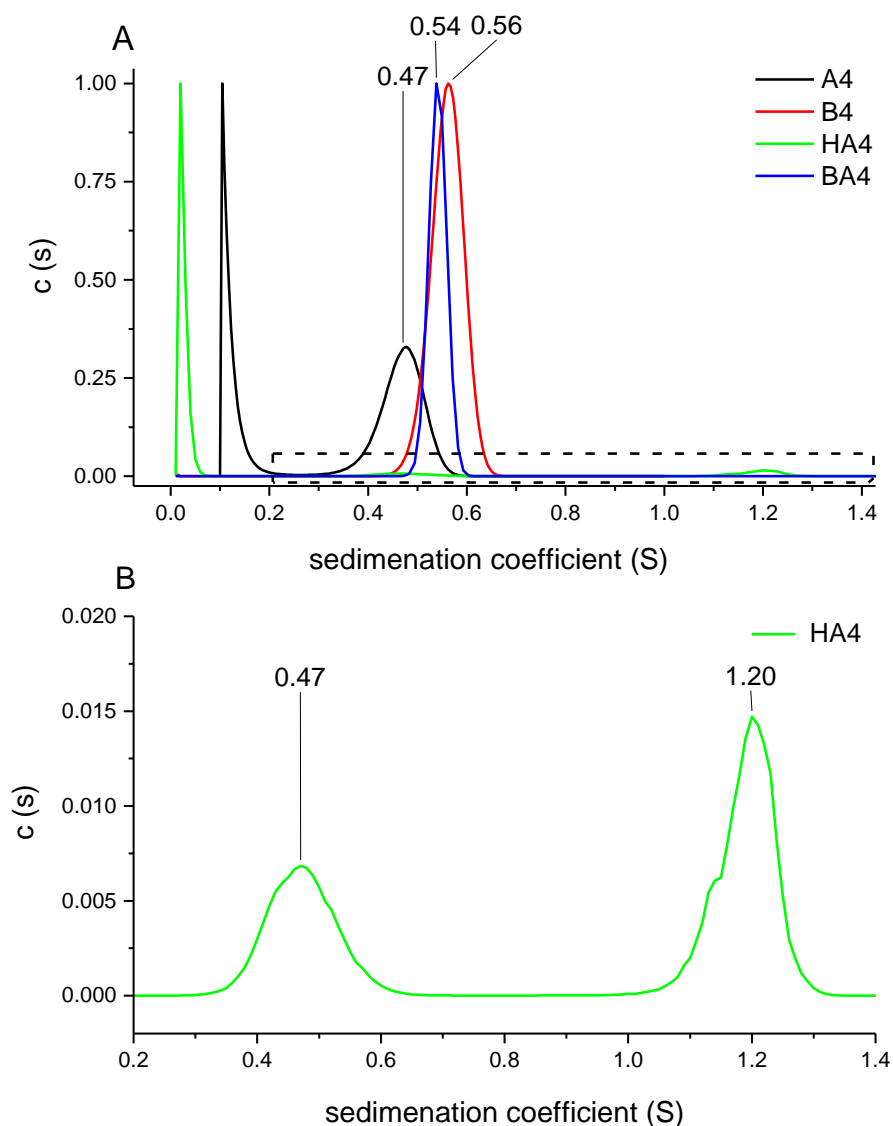


Figure 25: Sedimentation coefficient distribution of A4 (black), B4 (red), HA4 (green) and HB4 (blue). A: sedimentation coefficients of all peptides. B: Zoom-in to the dashed rectangle, distribution of HA4. The values were obtained with the interference detection at 60000 rpm and diffusion corrected.

4.6 Mechanical stability of the coiled coil is tuned by metal ion coordination

To create tunable hydrogels with metal coordinating coiled coils as mechano-sensitive crosslinkers, the mechanical response mechanism of the HA4HB4 system has to be well characterized. Figure 26 shows the His-modified coiled coil HA4HB4. The arrows indicate the point-of-origin of the shear force applied in single molecule force spectroscopy. The unfolding or dissociation process induced by the shear force should start at the terminus

where the peptide is coupled to the surface (N-terminus of CHA4) or the tip (C-terminus of CHB4), respectively. Thus, the His-metal coordination bonds introduced at these sites are expected to increase the force necessary to dissociate the coiled coil. In particular, the additional His-metal coordination bonds should decrease the free energy of the coiled coil in state A or increase the free energy of the transition state. In both cases, the free energy difference ΔG_1 would increase and thus, the thermal off rate (k_{off}) at zero force should decrease (see Figure 11). Stabilizing the coiled coil helices against deformation, His-metal coordination could also lead to a decrease of the potential width Δx_{AT} .

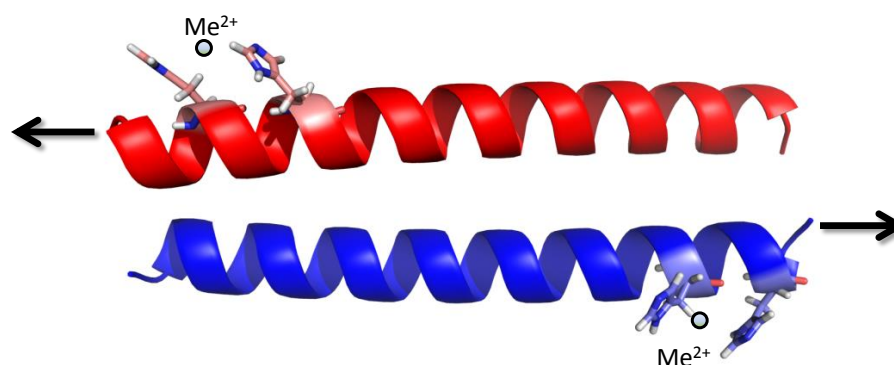


Figure 26: The dimeric coiled coil HA4HB4 tuned by His-metal coordination. The structure was predicted by CC-Builder [54]. Black arrows indicate the point-of-origin of the shear force in single molecule force spectroscopy. The A peptide (red) has two His in the first heptad and the B peptide (blue) has two His in the fourth heptad repeat. The coiled coil should be stabilized by the coordination of metal ions to the His residues.

Determining the rupture force F_R as a function of the loading rate of single molecule interactions reveals important information about the energy landscape of a system [109]. To obtain the most probably rupture force F_R as a function of the loading rate \dot{F} , different pulling speeds were used to probe the coiled coil interaction. Specifically, the cantilever was retracted from the surface at speeds of 50, 200, 400, 1000, 2500 and 5000 nm/s. Taking into account that HA4 could form oligomers, the concentration of HA4 was kept low on the surface. Moreover, it was shown for a heterotrimeric coiled coil, that heteromers are favored over homomers if the different coiled coil peptides were present in solution [110]. Thus, the formation of HA4HB4 should be favored over HA4 homomerization in the AFM experiment. To study the effect of metal ions, it is essential to avoid concentration effects due to evaporation of water. Thus, the SmallCell, which is a closed chamber, was used to study the influence of metal ions while preventing evaporation effects. To test the influence of metal ions on the HA4HB4 coiled coil, Ni^{2+} was used, since the Raman spectra showed that His is able to coordinate Ni^{2+} in a sodium phosphate buffer (see Figure 17). The concentration of Ni^{2+} used in the experiment was 2 mM and cannot be correlated to a certain His: Ni^{2+} ratio,

since the density or concentration of the peptides on the glass surface could not be accurately determined. After fitting the force curves with the WLC model and selecting the specific “single pulls”, the most probable values for F_R and \dot{F} were extracted from the data. This was done by fitting a Gaussian distribution to the F_R histograms with IGOR Pro. To obtain the most probable \dot{F} , a semi-logarithmic plot and a LogNormal-fit were used.

Since the data for the A4B4 system of Melis Göktaş were obtained with an open system (regular spring holder), a control measurement was performed with this setup to prove the comparability with the SmallCell data (Figure 27). At a pulling speed of 1000 nm/s in PBS (pH 7.4), the most probable F_R of HA4HB4 with the open system was 43 ± 1 pN and the most probable \dot{F} was 502 ± 4 pN/s (number of force curves $n=543$) (Figure 27 A, B). The most probable values obtained using the SmallCell (closed system) are $F_R=42 \pm 1$ pN and $\dot{F}=775 \pm 19$ pN/s (Figure 27 C, D) ($n=184$). The slight shifts of the values can result from the small number of curves obtained for the SmallCell and the systematic error originating from the different tips used for the experiments. Thus, the HA4HB4 system is comparable with the A4B4 system studied by Melis Göktaş (Mechano(bio)chemistry), which has a F_R of 45-48 pN at 1000 nm/s pulling speed (unpublished results).

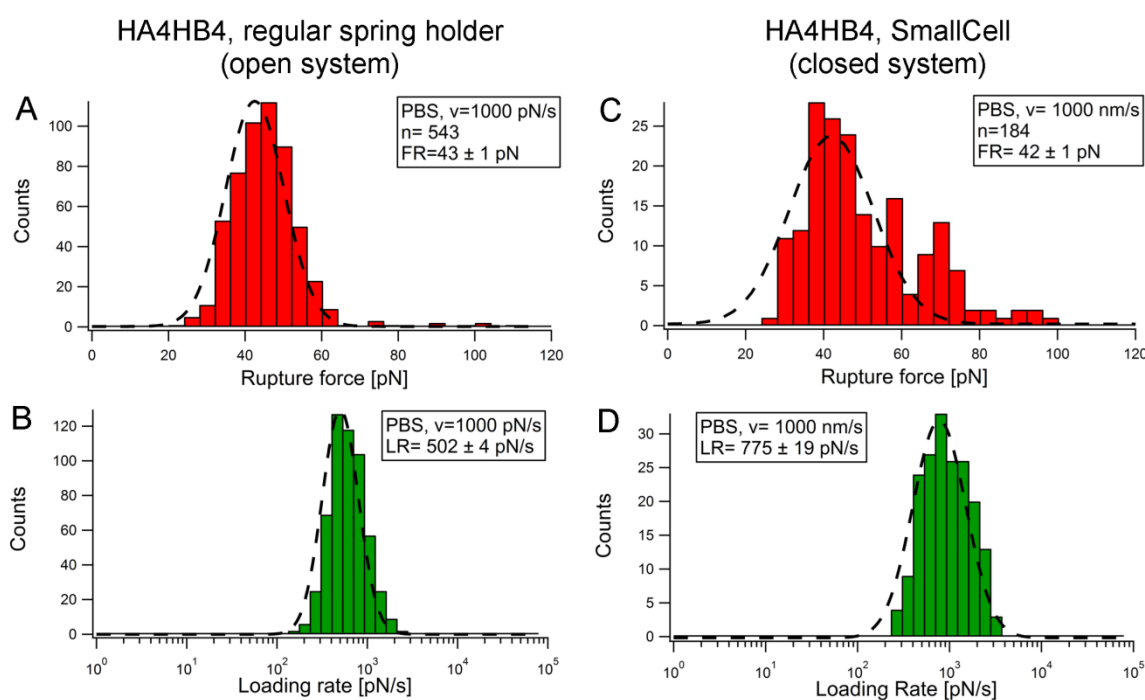


Figure 27: Comparison of the HA4HB4 system measured with a regular spring holder and the SmallCell. The rupture force (F_R) histogram (A) and the loading rate (\dot{F}) histogram (B) of HA4HB4 measured with an open system. C and D are the corresponding rupture force and loading rate histograms obtained with the SmallCell. CHA4 was coupled to the surface and CHB4 to the tip. Measurements were carried out in PBS at 1000 nm/s pulling speed. The most probable values were determined using a Gauss-fit, respectively a LogNormal-fit for \dot{F} in IGOR Pro. n is the number of curves.

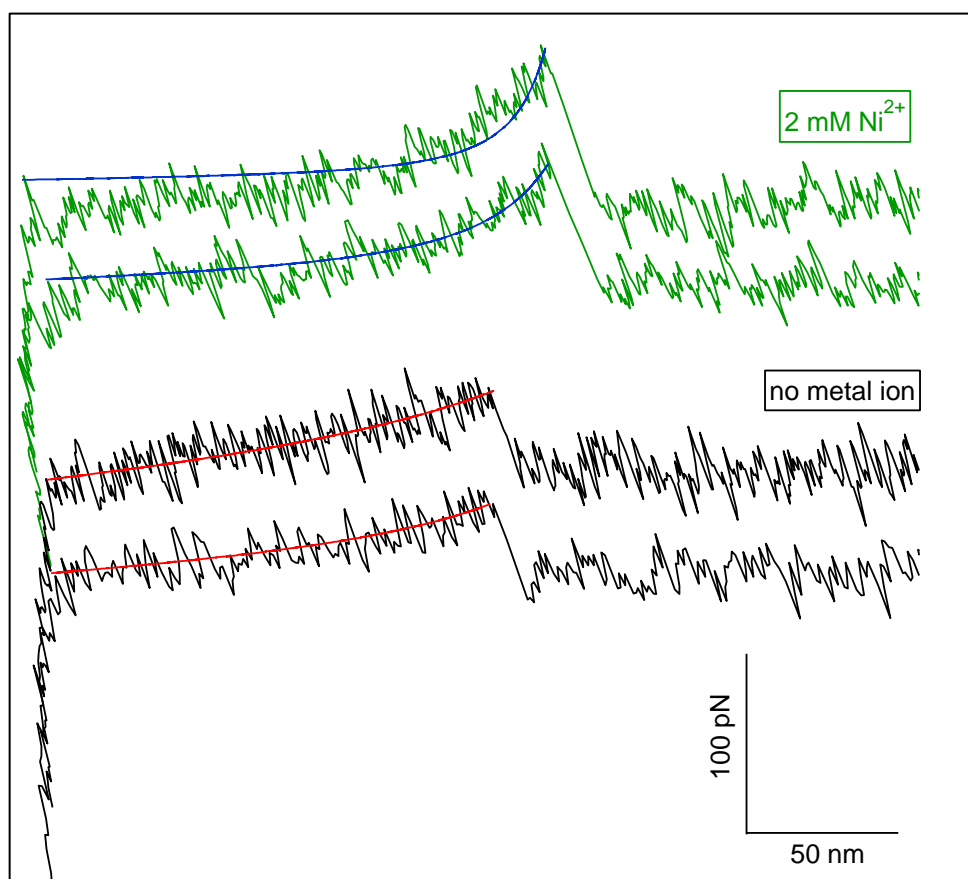


Figure 28: Force curves obtained for 1000 nm/s pulling speed in without metal ions (black) and with 2 mM Ni^{2+} (green) in PBS at 25°C. The WLC fits were performed with IGOR Pro (custom script) and are represented by the blue and red lines. The rupture force F_R is the force magnitude between the last adhesion point and the baseline. In the presence of Ni^{2+} the rupture force is about 13 pN higher than without metal ions. The curves are off set to increase the visibility of the differences between them.

In the presence of 2 mM Ni^{2+} , there is a general trend towards higher F_R compared to the measurements without metal. This is emphasized when comparing the force curves at 1000 nm/s pulling speed (Figure 28): the rupture force is about 13 pN higher if 2 mM Ni^{2+} is present, which corresponds to a 30 % increase. This is further confirmed by the histograms for F_R of the HA4HB4 coiled coil at different loading rates in the absence and presence of 2 mM Ni^{2+} (Figure 29, Figure 30). In PBS in the absence of Ni^{2+} , force curves were obtained for a range of loading rates from 31-7754 pN/s. In the presence of 2 mM Ni^{2+} the loading rate values cover the range from 21-1326 pN/s. The data for the most probable values of F_R and \dot{F} are summarized in Table 7. The number of single molecule pulling events was almost always below 200, because of the low density of peptides and thus low probability of binding. Hence, the data does not exhibit an ideal Gaussian distribution. Moreover, the F_R histograms at higher pulling speeds show a “tail” at higher rupture forces (Figure 29 D, F, Figure 30 D). The origin of this “tail” is currently unclear and requires further investigation.

Results

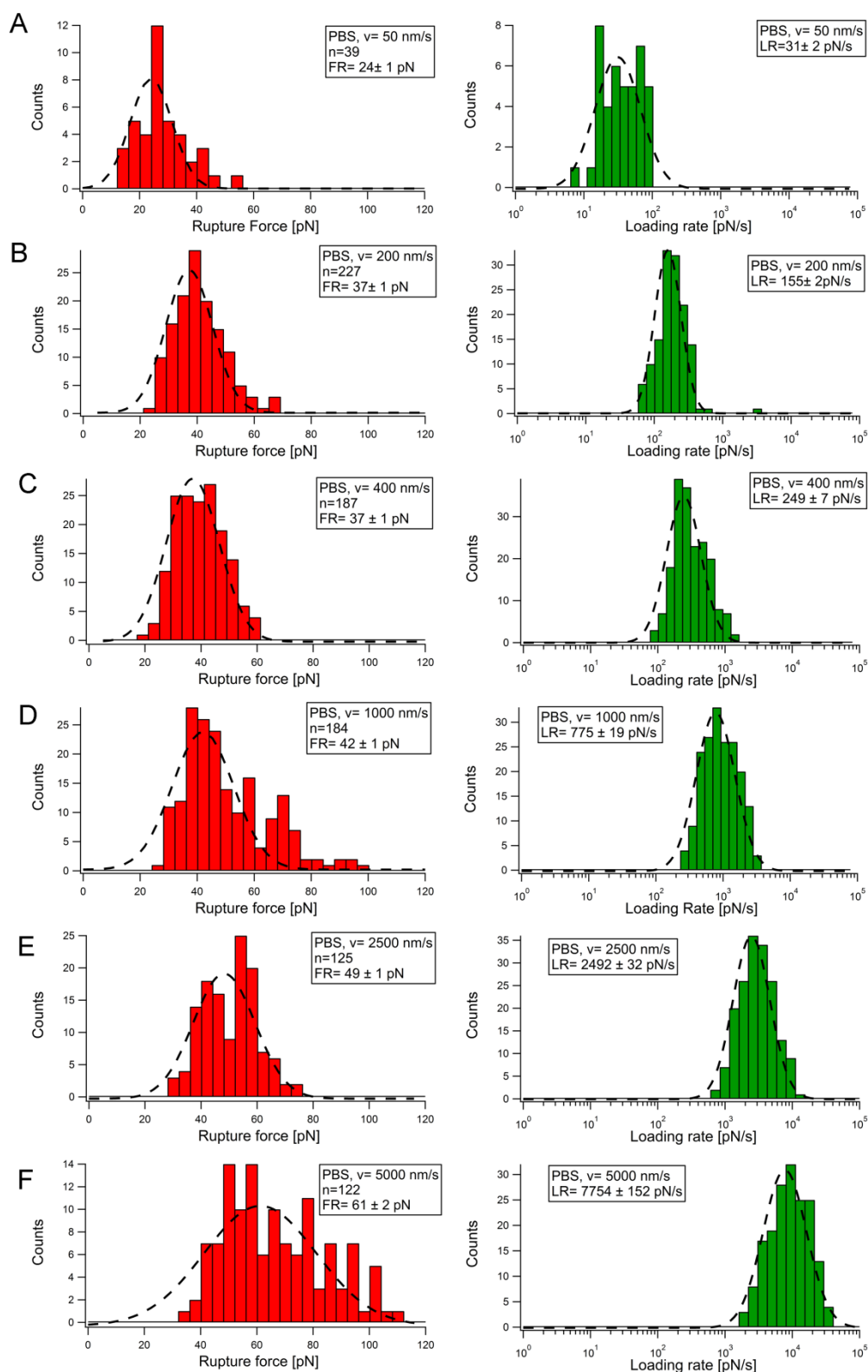


Figure 29: Rupture force and loading rate histograms for the HA4HB4 system in the absence of Ni^{2+} . Rupture force (F_R) and loading rate (\dot{F}) histograms for the pulling speeds $v=50$ (A), 200 (B), 400 (C), 1000 (D), 2500 (E) and 5000 nm/s (F). Data were obtained with the SmallCell in PBS (pH 7.4) at 25°C. CHA4 was coupled to the surface and CHB4 to the tip. The most probable values were determined using a Gauss-fit for the F_R and LogNormal-fit for the loading rate histogram. n is the number of force curves for each pulling speed.

Results

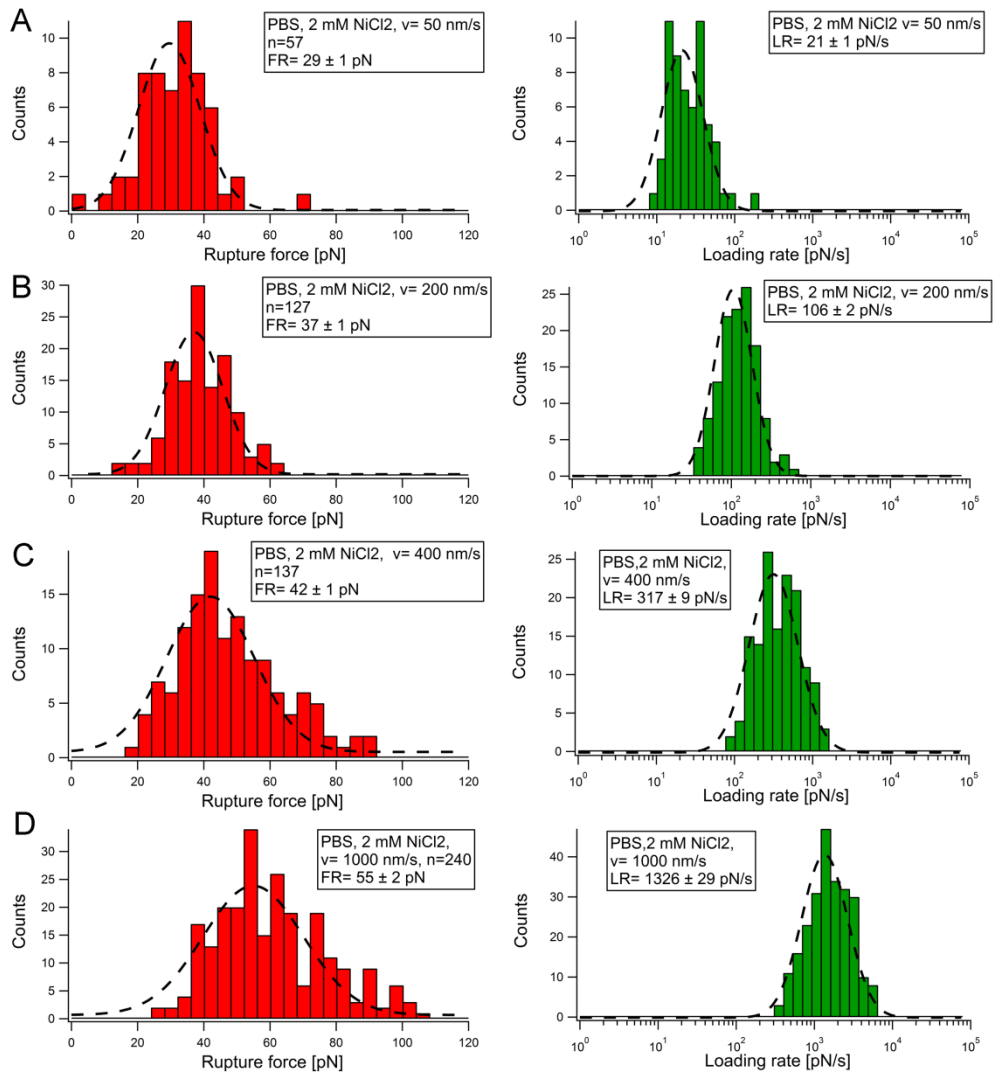


Figure 30: Rupture force and Loading rate histograms for the HA4HB4 system in the presence of 2 mM Ni^{2+} . Rupture force (F_R) and loading rate (\dot{F}) for the pulling speeds $v=50$ (A), 200 (B), 400 (C), 1000 pN/s(D). Data were obtained with the SmallCell in PBS (pH 7.4) at 25°C. CHA4 was coupled to the surface and CHB4 to the tip. The most probable values were determined using a Gauss-fit for the F_R and LogNormal-fit for the loading rate histogram. n is the number of force curves for each pulling speed.

Results

Table 7: Loading rate (\dot{F}) dependency of the rupture force (F_R) of the HA4HB4 system without and with 2 mM Ni^{2+} . The error is one standard deviation. A dash means no data could be obtained.

Pulling speed (nm/s)	without metal			with 2 mM Ni^{2+}		
	Number of curves	F_R (pN)	\dot{F} (pN/s)	Number of curves	F_R (pN)	\dot{F} (pN/s)
50	39	24 ± 1	31 ± 2	57	29 ± 1	21 ± 1
200	227	37 ± 1	155 ± 2	127	37 ± 1	106 ± 2
400	187	37 ± 1	249 ± 7	133	42 ± 1	317 ± 9
1000	184	42 ± 1	775 ± 19	240	55 ± 2	1326 ± 29
2500	125	49 ± 1	2492 ± 32	-	-	-
5000	122	61 ± 2	7754 ± 152	-	-	-

Information about the response mechanism of the HA4HB4 system in the shear geometry can be obtained by having a closer look at the free energy landscape in the presence and absence of Ni^{2+} . The distance between the native state A and the transition state T (Δx_{AT}) as well as the thermal off-rate k_{off} of the HA4HB4 coiled coil were determined using the Bell-Evans model (equation 17). The Bell-Evans model is valid if there is a linear dependency of the most probable F_R with the logarithm of the most probable \dot{F} (Figure 31). As only one data set covering a range of different loading rates is currently available, the standard error of the kinetic parameters is high. For k_{off} the error is in the same order of magnitude. The value for Δx_{AT} is 0.665 ± 0.087 nm in the presence of 2 mM Ni^{2+} and 0.671 ± 0.059 nm in the absence of Ni^{2+} . Thus the transition state energy barrier is not changed. In contrast, there is a nearly 2.5-fold decrease of the thermal off-rate k_{off} if Ni^{2+} is present ($k_{off,Ni}=0.038 \pm 0.029$ s⁻¹) compared to the system without Ni^{2+} ($k_{off,wo}=0.092 \pm 0.049$ s⁻¹). These results have to be reproduced to securely confirm the effect of the Ni^{2+} , but the trend towards higher stability is promising in terms of creating mechanosensitive crosslinkers, which are tunable with metal ion coordination.

Results

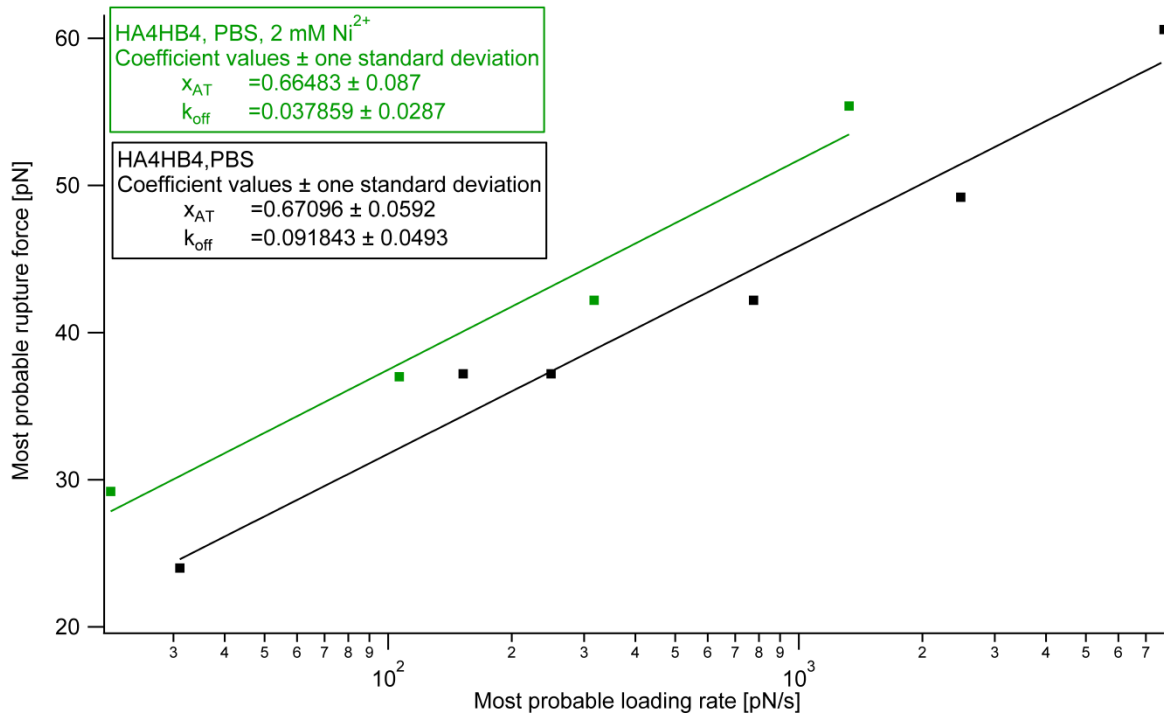


Figure 31: Loading rate dependency of the most probable rupture force. Black squares: HA4HB4 in PBS (pH7.4) without metal ions, green squares: HA4HB4 with 2 mM Ni²⁺. The Bell-Evans model was fitted to the data (lines) to obtain the potential width Δx_{AT} and the thermal off-rate at zero force k_{off} .

5 Discussion

The aim of this work was to characterize a coiled coil tuned with bi-histidine-metal chelation sites in order to address the need for tunable mechano-responsive crosslinks in hybrid hydrogels. Moreover, the effect of His-metal coordination on the mechanical response mechanism of coiled coils in the shear geometry was investigated. For this purpose, two His residues were introduced in the N-terminal heptad of A4 and the C-terminal heptad of B4. Spectroscopic techniques revealed that the His-modified peptides maintained an α -helical structure and were able to coordinate different transition metal ions. The chelation of metal ions by the engineered His residues was shown to increase the thermodynamic and the mechanical stability of the modified coiled coil.

In order to characterize the HA4HB4 coiled coil mechanically and thermodynamically it was important to investigate if the introduced His residues affect the secondary structure of the peptides. The His residues were placed in the solvent exposed register positions *b* and *f* with a three-amino-acid spacing (HXXXH) so that each individual peptide is able to chelate one single metal ion [50]. ATR-FTIR, CD spectroscopy as well as Raman spectroscopy clearly showed that the modified coiled coil peptides maintained a predominantly α -helical conformation. Surprisingly, in ATR-FTIR, the amide I peaks for all peptides, but A4, had a shoulder at $1674/75\text{ cm}^{-1}$, usually assigned to β -turns [95]. However, in the α -helical protein hemoglobin, this shoulder corresponds to the short segments connecting the helices [58]. For the peptides used in this work, the shoulder could originate from the two Gly placed at the termini of the peptides, which should not be part of the α -helix due to their low helix propensity [111]. The reason for the absence of this shoulder in A4 is still unclear. A predominantly α -helical structure of the peptides is also confirmed by the amide III band in Raman spectroscopy, which is dependent on the dihedral angles of the peptide backbone. The amide III band shows peaks assigned to α -helix in the range of $1270\text{-}1350\text{ cm}^{-1}$ (Table 5), while there is no such band for more extended conformations (e.g. β -sheet) around 1230 cm^{-1} [101].

In the literature, it is reported that buffer components can have an effect on the structure and stability of proteins and peptides and that they can interfere with metal coordination [97]. This is also true for the coiled coil peptides used in this work. In NaP buffer, the secondary structure of the His-modified and the control peptides was very similar to the structure of the original peptides measured in PBS [53]. A4 was unordered, while all the other individual

peptides as well as the coiled coil peptides HA4HB4 and A4B4 had an α -helical conformation. In water and in the non-coordinating PIPPS buffer, HB4, A4 and B4 were unordered, while HA4, HA4HB4 and A4B4 were α -helical. This indicates that the individual peptides, except HA4, are unfolded in PIPPS buffer. However, if HA4 and HB4, as well as A4 and B4 are mixed, they fold into α -helices and maintain their α -helical structure, even at the low concentration (50 μ M) used for the CD measurements. Thus, the folding and association of the coiled coil peptides is cooperative, which was also reported for other coiled coils [107], [112]. It was described by Ugwu and Apte [97], that the buffer and further components, such as salts, highly affect the activity and conformation of proteins. Thus, B4 and HB4 might be stabilized by the Na^+ and phosphate ions in the NaP buffer. Considering that the PIPPS buffer also contains Na^+ (NaOH, was used to raise the pH to 8.1), it appears unlikely that Na^+ affects the secondary structure of B4 and HB4. Most likely, the negative phosphate ions in the NaP buffer, interact with the positive Lys residues and stabilize the helical structure of B4 and HB4 in this buffer. To obtain further information about the structure of the coiled coils, NMR or X-ray diffraction experiments could be performed. In addition to buffer effects on the coiled coil structure, it was also observed using Raman spectroscopy that NaP buffer interfered with the ability of the coiled coil peptides to coordinate Zn^{2+} , which may arise from the ability of phosphate to form complexes of low solubility with Zn^{2+} [103], [104].

Different metal ions can bind to His with different affinities and in different coordination geometries. For the development of tunable His-modified coiled coils as crosslinkers, it is important to know, which metal ions can be bound by the peptides. To get information about the ability of the His residues to coordinate divalent metal ions, Raman spectroscopy was used [66]. The spectra in the non-coordinating PIPPS buffer for HA4, HB4 and HA4HB4 reveal that Ni^{2+} , Cu^{2+} and Zn^{2+} are coordinated by the His, because there is a shoulder at 1605 cm^{-1} (Figure 18) [66]. This is promising in terms of creating tunable materials, since the stability of His-metal complexes is dependent on the metal ion used and the compatibility of the α -helical structure of the coiled coil with the coordination geometry [72]. For example, Fullenkamp et al. [113] as well as Grindy et al. [114] observed that the rheological properties of a PEG hydrogel functionalized with His residues and crosslinked via His-metal coordination are dependent on the specific metal ion used for crosslinking. Furthermore, Ghadiri and Choi [72] showed that also the α -helicity of His containing peptides can be increased by adding metal ions. To investigate if Ni^{2+} has a similar effect on the secondary

structure of the peptides, CD spectroscopy was used. With exception of HA4, which exhibited an increased $r_{222/208}$ (Figure 19), an effect of the metal ions on the structure of the peptides could not be observed. This shows that the Ni^{2+} ratios used are not able to induce a structural change of the individual peptides, which are unfolded at 20°C in PIPPS buffer. Moreover, the coiled coil HA4HB4 already shows an α -helical conformation in the absence of Ni^{2+} so that no increase in α -helicity in the presence of Ni^{2+} may be detectable anymore. However, this is contradictory to the increase in ellipticity of HA4HB4 in the presence of Ni^{2+} , which was observed in the unfolding experiments. But in the unfolding experiments 2 M GdmCl was used, which leads to a destabilization of HA4HB4. In this setup, the stabilizing effect of Ni^{2+} on the secondary structure of HA4HB4 may be enhanced and easier to detect with CD spectroscopy.

The main focus of this work was to investigate if His-metal chelation can thermodynamically and mechanically stabilize the modified coiled coil peptides. It was shown, that two chelating His residues are able to thermodynamically stabilize protein conformations in the presence of metal ions [50], [72], [115]. To investigate if there is a thermodynamic stabilization effect of His-metal chelation on the coiled coils, thermal unfolding curves were acquired using CD spectroscopy. The original peptides published by Thomas et al. [53] have a T_m of <5°C for A4, $25.3 \pm 0.6^\circ\text{C}$ for B4 and $81.0 \pm 0.5^\circ\text{C}$ for A4B4. Compared with the T_m obtained in NaP buffer for HA4, HB4 and HA4HB4 as well as the control peptides, the original coiled coil peptides seem to be less stable (Table 6). However, Thomas et al. [53] used PBS (pH 7.4) instead of NaP buffer (pH 8.1). The lower ionic strength in the NaP buffer and the higher pH could lead to the slightly higher T_m of B4 and HB4 under the conditions used in the present work. In PIPPS buffer with 2 M GdmCl, A4B4 is approximately 9.0°C more stable than HA4HB4. Most likely, replacing the original Ala and the Gln residues with His destabilizes the coiled coil structure, since His has a lower helix propensity than the amino acids in the original peptides [111], [116]. In contrast, HA4 has a $T_m > 90^\circ\text{C}$ and is far more stable than the control peptide A4 ($T_m < 8^\circ\text{C}$) and is α -helical independent of the buffer used for CD spectroscopy (Figure 16, Figure 19). A reason could be that, HA4 is stabilized by the interaction of the first His in the first heptad with the acetylated N-terminus of the peptide. The stabilization effect of His was also reported for His residues near the C-terminus, which also has a carboxylate group [45], [108]. The interaction of the carboxylate group with a His residue could also interfere with the ability of that His to chelate metal ions, which is supported by the low increase of T_m in the presence of Ni^{2+} compared to HA4HB4 (Table 6).

Alternatively, the formation of HA4 homo-oligomers could lead to the high stability of the peptide. This hypothesis is supported by the $r_{222/208}$, which is close to 1 for HA4 in the buffers tested, indicating that HA4 could form a coiled coil. Potential formation of a parallel HA4 homomer could also explain the small change of the T_m in the presence of Ni^{2+} : In this conformation with all His residues on one site of the parallel homomeric coiled coil, the His-metal coordination would just stabilize one end of the coiled coil, while the other end would not be stabilized and thus, the whole HA4 coiled coil would still unfold in a very similar way as without Ni^{2+} . However, since the HA4 peptide has negatively charged residues at the *e* and *g* positions oligomerization of HA4 should be prevented by electrostatic repulsion [16]. Nevertheless, AUC in the sedimentation velocity mode was performed on all individual peptides to test if they are capable of forming higher oligomerization states, indicating that HA4 may be able to form oligomers (Figure 25). To further investigate this, a sedimentation equilibrium experiment is required. This experiment has not been performed yet, because of the impurities in A4 and HA4. An appropriate method to remove of the impurities could be HPLC. Regardless of the oligomerization state of HA4, the heterodimerization of HA4 and HB4 should be favored, if both peptides are present in solution. The full heterodimerization of HA4HB4 is supported by the fact that there is only one transition in the thermal unfolding experiments. A similar phenomenon was also observed for a trimeric coiled coil, where the heterotrimers were favored 100-fold about other oligomeric states [110].

The His-modified coiled coil HA4HB4 is stabilized by the addition of Ni^{2+} (2:1 His: Ni^{2+} ratio) in PIPPS buffer (Figure 24, Table 6). The T_m of HA4HB4 in the presence of Ni^{2+} is 6.0°C higher than without metals. This stabilizing effect was also observed for α -helical peptides with His residues in the presence of Cu^{2+} by Ghadiri and Choi [72] and for cytochrome *c*, tuned with two His in the presence of Cu^{2+} [50]. In the latter case, cytochrome *c* with 1 mM Cu^{2+} -iminodiacetate was 4 kcal/mol more stable than in the absence of metal ions [50]. In contrast to HA4HB4, there is no change in the T_m for A4B4 in the presence of Ni^{2+} , but the T_m of A4B4 is still 3.0°C higher than for HA4HB4 with Ni^{2+} . A reason for this could be that His has a lower helix propensity than the original amino acids Ala and Gln. Thus, His is destabilizing the α -helix in the absence of metal ions [111]. A similar effect was also reported for a His-modified cytochrome *c* [116]. The effect of different His-metal ratios and different metal ions on the thermodynamic stability of the peptides remains to be investigated in further studies.

In addition to thermodynamic stability measurements, the mechanism of how coiled coils respond to mechanical loading in the shear geometry was studied in the current work. Root et al. [52] performed Molecular Dynamics simulations to study the response of the myosin coiled coil to shear forces. These simulations suggested that the coiled coil starts to unfold at the point-of-origin of the force. Thus, the shear forces would first cause unfolding of the terminal heptads, carrying the Cys for surface attachment in the single molecule force spectroscopy experiments. If this hypothesis is true, the HA4HB4 coiled coil should be more stable in the presence of Ni^{2+} , because of the additional, stabilizing His-metal coordination bonds in these heptads. AFM force spectroscopy at the single molecule level was performed to test this hypothesis. It is shown in this work, that the rupture force F_R of HA4HB4 in the presence of Ni^{2+} is higher than in the absence of Ni^{2+} . Thus, stabilizing a terminal heptad repeat of the α -helices leads indeed to a higher stability of the whole coiled coil in the shear geometry. Furthermore, it supports the mechanism suggested by Root et al. [52] that the unfolding starts at that site of the α -helix, where the force is applied. A stabilizing effect of His-metal coordination was also reported by Cao et al. [12], who inserted two His into a β -sheet of the small protein GB1. In the presence of 4 mM Ni^{2+} the F_R for the modified protein was doubled. Moreover, the His modification also resulted in a decrease of the rupture force (≈ 120 pN) compared with the wildtype protein (≈ 180 pN). This is also in accordance with the result of the thermal unfolding experiments in the absence of metal ions: HA4HB4 is less stable than the control peptides A4B4 (Table 6), but the stability of HA4HB4 increases, if Ni^{2+} is present. However, it is important to note, that the AFM results cannot be directly related to a certain His: Ni^{2+} ratio used for CD spectroscopy, because the density of the peptides on the glass slide cannot to be determined easily. A possible method to measure the density of the peptides on the surface is to fluorescently label the peptides.

If the HA4HB4 coiled coil is stabilized by His- Ni^{2+} coordination, there should also be an effect on the potential energy landscape of the system. In particular, the bound or native state “A” should be stabilized by lowering the thermal off-rate k_{off} and eventually decreasing the potential width Δx_{AT} (see Figure 11). To investigate this effect, the loading rate dependency of F_R was studied by obtaining force curves at different pulling speeds of HA4HB4 in the presence and absence of Ni^{2+} . The resulting histograms of F_R and \dot{F} do not have an ideal Gaussian distribution, which would be expected if there is just variation around one mean value (Figure 29, Figure 30). A reason for that could be the low number of curves for each pulling speed. Future experiments should have at least 200-300 curves per condition.

Furthermore, the histograms for the rupture force at high speeds also show a “tail” of high rupture forces (Figure 29 D, F; Figure 30 D). Currently, the origin of the “tail” it is unclear and has to be further investigated. If Ni^{2+} is present, the “tail” can be explained by an increased heterogeneity of the HA4HB4 system, because there will be a statistic distribution of coiled coils with no Ni^{2+} bound, 1 Ni^{2+} bound to one of the α -helices and Ni^{2+} bound to both α -helices. However, there is also a “tail” of high F_R in PBS without Ni^{2+} .

The change of the kinetic parameters k_{off} and Δx_{AT} , in the presence and absence of Ni^{2+} , reveals valuable information about the response mechanism of HA4HB4 if a shear force is applied. To obtain the kinetic parameters, the loading rate \dot{F} and the rupture force F_R were determined and the most probable F_R at every pulling speed was plotted against the logarithm of the most probable values of the corresponding \dot{F} (Figure 31). The data were fitted with the Bell-Evans model, to obtain the dissociation constant k_{off} at zero force as well as the distance Δx_{AT} between the bound or native state A and the transition T. In the presence of Ni^{2+} , k_{off} was 2.5-fold lower than without Ni^{2+} , while the potential width Δx_{AT} remained unchanged. The possible effects of His- Ni^{2+} chelation on the shape of the free energy landscape of HA4HB4 are visualized in Figure 32.

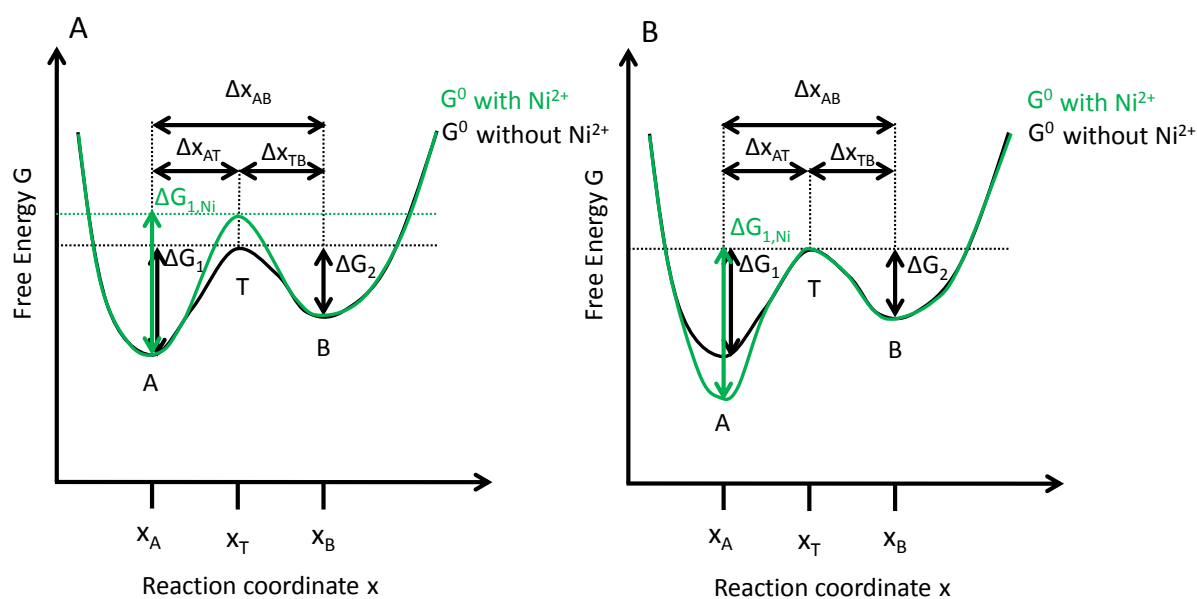


Figure 32: Possible shapes of the free energy landscape in the absence (black) and presence of Ni^{2+} (green). The arrows depicting the difference in the free energy between the bound/native state A and the transition state T are slightly shifted for better visualization. B is the unbound/unfolded state of the coiled coil peptides. The potential width between the state A and the state T is Δx_{AT} . In model A, the His- Ni^{2+} complex increases the free energy of the transition state T, whereas in model B the free energy of the bound state A of the coiled coil is decreased via His- Ni^{2+} coordination. Both models result in a higher energy barrier ΔG_1 and thus, in a decrease in the thermal off-rate k_{off} . The observed effect of Ni^{2+} on the coiled coil could also be the result of a combination of both models. The potential width Δx_{AT} remains unchanged according to the obtained data (Figure 31).

In model A, the additional His-metal coordination bonds increase the free energy of the transition state and, thus, the free energy ΔG_1 the coiled coil needs to overcome to reach the transition state T (Figure 32). Another possible model explaining the stabilizing effect of Ni^{2+} on the His-modified coiled coil structure is that the free energy of the bound state is decreased, while the free energy of the transition state remains unchanged, as depicted in Figure 32,B. However, also a combination of both effects is possible. Furthermore, since there was no detectable change of the potential width Δx_{AT} in the presence of His- Ni^{2+} chelation bonds, Δx_{AT} was assumed to be constant in the models. In both models, the predicted effect of the His- Ni^{2+} chelation is a higher energy barrier ΔG_1 , which results in the decrease of k_{off} , between the bound state A and the transition state T. Thus, the stabilization of the His-modified coiled coil in the presence of Ni^{2+} promotes the mechanical unfolding mechanism of coiled coils in the shear geometry predicted by Molecular Dynamics simulations, where the helices starts to unravel at the terminus, where the force is applied [52]. In conclusion, using SMFS to study coiled coils tuned with His-metal chelation can provide valuable information about the mechanical response mechanism of coiled coils under load. Further measurements have to be done to confirm the results, however, to characterize the response of the HA4HB4 system to different metal ions, like Ni^{2+} , Cu^{2+} or Zn^{2+} and to study the effect of the concentration of those metal ions on the mechanical stability of HA4HB4.

6 Conclusion and Outlook

Naturally occurring or *de novo* designed coiled coils can serve as crosslinkers in hybrid hydrogels with promising applications in cell culture or tissue engineering [6], [7]. Addressing the need for tunable, mechano-responsive hydrogel building blocks the current work shows that coiled coils can be stabilized with bioengineered His-metal coordination sites. The His-modified coiled coils studied in this work maintained an α -helical structure and were shown to coordinate transition metal ions, such as Ni^{2+} , Cu^{2+} and Zn^{2+} . More importantly, applying force in the shear geometry, the mechanical stability of the His-modified HA4HB4 is enhanced in the presence of Ni^{2+} . Thus, stabilizing the heptads where the pulling force is applied stabilizes the whole coiled coil (chapter 4.6). This result supports the response mechanism suggested by Root et al. [52] where the α -helices begin to unfold from the point-of-origin of the shear force. Furthermore, the coordination of the transition metal ion Ni^{2+} by the His residues thermodynamically stabilizes the HA4HB4 coiled coil (chapter 4.5). Although, further work has to be done, this thesis is a proof of principle for the mechanical stabilization of coiled coils by His-metal coordination.

Before HA4HB4 can be included into the toolkit of coiled coils usable as mechanosensitive material crosslinkers, several open questions need to be answered. The oligomerization state of HA4 needs to be determined and the influence of His-metal ion ratios on the mechanical stability of the HA4HB4 coiled coil needs to be investigated in more detail. Also the ability of the coiled coil to coordinate other metals, such as Co^{2+} , should be tested. SMFS performed with other metal ions will provide essential information about the tunable force range of the coiled coil. Furthermore, the effect of His-metal chelation on the stability of HA4HB4 in the unzipping mode could be investigated with SMFS to obtain information about the effect of His-metal coordination on the free energy landscape in this geometry. Preliminary rheology results of the Mechano(bio)chemistry group (MPIKG) for A4B4 hydrogels, indicate a difference in the mechanical behavior of hydrogels crosslinked in the shear versus the unzipping geometry (unpublished results). Also the coordination geometry of the His-metal complexes could be investigated further, e.g. with XAFS [117], and the binding constants of metal ions to the His residues could be determined with ITC [118]. Coordination geometry data and binding constants of the HA4HB4 system with different metal ions will be important to choose the right metal ion for a hydrogel setup with certain tunable characteristics. Future work should not only be focused on the characterization of the peptides used in this work, but

also on the bioengineering of new coiled coil variants with His residues at other positions to further elucidate the response mechanism of coiled coils to shear forces. For example, His-metal coordination sites could be inserted into a heptad in the middle of the α -helical peptides. In this case, the effect on the mechanical response of the coiled coil to the applied force should be smaller, because the distance between the heptad, on which the force is applied, and the metal-stabilization site is larger. Furthermore, the stabilizing effect could be enhanced by tuning more than one heptad with His-metal chelation sites. The final aim would be to create mechano-responsive hybrid hydrogels using a four-arm poly-ethylene glycol (star-PEG) framework crosslinked by metal coordinating coiled coils. These hydrogels may also exhibit self-healing capacity as observed in mussel byssus threads in which the His-metal coordination bonds are able to reform (when allowed to rest) after mechanical loading [11]. Along these lines, coiled coil hydrogels based on the His-modified peptides could be further characterized with rheological measurements to investigate the effect of metal ion coordination on the viscoelastic properties of the hydrogels. Moreover, the mechano-responsive coiled coils could eventually be equipped with a FRET pair, which reports on the mechanical state of the coiled coil. Combined with a fluorescence readout, the coiled coils can potentially serve as force sensors in self-reporting hybrid hydrogels, which can be used to study cell-matrix interactions.

In summary, coiled coils tuned with His-metal chelation sites are excellent candidates to address the necessity of bioengineering tunable crosslinkers to create mechano-responsive, materials. Metal-coordinating coiled coils could not only find application as self-reporting and self-healing hydrogels to study cell-matrix interaction but also be useful for protein purification and labeling, biosensing and antibody-fragment stabilization [7], [119].

References

1. Ariga, K., Mori, T. & Hill, J. P., Mechanical control of nanomaterials and nanosystems, *Adv. Mater. Deerfield Beach Fla*, **2012**, *24*, 158–176.
2. Davis, D. A. *et al.*, Force-induced activation of covalent bonds in mechanoresponsive polymeric materials, *Nature*, **2009**, *459*, 68–72.
3. Karthikeyan, S. & Sijbesma, R. P., Probing Strain in Thermoplastic Elastomers Using Fluorescence Resonance Energy Transfer, *Macromolecules*, **2009**, *42*, 5175–5178.
4. Fletcher, N. L., Lockett, C. V. & Dexter, A. F., A pH-responsive coiled-coil peptide hydrogel, *Soft Matter*, **2011**, *7*, 10210–10218.
5. Wang, C., Stewart, R. J. & Kopeček, J., Hybrid hydrogels assembled from synthetic polymers and coiled-coil protein domains, *Nature*, **1999**, *397*, 417–420.
6. Dånmark, S., Aronsson, C. & Aili, D., Tailoring Supramolecular Peptide–Poly(ethylene glycol) Hydrogels by Coiled Coil Self-Assembly and Self-Sorting, *Biomacromolecules*, **2016**, *17*, 2260–2267.
7. Zhang, L. G., Khademhosseini, A. & Webster, T. Tissue and Organ Regeneration: Advances in *Micro- and Nanotechnology*, **2016**, CRC Press.
8. Sim, J. Y. *et al.*, Spatial distribution of cell-cell and cell-ECM adhesions regulates force balance while maintaining E-cadherin molecular tension in cell pairs, *Mol. Biol. Cell*, **2015**, *26*, 2456–2465.
9. Wells, R. G., The role of matrix stiffness in regulating cell behavior, *Hepatology*, **2008**, *47*, 1394–1400.
10. Zemel, A., Rehfeldt, F., Brown, A. E. X., Discher, D. E. & Safran, S. A., Optimal matrix rigidity for stress-fibre polarization in stem cells, *Nat. Phys.*, **2010**, *6*, 468–473.
11. Degtyar, E., Harrington, M. J., Politi, Y. & Fratzl, P. The Mechanical Role of Metal Ions in Biogenic Protein-Based Materials, *Angew. Chem. Int. Ed.*, **2014**, *53*, 12026–12044.
12. Cao, Y., Yoo, T. & Li, H., Single molecule force spectroscopy reveals engineered metal chelation is a general approach to enhance mechanical stability of proteins, *Proc. Natl. Acad. Sci. U. S. A.*, **2008**, *105*, 11152–11157.

-
13. Zot, A. S. & Potter, J. D., Structural aspects of troponin-tropomyosin regulation of skeletal muscle contraction, *Annu. Rev. Biophys. Biophys. Chem.*, **1987**, *16*, 535–559.
 14. Lupas, A., Coiled coils: new structures and new functions, *Trends Biochem. Sci.*, **1996**, *21*, 375–382.
 15. Bragulla, H. H. & Homberger, D. G., Structure and functions of keratin proteins in simple, stratified, keratinized and cornified epithelia, *J. Anat.*, **2009**, *214*, 516–559.
 16. Mason, J. M. & Arndt, K. M., Coiled coil domains: stability, specificity, and biological implications, *ChemBiochem Eur. J. Chem. Biol.*, **2004**, *5*, 170–176.
 17. Liu, J. *et al.*, A seven-helix coiled coil, *Proc. Natl. Acad. Sci. U. S. A.*, **2006**, *103*, 15457–15462.
 18. Malashkevich, V. N., Kammerer, R. A., Efimov, V. P., Schulthess, T. & Engel, J., The crystal structure of a five-stranded coiled coil in COMP: a prototype ion channel?, *Science*, **1996**, *274*, 761–765.
 19. Miserez, A. & Guerette, P. A., Phase transition-induced elasticity of α -helical bioelastomeric fibres and networks, *Chem. Soc. Rev.*, **2013**, *42*, 1973–1995.
 20. Kohn, W. D., Mant, C. T. & Hodges, R. S., Alpha-helical protein assembly motifs, *J. Biol. Chem.*, **1997**, *272*, 2583–2586.
 21. Arndt, K. M., Pelletier, J. N., Müller, K. M., Plückthun, A. & Alber, T., Comparison of in vivo selection and rational design of heterodimeric coiled coils, *Struct. Lond. Engl. 1993*, **2002**, *10*, 1235–1248.
 22. Aronsson, C. *et al.*, Self-sorting heterodimeric coiled coil peptides with defined and tuneable self-assembly properties, *Sci. Rep.*, **2015**, *5*, No. 14063.
 23. Zhou, N. E., Kay, C. M. & Hodges, R. S., The role of interhelical ionic interactions in controlling protein folding and stability. De novo designed synthetic two-stranded alpha-helical coiled-coils, *J. Mol. Biol.*, **1994**, *237*, 500–512.
 24. Mao, Y.-J., Sheng, X.-R. & Pan, X.-M., The effects of NaCl concentration and pH on the stability of hyperthermophilic protein Ssh10b, *BMC Biochem.*, **2007**, *8*, 1–8.
 25. Lau, S. Y., Taneja, A. K. & Hodges, R. S. S., Synthesis of a model protein of defined secondary and quaternary structure. Effect of chain length on the stabilization and formation of two-stranded alpha-helical coiled-coils, *J. Biol. Chem.*, **1984**, *259*, 13253–13261.
-

-
26. Su, J. Y., Hodges, R. S. & Kay, C. M., Effect of chain length on the formation and stability of synthetic alpha-helical coiled coils, *Biochemistry (Mosc.)*, **1994**, *33*, 15501–15510.
 27. Hulko, M. et al., The HAMP domain structure implies helix rotation in transmembrane signaling, *Cell*, **2006**, *126*, 929–940.
 28. Carter, A. P. et al., Structure and functional role of dynein's microtubule-binding domain, *Science*, **2008**, *322*, 1691–1695.
 29. Kreplak, L., Doucet, J., Dumas, P. & Briki, F., New Aspects of the α -Helix to β -Sheet Transition in Stretched Hard α -Keratin Fibers, *Biophys. J.*, **2004**, *87*, 640–647.
 30. Kreplak, L., Herrmann, H. & Aebi, U., Tensile properties of single desmin intermediate filaments, *Biophys. J.*, **2008**, *94*, 2790–2799.
 31. Wasko, S. S. et al., Structural Proteins from Whelk Egg Capsule with Long Range Elasticity Associated with a Solid-state Phase Transition, *Biomacromolecules*, **2014**, *15*, 30–42.
 32. Apostolovic, B., Deacon, S. P. E., Duncan, R. & Klok, H.-A., Hybrid polymer therapeutics incorporating bioresponsive, coiled coil peptide linkers, *Biomacromolecules*, **2010**, *11*, 1187–1195.
 33. Wang, C., Kopecek, J. & Stewart, R. J., Hybrid hydrogels cross-linked by genetically engineered coiled-coil block proteins, *Biomacromolecules*, **2001**, *2*, 912–920.
 34. Apostolovic, B., Danial, M. & Klok, H.-A., Coiled coils: attractive protein folding motifs for the fabrication of self-assembled, responsive and bioactive materials, *Chem. Soc. Rev.*, **2010**, *39*, 3541–3575.
 35. Arndt, K. M., Müller, K. M. & Plückthun, A., Helix-stabilized Fv (hsFv) antibody fragments: substituting the constant domains of a Fab fragment for a heterodimeric coiled-coil domain, *J. Mol. Biol.*, **2001**, *312*, 221–228.
 36. Jing, P., Rudra, J. S., Herr, A. B. & Collier, J. H., Self-Assembling Peptide-Polymer Hydrogels Designed From the Coiled Coil Region of Fibrin, *Biomacromolecules*, **2008**, *9*, 2438–2446.
 37. Bornschlögl, T. & Rief, M., Single molecule unzipping of coiled coils: sequence resolved stability profiles, *Phys. Rev. Lett.*, **2006**, *96*, 118102.
-

-
38. Qin, Z. & Buehler, M. J., Molecular dynamics simulation of the α -helix to β -sheet transition in coiled protein filaments: evidence for a critical filament length scale, *Phys. Rev. Lett.*, **2010**, 104, 198304.
 39. Schwaiger, I., Sattler, C., Hostetter, D. R. & Rief, M., The myosin coiled-coil is a truly elastic protein structure,” *Nat. Mater. Nat. Mater.*, **2002**, 1, 232–235.
 40. Lovell, T., Himo, F., Han, W.-G. & Noodleman, L., Density functional methods applied to metalloenzymes, *Coord. Chem. Rev.*, **2003**, 238–239, 211–232.
 41. Dudev, T. & Lim, C., Metal binding affinity and selectivity in metalloproteins: insights from computational studies, *Annu. Rev. Biophys.*, **2008**, 37, 97–116.
 42. Dokmanić, I., Sikić, M. & Tomić, S., Metals in proteins: correlation between the metal-ion type, coordination number and the amino-acid residues involved in the coordination, *Acta Crystallogr. D Biol. Crystallogr.*, **2008**, 64, 257–263.
 43. Andreini, C., Bertini, I., Cavallaro, G., Holliday, G. L. & Thornton, J. M., Metal ions in biological catalysis: from enzyme databases to general principles, *J. Biol. Inorg. Chem. JBIC Publ. Soc. Biol. Inorg. Chem.*, **2008**, 13, 1205–1218.
 44. Edgcomb, S. P. & Murphy, K. P., Variability in the pKa of histidine side-chains correlates with burial within proteins, *Proteins*, **2002**, 49, 1–6.
 45. Sancho, J., Serrano, L. & Fersht, A. R., Histidine residues at the N- and C-termini of alpha-helices: perturbed pKas and protein stability, *Biochemistry (Mosc.)*, **1992**, 31, 2253–2258.
 46. Zhang, X. & van Eldik, R., A functional model for carbonic anhydrase: thermodynamic and kinetic study of a tetraazacyclododecane complex of zinc(II), *Inorg. Chem.*, **1995**, 34, 5606–5614.
 47. Schmitt, C. N. Z., Politi, Y., Reinecke, A. & Harrington, M. J., Role of Sacrificial Protein–Metal Bond Exchange in Mussel Byssal Thread Self-Healing, *Biomacromolecules*, **2015**, 16, 2852–2861.
 48. Waite, J. H., Qin, X. X. & Coyne, K. J., The peculiar collagens of mussel byssus, *Matrix Biol. J. Int. Soc. Matrix Biol.*, **1998**, 17, 93–106.
 49. Schmidt, S. *et al.*, Metal-Mediated Molecular Self-Healing in Histidine-Rich Mussel Peptides, *Biomacromolecules*, **2014**, 15, 1644–1652.
-

-
50. Arnold, F. H. & Haymore, B. L., Engineered metal-binding proteins: purification to protein folding, *Science*, **1991**, *252*, 1796–1797.
 51. Zheng, P., Cao, Y., Bu, T., Straus, S. K. & Li, H., Single Molecule Force Spectroscopy Reveals that Electrostatic Interactions Affect the Mechanical Stability of Proteins, *Biophys. J.*, **2011**, *100*, 1534–1541.
 52. Root, D. D., Yadavalli, V. K., Forbes, J. G. & Wang, K., Coiled-Coil Nanomechanics and Uncoiling and Unfolding of the Superhelix and α -Helices of Myosin, *Biophys. J.*, **2006**, *90*, 2852–2866.
 53. Thomas, F., Boyle, A. L., Burton, A. J. & Woolfson, D. N., A Set of de Novo Designed Parallel Heterodimeric Coiled Coils with Quantified Dissociation Constants in the Micromolar to Sub-nanomolar Regime, *J. Am. Chem. Soc.*, **2013**, *135*, 5161–5166.
 54. Wood, C. W. *et al.*, CCBuilder: an interactive web-based tool for building, designing and assessing coiled-coil protein assemblies, *Bioinforma. Oxf. Engl.*, **2014**, *30*, 3029–3035.
 55. Movasaghi, Z., Rehman, S. & Rehman, D. I. ur., Fourier Transform Infrared (FTIR) Spectroscopy of Biological Tissues, *Appl. Spectrosc. Rev.* **2008**, *43*, 134–179.
 56. Peter Larkin, *Infrared and Raman Spectroscopy; Principles and Spectral Interpretation*, 1st Edition, Elsevier, **2011**, ISBN 9780123870186.
 57. Baker, M. J. *et al.*, Using Fourier transform IR spectroscopy to analyze biological materials, *Nat. Protoc.*, **2014**, *9*, 1771–1791.
 58. Byler, D. M. & Susi, H., Examination of the secondary structure of proteins by deconvolved FTIR spectra, *Biopolymers*, **1986**, *25*, 469–487.
 59. Heimburg, T., Schünemann, J., Weber, K. & Geisler, N. F, FTIR-Spectroscopy of Multistranded Coiled Coil Proteins, *Biochemistry (Mosc.)*, **1999**, *38*, 12727–12734.
 60. Pike Technologies, *ATR–Theory and Applications*, Application note, *Pike Technologies*, **2011**.
 61. Perkin Elmer, *FT-IR Spectroscopy Attenuated Total Reflectance (ATR)*, Perkin Elmer inc. USA, **2005**.
 62. Movasaghi, Z., Rehman S. & Rehman I.U., Raman Spectroscopy of Biological Tissues, *Appl. Spectrosc. Rev.*, **2007**, 493–541.
-

-
63. Shetty, G., Kendall, C., Shepherd, N., Stone, N. & Barr, H., Raman spectroscopy: elucidation of biochemical changes in carcinogenesis of oesophagus, *Br. J. Cancer*, **2006**, *94*, 1460–1464.
 64. Huang, Z. *et al.*, Near-infrared Raman spectroscopy for optical diagnosis of lung cancer, *Int. J. Cancer*, **2003**, *107*, 1047–1052.
 65. Jyothi Lakshmi, R. *et al.*, Tissue Raman spectroscopy for the study of radiation damage: brain irradiation of mice, *Radiat. Res.*, **2002**, *157*, 175–182.
 66. Takeuchi, H., Raman structural markers of tryptophan and histidine side chains in proteins, *Biopolymers*, **2003**, *72*, 305–317.
 67. Greenfield, N. J., Using circular dichroism spectra to estimate protein secondary structure, *Nat. Protoc.*, **2006**, *1*, 2876–2890.
 68. Greenfield, N. J., Using circular dichroism collected as a function of temperature to determine the thermodynamics of protein unfolding and binding interactions, *Nat. Protoc.*, **2006**, *1*, 2527–2535.
 69. Wendt, H. *et al.*, Very rapid, ionic strength-dependent association and folding of a heterodimeric leucine zipper, *Biochemistry (Mosc.)*, **1997**, *36*, 204–213.
 70. Zitzewitz, J. A., Bilsel, O., Luo, J., Jones, B. E. & Matthews, C. R. P, *Biochemistry (Mosc.)*, **1995**, *34*, 12812–12819.
 71. Rabe, M., Boyle, A., Zope, H. R., Versluis, F. & Kros, A., Probing the folding mechanism of a leucine zipper peptide by stopped-flow circular dichroism spectroscopy, *Pept. Sci.*, **2015**, *104*, 65–72.
 72. Ghadiri, M. R. & Choi, C., Secondary structure nucleation in peptides. Transition metal ion stabilized alpha-helices, *J. Am. Chem. Soc.*, **1990**, *112*, 1630–1632.
 73. Greenfield, N. J., Circular dichroism analysis for protein-protein interactions, *Methods Mol. Biol. Clifton NJ*, **2004**, *261*, 55–78.
 74. Kemmer, G. & Keller, S., Nonlinear least-squares data fitting in Excel spreadsheets, *Nat. Protoc.*, **2010**, *5*, 267–281.
 75. Rutherford, S. M. & Gilani, G. S., Ed. John E, Coligan Al, Amino acid analysis, *Curr. Protoc. Protein Sci*, John Wiley and Sons, **2009**, Chapter 11, Unit 11.9.
-

References

76. Cole, J. L., Lary, J. W., P Moody, T. & Laue, T. M., Analytical ultracentrifugation: sedimentation velocity and sedimentation equilibrium, *Methods Cell Biol.*, **2008**, *84*, 143–179.
77. Schuck, P. & Rossmanith, P., Determination of the sedimentation coefficient distribution by least-squares boundary modeling, *Biopolymers*, **2000**, *54*, 328–341.
78. Laidler, K. J. & King, M. C., Development of transition-state theory, *J. Phys. Chem.*, **1983**, *87*, 2657–2664.
79. Kramers, H. A., Brownian motion in a field of force and the diffusion model of chemical reactions, *Physica*, **1940**, *7*, 284–304.
80. Bell, G. I., Models for the specific adhesion of cells to cells, *Science*, **1978**, *200*, 618–627.
81. Evans, E. & Ritchie, K., Dynamic strength of molecular adhesion bonds., *Biophys. J.*, **1997**, *72*, 1541–1555.
82. Guthold, M., Superfine, R. & Taylor, R. M. T, The Rules are Changing: Force Measurements on Single Molecules and How They Relate to Bulk Reaction Kinetics and Energies, *Biomed. Microdevices*, **2001**, *3*, 9–18
83. Zlatanova, J., Lindsay, S. M. & Leuba, S. H., Single molecule force spectroscopy in biology using the atomic force microscope, *Prog. Biophys. Mol. Biol.*, **2000**, *74*, 37–61.
84. Bouchiat, C. et al., Estimating the persistence length of a worm-like chain molecule from force-extension measurements, *Biophys. J.*, **1999**, *76*, 409–413.
85. Rief, M., Fernandez, J. M. & Gaub, H. E., Elastically Coupled Two-Level Systems as a Model for Biopolymer Extensibility, *Phys. Rev. Lett.*, **1998**, *81*, 4764–4767.
86. Milstein, J. N. & Meiners, J.-C., Ed. Roberts, G. C. K., Worm-Like Chain (WLC) Model, *Encyclopedia of Biophysics*, Springer Berlin, Heidelberg, **2013**, 2757–2760.
87. Marko, J. F. & Siggia, E. D., Stretching DNA, *Macromolecules*, **1995**, *28*, 8759–8770.
88. Schuck, P., Size-distribution analysis of macromolecules by sedimentation velocity ultracentrifugation and lamm equation modeling, *Biophys. J.*, **2000**, *78*, 1606–1619.
89. Zimmermann, J. L., Nicolaus, T., Neuert, G. & Blank, K., Thiol-based, site-specific and covalent immobilization of biomolecules for single-molecule experiments, *Nat. Protoc.*, **2010**, *5*, 975–985.

-
90. Suh, S.-S., Haymore, B. L. & Arnold, F. H., Characterization of His-X3-His sites in α -helices of synthetic metal-binding bovine somatotropin, *Protein Eng.*, **1991**, *4*, 301–305.
 91. Krantz, B. A. & Sosnick, T. R., Engineered metal binding sites map the heterogeneous folding landscape of a coiled coil, *Nat. Struct. Biol.*, **2001**, *8*, 1042–1047.
 92. Alexander, P. A., He, Y., Chen, Y., Orban, J. & Bryan, P. N., A minimal sequence code for switching protein structure and function, *Proc. Natl. Acad. Sci U. S. A.*, **2009**, *106*, 21149–21154.
 93. Heimburg, T., Schuenemann, J., Weber, K. & Geisler, N., Specific Recognition of Coiled Coils by Infrared Spectroscopy: Analysis of the Three Structural Domains of Type III Intermediate Filament Proteins, *Biochemistry (Mosc.)*, **1996**, *35*, 1375–1382.
 94. Nevskaya, N. A. & Chirgadze, Y. N., Infrared spectra and resonance interactions of amide-I and II vibration of alpha-helix, *Biopolymers*, **1976**, *15*, 637–648.
 95. Kong, J. & Yu, S., Fourier Transform Infrared Spectroscopic Analysis of Protein Secondary Structures, *Acta Biochim. Biophys. Sin.*, **2007**, *39*, 549–559.
 96. Navarrete, J. T. L., Hernández, V. & Ramírez, F. J., Molecular Spectroscopy and Molecular Structure 1994Vibrational study of aspartic acid and glutamic acid dipeptides, *J. Mol. Struct.*, 1995, *348*, 249–252.
 97. Ugwu, S. O.; Apte, S. P., *Pharm. Technol.*, 2004, *28*, 86.
 98. Kandegedara, A. & Rorabacher, D. B., Noncomplexing Tertiary Amines as ‘Better’ Buffers Covering the Range of pH 3-11. Temperature Dependence of Their Acid Dissociation Constants, *Anal. Chem.*, **1999**, *71*, 3140–3144.
 99. Silva, J. L., Silveira, C. F., Correia, A. & Pontes, L., Dissociation of a native dimer to a molten globule monomer, *J. Mol. Biol.*, **1992**, *223*, 545–555.
 100. Rulíšek, L. & Vondrášek, J., Coordination geometries of selected transition metal ions (Co^{2+} , Ni^{2+} , Cu^{2+} , Zn^{2+} , Cd^{2+} , and Hg^{2+}) in metalloproteins, *J. Inorg. Biochem.*, **1998**, *71*, 115–127.
 101. Mikhonin, A. V., Bykov, S. V., Myshakina, N. S. & Asher, S. A., Peptide secondary structure folding reaction coordinate: correlation between uv raman amide III frequency, Psi Ramachandran angle, and hydrogen bonding, *J. Phys. Chem. B*, **2006**, *110*, 1928–1943.
-

-
102. Laity, J. H., Lee, B. M. & Wright, P. E., Zinc finger proteins: new insights into structural and functional diversity, *Curr. Opin. Struct. Biol.*, **2006**, *11*, 39–46.
 103. Singh, S. P., Ma, L. Q. & Harris, W. G., Heavy metal interactions with phosphatic clay: Sorption and desorption behavior, *J. Environ. Qual.*, **2000**, *30*, 1961–1968.
 104. Cotter-Howells, J. & Caporn, S., Environmental Geochemistry Remediation of contaminated land by formation of heavy metal phosphates, *Appl. Geochem.*, **1996**, *11*, 335–342.
 105. Fletcher, J. M. *et al.*, A Basis Set of de Novo Coiled-Coil Peptide Oligomers for Rational Protein Design and Synthetic Biology, *ACS Synth. Biol.*, **2012**, *1*, 240–250.
 106. Pace, C. N. & Vanderburg, K. E., Determining globular protein stability: guanidine hydrochloride denaturation of myoglobin, *Biochemistry (Mosc.)*, **1979**, *18*, 288–292.
 107. Thompson, K. S., Vinson, C. R. & Freire, E., Thermodynamic characterization of the structural stability of the coiled-coil region of the bZIP transcription factor GCN4, *Biochemistry (Mosc.)*, **1993**, *32*, 5491–5496.
 108. Armstrong, K. M. & Baldwin, R. L., Charged histidine affects alpha-helix stability at all positions in the helix by interacting with the backbone charges., *Proc. Natl. Acad. Sci. U. S. A.*, **1993**, *90*, 11337–11340.
 109. Sekatskii, S. K., Benedetti, F. & Dietler, G., Dependence of the most probable and average bond rupture force on the force loading rate: First order correction to the Bell–Evans model, *J. Appl. Phys.*, **2013**, *114*, 034701.
 110. Nautiyal, S., Woolfson, D. N., King, D. S. & Alber, T., A Designed Heterotrimeric Coiled Coil, *Biochemistry (Mosc.)*, **1995**, *34*, 11645–11651.
 111. Pace, C. N. & Scholtz, J. M., A helix propensity scale based on experimental studies of peptides and proteins., *Biophys. J.*, **1998**, *75*, 422–427.
 112. Kitakuni, E., Kuroda, Y., Oobatake, M., Tanaka, T. & Nakamura, H., Thermodynamic characterization of an artificially designed amphiphilic alpha-helical peptide containing periodic prolines: observations of high thermal stability and cold denaturation, *Protein Sci. Publ. Protein Soc.*, **1994**, *3*, 831–837.
 113. Fullenkamp, D. E., He, L., Barrett, D. G., Burghardt, W. R. & Messersmith, P. B., Mussel-inspired histidine-based transient network metal coordination hydrogels, *Macromolecules*, **2013**, *46*, 1167–1174.
-

114. Grindy, S. C. *et al.*, Control of hierarchical polymer mechanics with bioinspired metal-coordination dynamics. *Nat. Mater.*, **2015**, *14*, 1210–1216.
115. Kellis, J. T., Todd, R. J. & Arnold, F. H., Protein stabilization by engineered metal chelation, *Biotechnol. Nat. Publ. Co.*, **1991**, *9*, 994–995.
116. Arnold, F. H. & Zhang, J. H., Metal-mediated protein stabilization, *Trends Biotechnol.*, **1994**, *12*, 189–192.
117. Kau, L. S., Spira-Solomon, D. J., Penner-Hahn, J. E., Hodgson, K. O. & Solomon, E. I., X-ray absorption edge determination of the oxidation state and coordination number of copper. Application to the type 3 site in *Rhus vernicifera* laccase and its reaction with oxygen, *J. Am. Chem. Soc.*, **1987**, *109*, 6433–6442.
118. Zhang, Y., Akilesh, S. & Wilcox, D. E., Isothermal titration calorimetry measurements of Ni(II) and Cu(II) binding to His, GlyGlyHis, HisGlyHis, and bovine serum albumin: a critical evaluation, *Inorg. Chem.*, **2000**, *39*, 3057–3064.
119. Wang, H. & Heilshorn, S. C., Adaptable hydrogel networks with reversible linkages for tissue engineering, *Adv. Mater. Deerfield Beach Fla.*, **2015**, *27*, 3717–3736.

Appendix

List of Figures

Figure A 1: ATR-FTIR spectra for A4 (A), B4 (B) and A4B4 (C) in the presence of metal ions.	79
Figure A 2: ATR-FTIR spectra for HA4 (A), HB4 (B) and HA4HB4 (C) in the presence of metal ions.....	80
Figure A 3: Raman spectra of A4 (A), B4 (B) and A4B4 (C) in 10 mM PIPPS pH 8.1.....	81
Figure A 4: Thermal unfolding for the peptides in 10 mM NaP (pH 8.1) from 10-90°C in the time course measurement mode.	82
Figure A 5: Thermal unfolding curves of B4 (A) and HB4 (B) in 10 mM NaP (pH 8.1) at 222 nm fitted to equation 5 to obtain T_m	84
Figure A 6: Replicates of the unfolding curves of HA4 (A, B) in 2 M GdmCl with and without Ni^{2+} at 222 nm.	85
Figure A 7: Replicates of the unfolding curves of HA4HB4 (A-C) and A4B4 (D,E) in 2 M GdmCl with and without Ni^{2+} at 222 nm.	86
Figure A 8: CD spectra for HA4HB4 before (black) and after (red) the heating process without (A) and with 2:1 His: Ni^{2+} ratio (B) at 20°C.	87
Figure A 9: Apparent sedimentation coefficient distribution (ls g*) of the individual peptides.	88

List of Tables

Table A 1: Concentration of peptide stock solution used for the CD measurements.....	82
Table A 2: Parameters obtained by fitting the thermal unfolding curves with equation 5.....	83

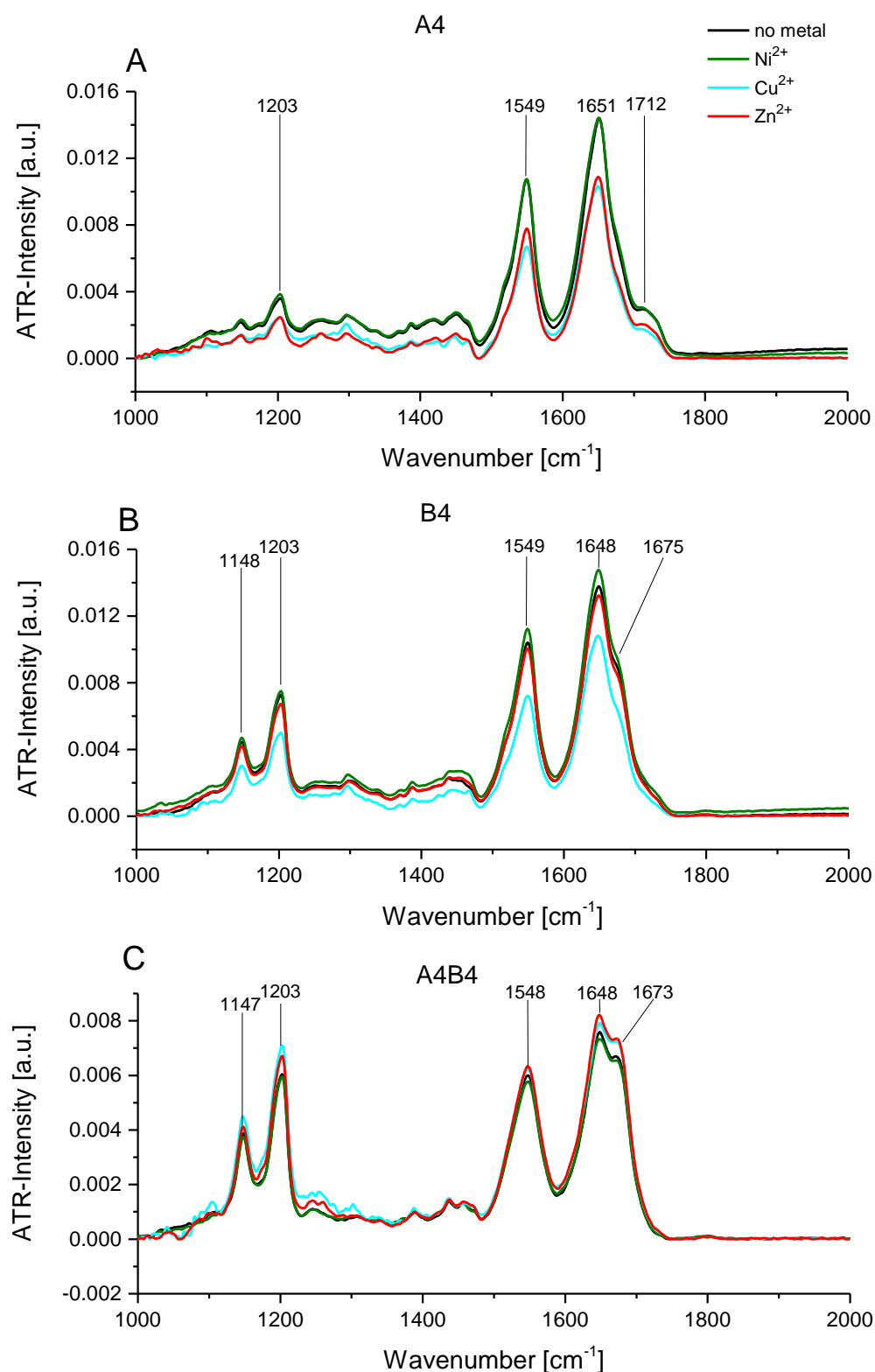


Figure A 1: ATR-FTIR spectra for A4 (A), B4 (B) and A4B4 (C) in the presence of metal ions. No metal ions (black), Ni²⁺ (green), Cu²⁺ (blue) and Zn²⁺ (red) were added in a ratio of 2:1 His:Me²⁺. The peptides (1.5 mM) were measured in water in the ATR-mode. Number of scans: 32, smoothing: 5 points, baseline correction: 1 iteration (rubberband method, linear).

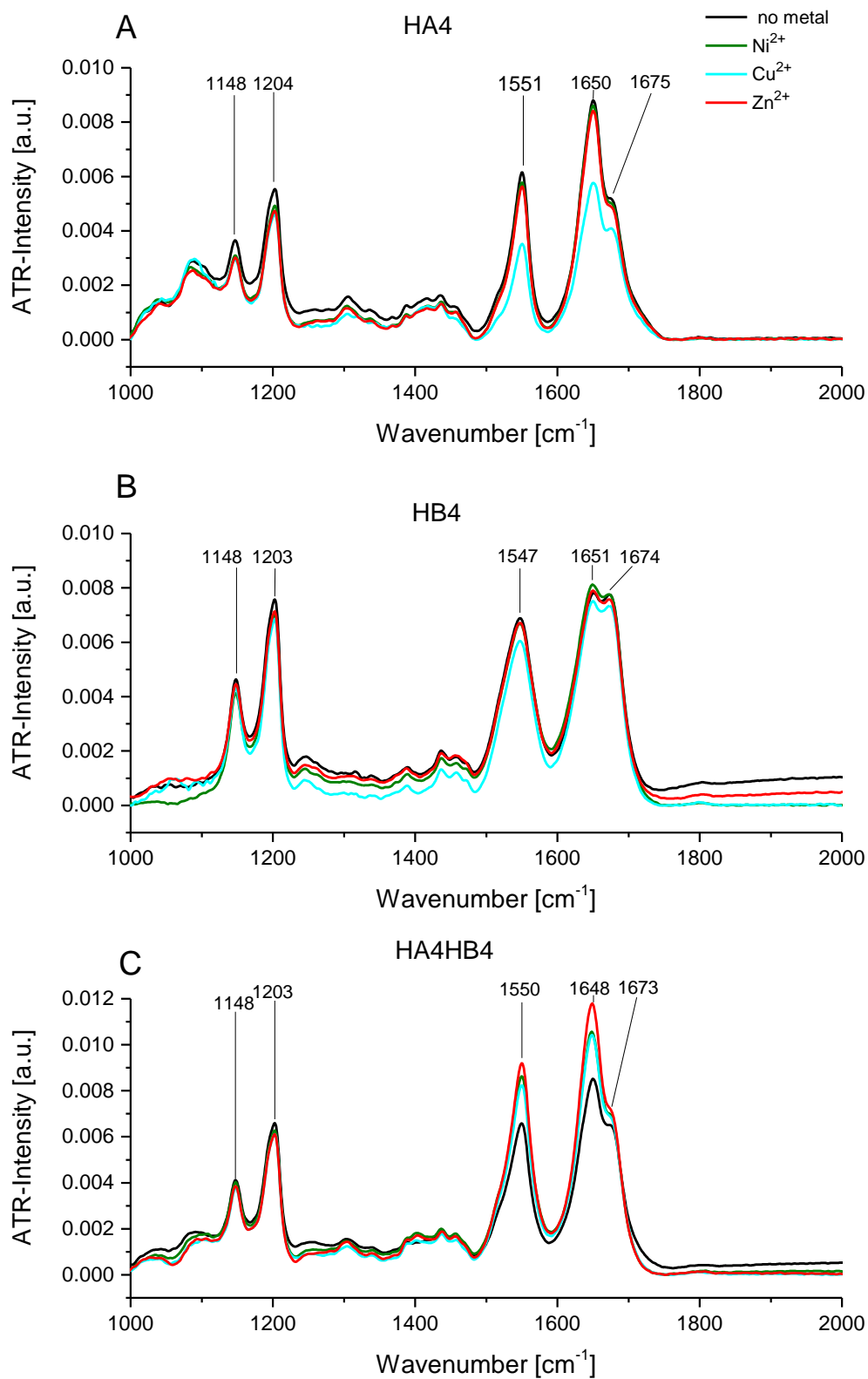


Figure A 2: ATR-FTIR spectra for HA4 (A), HB4 (B) and HA4HB4 (C) in the presence of metal ions. No metal ions (black), Ni²⁺ (green), Cu²⁺ (blue) and Zn²⁺ (red) were added in a ratio of 2:1 His:Me²⁺. The peptides (1.5 mM) were measured in water in the ATR-mode. Number of scans: 32, smoothing: 5 points, baseline correction: 1 iteration (rubberband method, linear).

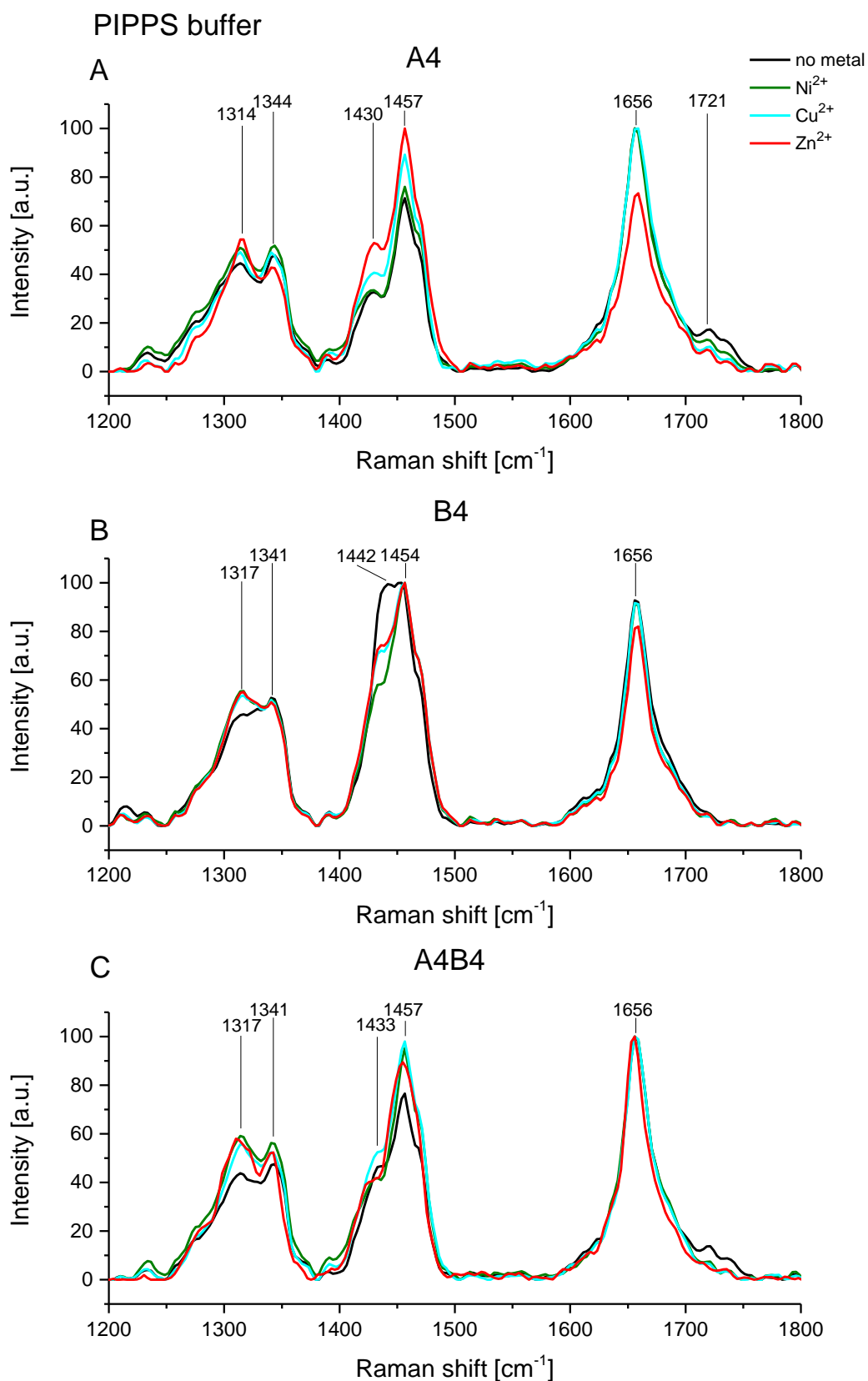


Figure A 3: Raman spectra of A4 (A), B4 (B) and A4B4 (C) in 10 mM PIPPS pH 8.1. Metal ions were added in 2:1 His:Me²⁺ ratio. No metal ions (black), Ni²⁺ (green), Cu²⁺ (blue) and Zn²⁺ (red). A 20x objective (Nikon, NA 0.4) was used with 0° polarization and no analyzer in the light path. Spectra from at least three points of the sample were measured (Integration of 1 s and 30 accumulations) and averaged. The spectra are baseline corrected (1 pt) and smoothed (5 pt).

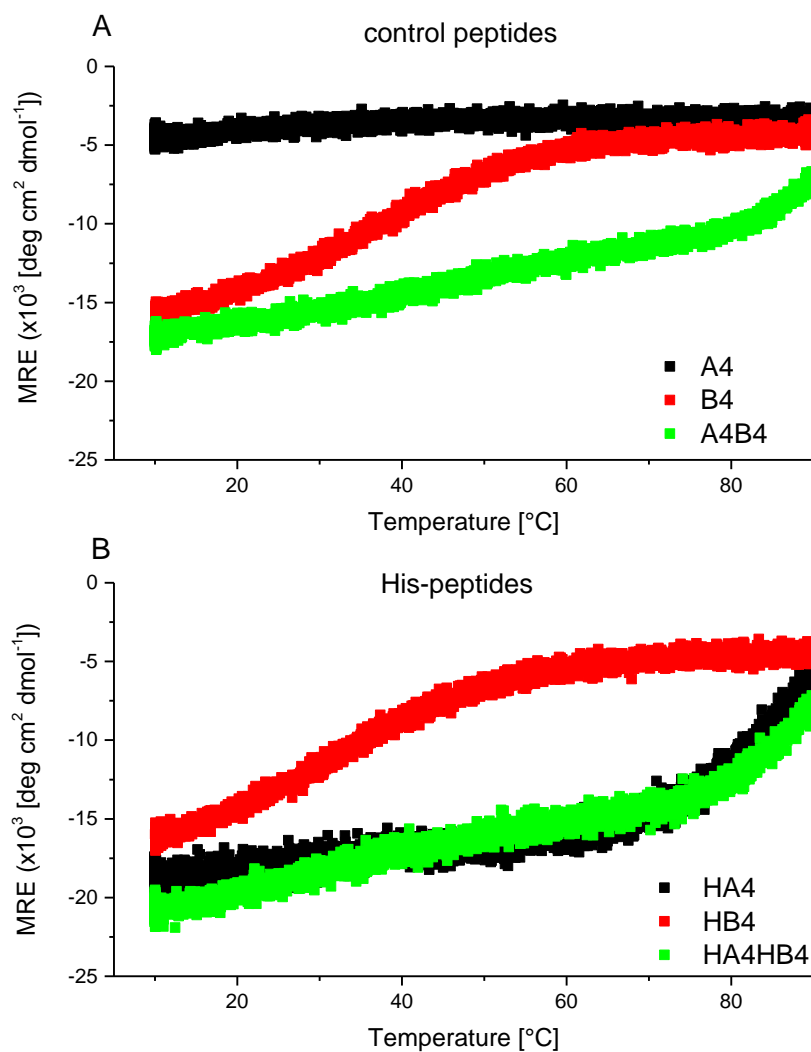


Figure A 4: Thermal unfolding for the peptides in 10 mM NaP (pH 8.1) from 10-90°C in the time course measurement mode. The spectra were taken at 222 nm with a bandwidth of 2 nm, an integration time of 1 s and 2 s intervals.

Table A 1: Concentration of peptide stock solution used for the CD measurements. The concentrations were determined with Amino Acid Analysis after acid hydrolysis of the peptides (chapter 3.6). Calculation of total amino acid concentration was based on the standard amino acid mixture with known concentration.

Peptide	Concentration [mM]
A4	1.32
B4	1.33
HA4	0.73
HB4	1.17

Appendix

Table A 2: Parameters obtained by fitting the thermal unfolding curves with equation 5. The ΔC_p was hold constant at 0 J/(mol K) and the m_n was hold constant at 14 deg cm²/(dmol K) for all the fits. SSR is the sum of squared residuals.

Sample	T_m [°C]	ΔH_m [kJ/mol]	θ_u [x 10 ³ deg cm ² / dmol]	θ_n [x 10 ³ deg cm ² / dmol]	m_u [deg cm ² /dmol K]	SSR (x10 ⁵)
B4 in NaP	38.3	-75.1	0.0	-20.2	-11.4	1939
HB4 in NaP	33.8	-68.1	0.0	-21.5	-12.0	2560
HA4 PIPPS, 2 M GdmCl	33.1	-112.7	0.0	-29.2	-9.2	169
	31.4	-109.3	0.0	-26.4	-9.9	134
	30.4	-111.9	0.0	-22.4	-8.7	84
HA4 PIPPS, 2 M GdmCl, Ni ²⁺	32.4	-110.3	0.0	-27.8	-12.0	327
	32.8	-103.4	0.0	-30.9	-9.9	219
	33.6	-113.2	0.0	-24.4	-8.1	157
HA4HB4 PIPSS, 2 M GdmCl	27.6	-115.8	0.0	-20.3	-8.8	103
	30.5	-110.3	0.0	-21.9	-8.3	45
	30.6	-106.8	0.0	-21.4	-7.8	53
HA4HB4 PIPSS, 2 M GdmCl, Ni ²⁺	34.3	-105.7	0.0	-22.8	-8.7	161
	36.7	-112.6	0.0	-23.1	-7.9	81
	36.4	-113.4	0.0	-23.2	-8.6	103
A4B4 PIPPS, 2 M GdmCl	39.8	-113.0	0.0	-19.7	-9.2	69
	38.1	-118.7	0.0	-20.0	-8.9	65
	37.7	-120.5	0.0	-18.4	-8.1	69
A4B4 PIPPS, 2 M GdmCl, Ni ²⁺	39.4	-116.9	0.0	-20.0	-9.1	75
	38.4	-114.5	0.0	-20.4	-8.8	853
	35.8	-117.3	0.0	-19.2	-9.1	29
HA4HB4 PIPSS, 2 M GdmCl (university)	31.2	-98.8	0.0	-22.2	-8.7	52
HA4HB4 PIPSS, 2 M GdmCl, Ni ²⁺ (university)	36.4	-92.8	0.0	-24.5	-8.4	163

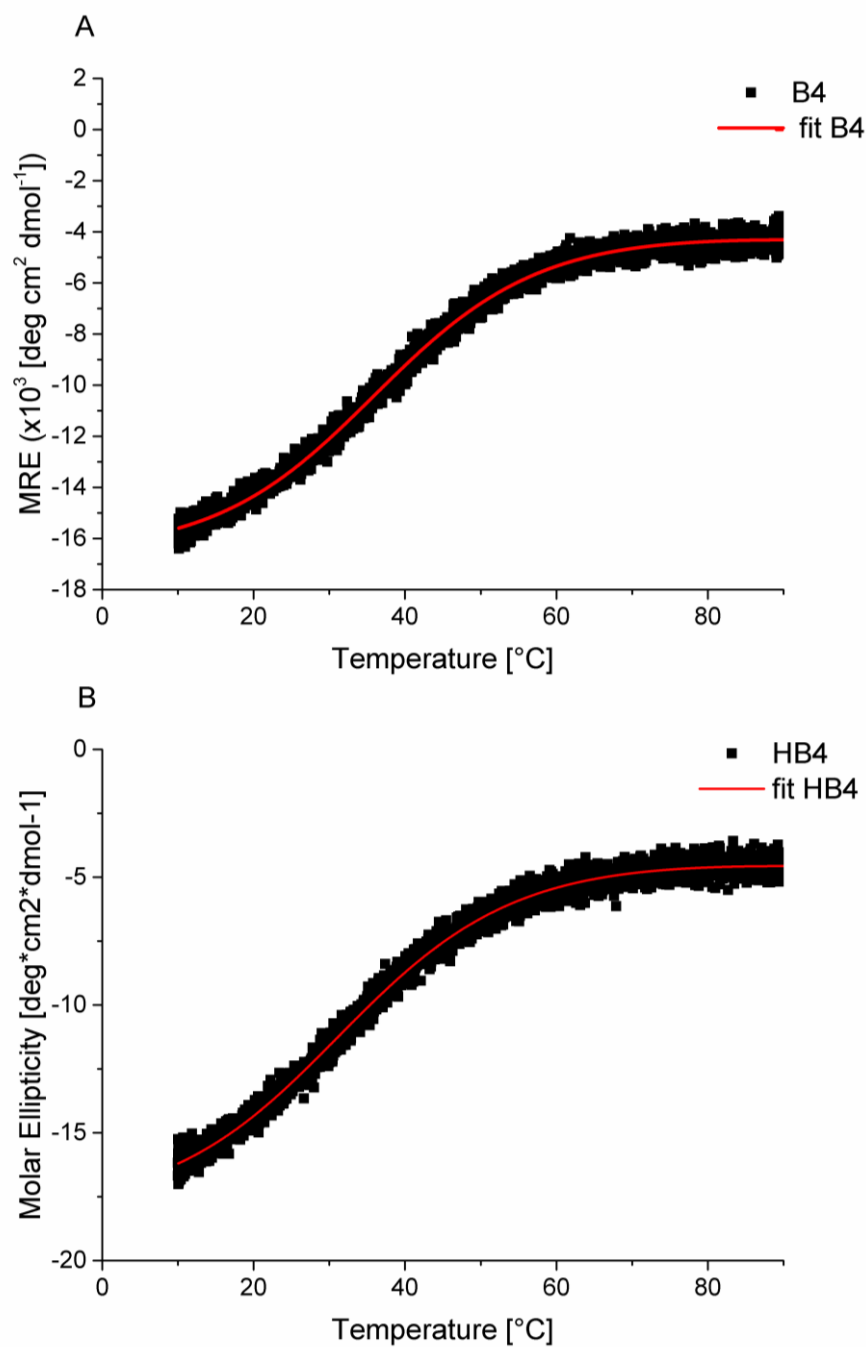


Figure A 5: Thermal unfolding curves of B4 (A) and HB4 (B) in 10 mM NaP (pH 8.1) at 222 nm fitted to equation 5 to obtain T_m . The spectra were taken at 222 nm from 10 to 90°C with a bandwidth of 2 nm, an integration time of 1 s and 2 s intervals in the time course measurement mode.

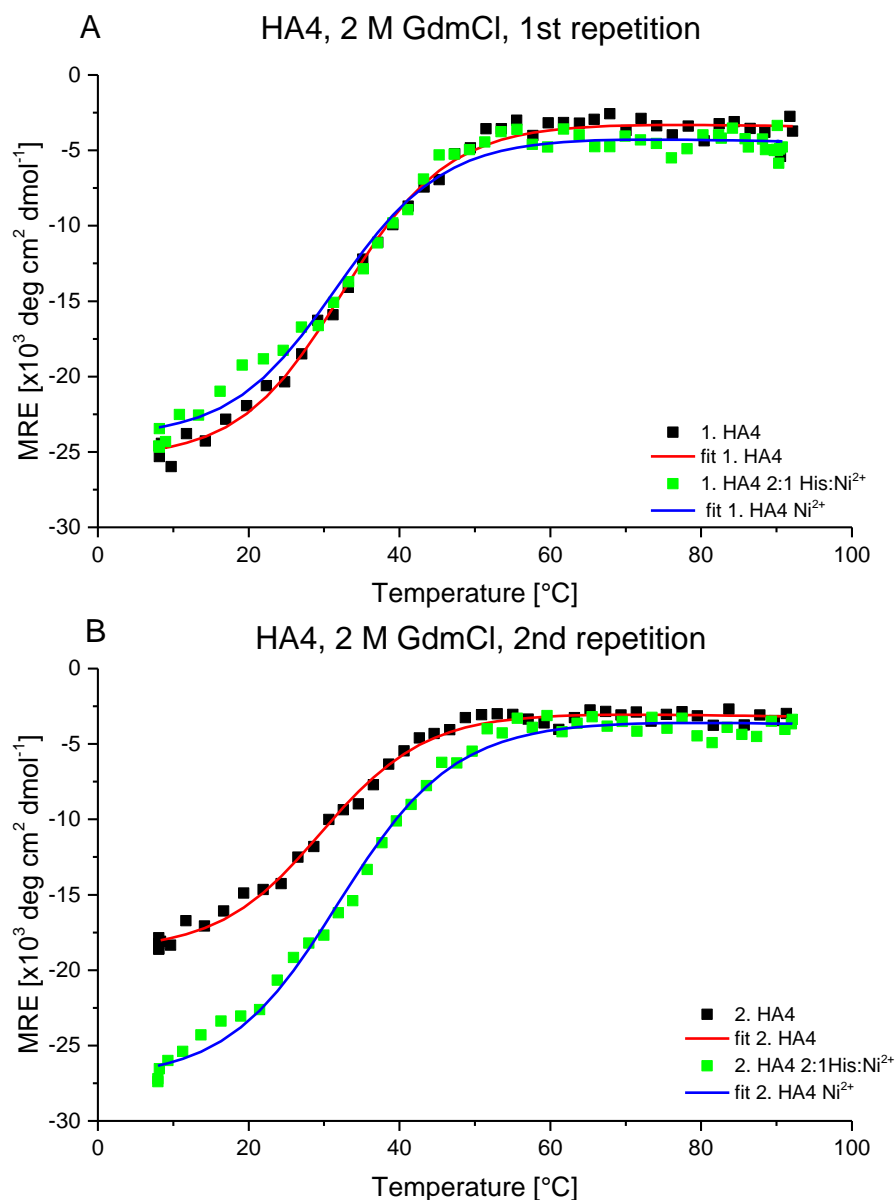


Figure A 6: Replicates of the unfolding curves of HA4 (A, B) in 2 M GdmCl with and without Ni^{2+} at 222 nm. The His: Ni^{2+} ratio was 2:1. The data were fitted with equation 5 to obtain the T_m . The unfolding curves were acquired with the following setup: The heating rate was $1^{\circ}\text{C}/\text{min}$. Measurements were performed in 5 mM PIPPS pH 8.1 in the interval scan mode (interval: 2 min, 1 accumulation, bandwidth: 1 nm, 2 s integration time). The mean residue molar ellipticity was calculated using equation 1.

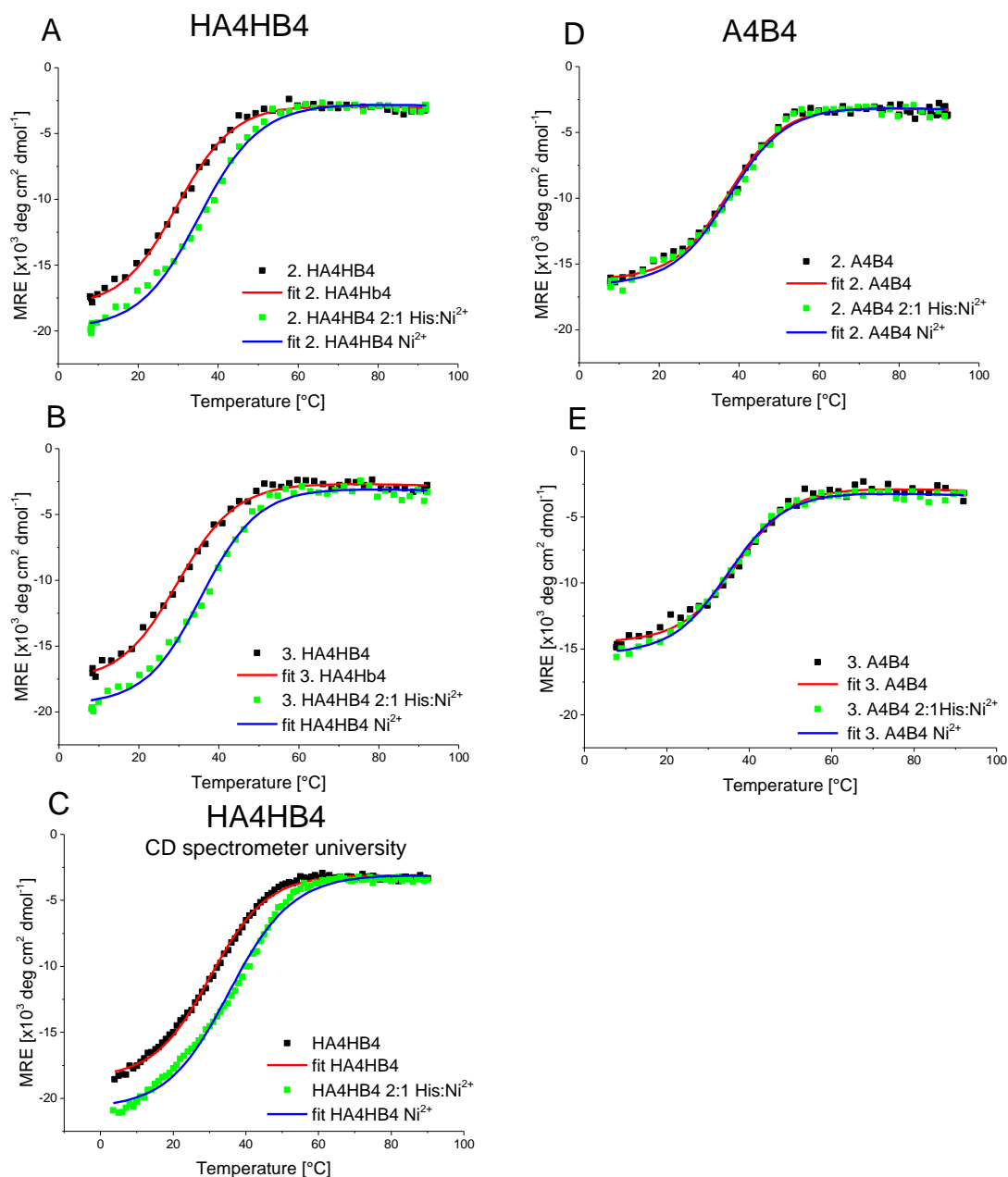


Figure A 7: Replicates of the unfolding curves of HA4HB4 (A-C) and A4B4 (D,E) in 2 M GdmCl with and without Ni²⁺ at 222 nm. The His:Ni²⁺ ratio was 2:1. The data were fitted with equation 5 to obtain the T_m .

The unfolding curves in A, B, D, E were acquired with the following setup: The heating rate was 1°C/min. Measurements were performed in 5 mM PIPPS pH 8.1 in the interval scan mode (interval: 2 min, 1 accumulation, bandwidth: 1 nm, integration time 2 s). The curves in graph C were taken at a Jasco J-815 CD Spectropolarimeter equipped with a Jasco PTC 423s peltier element (University of Potsdam) in 5 mM PIPPS, 2 M GdmCl (pH 8.1) at 222 nm from 4 to 90°C (heating rate: 1°C/min). The measurement mode was the temperature-wavelength scan with a step width of 1°C, a bandwidth of 2 nm, an integration time of 4 s after 5 s with a change smaller than 0.1°C. The mean residue molar ellipticity (MRE) was calculated using equation 1.

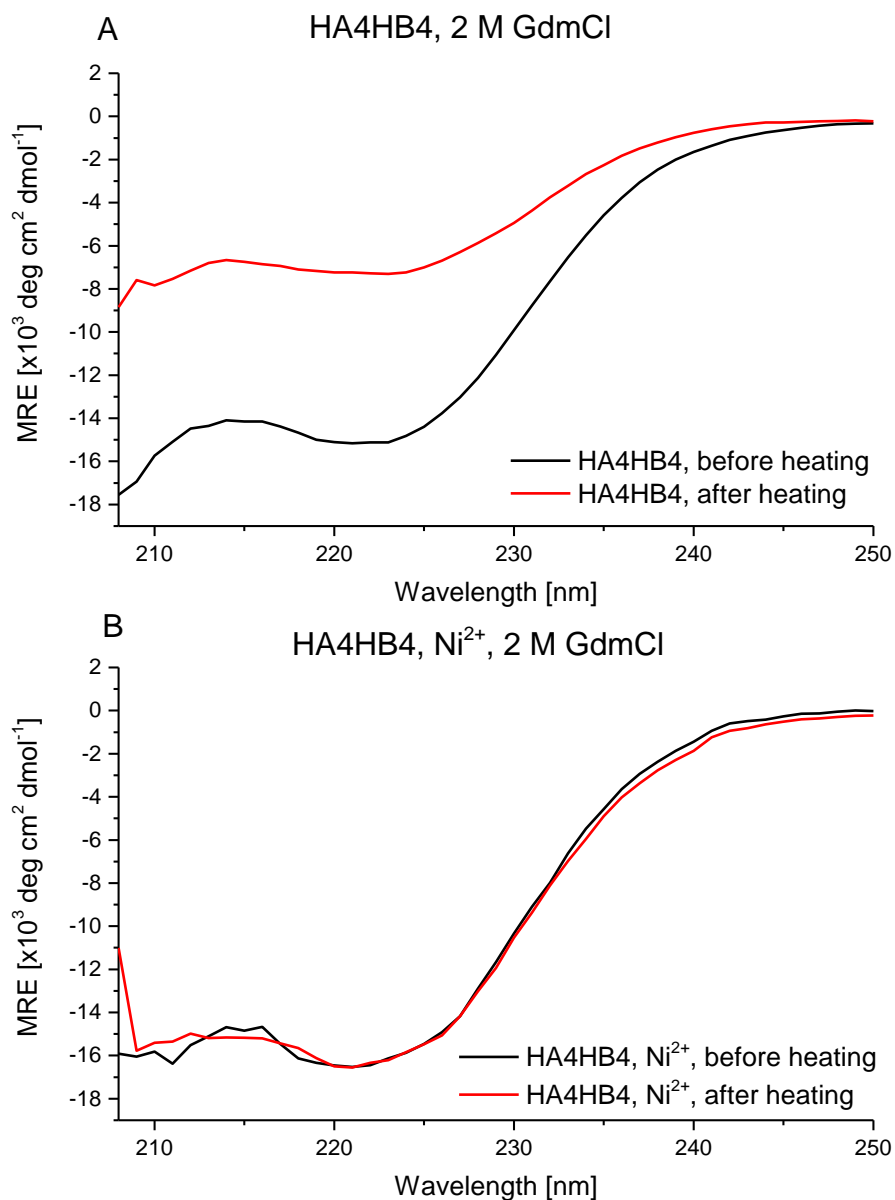


Figure A 8: CD spectra for HA4HB4 before (black) and after (red) the heating process without (A) and with 2:1 His:Ni²⁺ ratio (B) at 20°C. The spectra were taken in 5 mM PIPPS, 2M GdmCl (pH 8.1) from 250 to 208 nm with a step resolution of 1 nm, a bandwidth of 1 nm, a scanning speed of 50 nm/min, an integration time of 2 s and 10 scans were accumulated. The mean residue molar ellipticity (MRE) was calculated using equation 1.

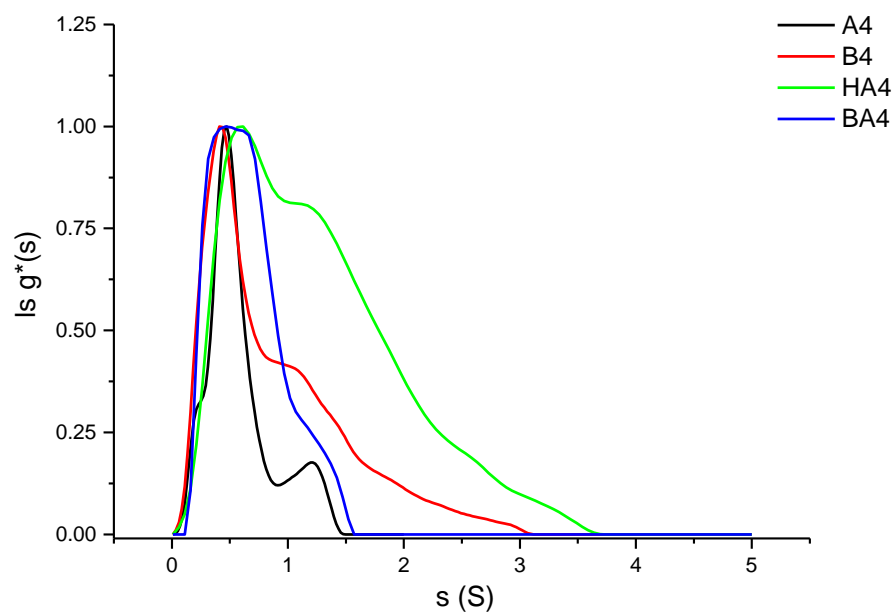


Figure A 9: Apparent sedimentation coefficient distribution ($s g^*$) of the individual peptides. The peptides (1 mg/ml) were measured in 5 mM PIPPS buffer (pH 8.1). Data were obtained using AUC in the sedimentation velocity mode (60000 rpm) with an interference detector.

Acknowledgements

First of all, I thank my supervisor Matthew Harrington for giving me the opportunity to do this project in his group and all his help and advice. Furthermore, I would like to thank Kerstin Blank, the head of the Mechano(bio)chemistry group, for sharing her “know how” about single molecule force spectroscopy with me and all her helpful advice regarding this thesis.

I would also like to thank Prof. Robert Seckler for giving me the opportunity to use their CD spectrometer and his advice regarding the method for analyzing the thermal unfolding data. Furthermore, I thank Anja Thalhammer and Klaus Gast, who are the Circular Dichroism experts working in Prof. Secklers group at the University of Potsdam, for giving me the instructions for the CD spectrometer.

Moreover, I would like to thank all the people working at the MPIKG, especially in the groups of Matthew Harrington and Kerstin Blank, for creating a great atmosphere in the labs and coffee corners. In particular, I like to mention Ana Trapaidze, for her help in the development of experimental setups and troubleshooting and for always giving me positive energy. Thanks to Jeannette Steffen, for helping me with the Amino Acid Analysis. A huge “thank you” to Ruby Sullan, for teaching me how the AFM works and how to analyze the AFM data as well as for all her patience in answering all my questions regarding IGOR Pro. Many thanks to Melis Göktas and Patricia López García for helping me with the AFM data interpretation and Lorena Ruiz Rodriguez for spending many hours with me solving the teething troubles of the custom built heating system for the CD spectrometer. Furthermore, I would like to thank Antje Völkl for performing the AUC measurements, Antje Reinecke for her helpful advice and Klaus Bienert for all his effort during the development and set up the heating system for the thermal unfolding measurements.

Finally, I could not have done this work without my family. I am thankful to my mother and my siblings for all their support and acceptance. Last but not least, I would like to thank my husband Jakob for providing me with delicious cakes and chocolate, while I was writing and his unconditional love.